UNLV | UNIVERSITY LIBRARIES

UNLV Retrospective Theses & Dissertations

1-1-1989

The dynamic response of a flexible three-link robot using strain gages, Lagrange polynomials, Fourier series, and the finite element analysis

Robert Frank Marceau
University of Nevada, Las Vegas

Follow this and additional works at: https://digitalscholarship.unlv.edu/rtds

Repository Citation

Marceau, Robert Frank, "The dynamic response of a flexible three-link robot using strain gages, Lagrange polynomials, Fourier series, and the finite element analysis" (1989). *UNLV Retrospective Theses & Dissertations*. 67.
http://dx.doi.org/10.25669/rtko-65ep

This Thesis is protected by copyright and/or related rights. It has been brought to you by Digital Scholarship@UNLV with permission from the rights-holder(s). You are free to use this Thesis in any way that is permitted by the copyright and related rights legislation that applies to your use. For other uses you need to obtain permission from the rights-holder(s) directly, unless additional rights are indicated by a Creative Commons license in the record and/or on the work itself.

This Thesis has been accepted for inclusion in UNLV Retrospective Theses & Dissertations by an authorized administrator of Digital Scholarship@UNLV. For more information, please contact digitalscholarship@unlv.edu.

INFORMATION TO USERS

The most advanced technology has been used to photograph and reproduce this manuscript from the microfilm master. UMI films the text directly from the original or copy submitted. Thus, some thesis and dissertation copies are in typewriter face, while others may be from any type of computer printer.

The quality of this reproduction is dependent upon the quality of the copy submitted. Broken or indistinct print, colored or poor quality illustrations and photographs, print bleedthrough, substandard margins, and improper alignment can adversely affect reproduction.

In the unlikely event that the author did not send UMI a complete manuscript and there are missing pages, these will be noted. Also, if unauthorized copyright material had to be removed, a note will indicate the deletion.

Oversize materials (e.g., maps, drawings, charts) are reproduced by sectioning the original, beginning at the upper left-hand corner and continuing from left to right in equal sections with small overlaps. Each original is also photographed in one exposure and is included in reduced form at the back of the book.

Photographs included in the original manuscript have been reproduced xerographically in this copy. Higher quality 6" x 9" black and white photographic prints are available for any photographs or illustrations appearing in this copy for an additional charge. Contact UMI directly to order.

U·M·I

University Microfilms International
A Bell & Howell Information Company
300 North Zeeb Road, Ann Arbor, MI 48106-1346 USA
313/761-4700 800/521-0600

Order Number 1339578

The dynamic response of a flexible three-link robot using strain gages, Lagrange polynomials, Fourier series, and the finite element analysis

Marceau, Robert Frank, M.S.

University of Nevada, Las Vegas, 1989

U·M·I
300 N. Zeeb Rd.
Ann Arbor, MI 48106

THE DYNAMIC RESPONSE OF A FLEXIBLE THREE–LINK ROBOT USING STRAIN GAGES, LAGRANGE POLYNOMIALS, FOURIER SERIES, AND THE FINITE ELEMENT ANALYSIS

by

Robert Frank Marceau

A Thesis Submitted in Partial Fulfillment
of the Requirements for the Degree of

Masters of Science in Civil Engineering
(Structural)

Department of Civil & Mechanical Engineering
University of Nevada, Las Vegas
June 1989

This Research was Supported by the U.S. Army Research Office
under Grant No.DAAL03–87–G–0004

The thesis of Mr. Robert Frank Marceau for the degree of Masters in Civil Engineering is approved.

Prof. Samaan G. Ladkany, Ph.D., Chairperson

Prof. James Cardle, Ph.D., Examining Committee Member

Prof. Mohamed B.Trabia Ph.D., Examining Committee Member

Prof. Yahia Baghzouz Ph.D., Graduate Faculty Representative

Prof. Ronald Smith, Ph.D., Graduate Dean

University of Nevada, Las Vegas
June, 1989

ABSTRACT

This thesis presents theoretical and experimental methods for determining the static and dynamic response, in three dimensional space, of a flexible three–link robotic manipulator. The Links are designed to deform elastically under static and dynamic loads. Lagrange polynomials are derived to determine the defected shape of the robotic links. All coefficients of the Lagrange polynomials are functions of the elastic strain at three specific locations on each link. The strain gages at these locations act as variable resisters when connected to Wheatstone bridge amplification circuitry. Strains are converted to voltage differentials and are read into a micro–computer through an A–to–D board system, where they are converted to digital strain values. Angular encoder sensors connected to each joint read the angular position of each joint. The angular readings along with the strain values are then read into a FORTRAN program which utilizes the Lagrange polynomials to determine the elastic deformations of each link in two orthogonal planes defined by the axes of the links, while the actions of twist along the axes are determined by rectangular rosettes. The deflected global position of the joints and the end effector are determined by three dimensional coordinate transformations. Expressions for the dynamic response of the end effector near a destination point, for a defined path of motion within the workspace, are found at any time by numerical integration, Fourier series expansion, and a damping function using a number of known vibration amplitudes over a predetermined time interval. Coefficients defining the damped response of the robot are determined experimentally. The dynamic response of the robotic manipulator is also studied using the finite element method. Given

the readings of the angular encoders, a FORTRAN code is presented that prepares complete source files for the robot. A finite element code uses the source files to determine the dynamic response of the robot at any position within its workspace.

ACKNOWLEDGEMENTS

The author would like to express his gratitude to Dr. Samaan G. Ladkany, for his effort as advisor and major professor on this research project. The author is also very thankful to the Army Research Office (ARO) for funding this research project, providing him with the opportunity to work in this area of research. The author would also like to specifically thank Dr. Richard Wyman for his help and encouragement along with Dr. William Culbreth, Dr. Mohamed Trabia, Dr. Doug Reynolds and the entire research team at the University of Nevada, Las Vegas, for their help and cooperation, and Elaine Smith for her help in proofreading.

The author is also grateful to have parents who throughout his life have continued to encourage and support his efforts in fulfilling his educational desires.

Robert Frank Marceau

NOTATIONS

Mathematical Symbols

$\{\ \}$	Matrix notation for a column vector.
$[\ ]$	Matrix notation for a row vector.
$\int$	Integral sign notation.
$\sum$	Summation sign notation.

Latin Symbols

A	Cross sectional area.
a_o	Fourier series coefficient.
a_n	Fourier series coefficient.
${}^{i}a_m$	Constant Lagrange polynomial coefficients (i = 2,3) (m = 1,2,3,...).
b_n	Fourier series coefficient.
${}^{i}b_m$	Constant Lagrange polynomial coefficients (i = 2,3) (m = 1,2,3,...).
C_m	Constants of Integration (m = 1,2,3,...)
c	Experiment No.1 beam thickness divided by 2.(0.125").
${}^{r}D_m$	Discrete global displacements at the end effector at time points (t_m) (r = 1,2,3,4,5,6) (m = 1,2,3...N)

${}^{r}\{D\}$	Global displacements in row matrix form at the end effector (r = 1,2,3,4,5,6).
${}^{r}\{\dot{D}\}$	Velocity row matrix (r = 1,2,3,4,5,6).
${}^{r}\{\ddot{D}\}$	Acceleration row matrix (r = 1,2,3,4,5,6).
${}^{i}c_{m}$	Constant Lagrange polynomial coefficients (i = 2,3) (m = 1,2,3,...).
${}^{i}d_{m}$	Constant Lagrange polynomial coefficients (i = 2,3) (m = 1,2,3,...).
$d\varphi$	Change in angle due to fluctuation in actuator ab.
$d\alpha$	Change in angle due to fluctuation in actuator de.
E	Young's Modulus of Elasticity (for steel E = 29,000,000 psi).
EECP	End effector center point.
F	Axial force.
f_{d}	Natural frequency of vibration in hertz.
${}^{i}f_{m}$	Constant Lagrange polynomial coefficients (i = 2,3) (m = 1,2,3,...).
G	Shear Modulus = $E/(2(1+\mu))$
${}^{i}g_{m}$	Constant Lagrange polynomial coefficients (i = 2,3) (m = 1,2,3,...).
h	Out–to–out dimension of cross section of link 2 & 3 (h = 1.5 inch).
I	Moment of inertia.
i	An integer equal to 2 for *link 2* and 3 for *link 3.*
J	Polar moment of inertia.
j	An integer equal to 1,2,or 3.
K	An integer which defines the number of Fourier terms.
k	An integer equal to 1,2,3,or 4.
ℓ	An integer which defines the correct strain gage combination from the positions on each link.
L	Length of a cantilever beam.

L_j	Length in inches from P load to strain gage set j.
L_1	Length of the link No. 1 in inches.
L_2	Length of the link No. 2 in inches.
L_3	Length of the link No. 3 in inches.
M	Bending moment.
m	An integer equal to 1,2,3,...∞)
m_s	Mass per unit length in slugs/in^2.
N	Even number equal to the period T divided by the time increment.
n	An integer which depicts the number of Fourier series terms.
^iN_j	Shape function terms (i = 2,3) (j = 1,2,3).
$^i[N]$	Row matrix of shape functions (i = 2,3).
P	Consentrated load.
r	An integer equal to 1,2,3,4,5,6.
RBME	Rigid body motion effects.
s	An integer which refers to joints 2,and 3,and EECP 4.
T	Torque.
T	Period of vibration.
T_d	Period of damped vibration.
t_m	Time data points evenly distributed over the period T_d.
^iu	Axial displacements in the direction of the local ^ix axis (i = 2,3).
^iu_o	Axial displacements at $^ix = 0$ in the direction of the local ^ix axis (i = 2,3).
U	Axial displacement in the direction of the global X–axis.
^iv	Flexural displacements in the direction of the local ^iy axis (i = 2,3).
^iv_o	Flexural displacements at $^ix = 0$ in the direction of the local ^iy axis (i = 2,3).

V	Flexural displacement in the direction of the global Y–axis.
^{i}w	Flexural displacement in the direction of the local ^{i}z axis (i = 2,3).
$^{i}w_{o}$	Flexural displacement at $^{i}x = 0$ in the direction of the local ^{i}z axis (i = 2,3).
W	Flexural displacement in the direction of the global Z–axis.
X	Indicates x coordinate in global coordinate system.
^{i}x	Indicates x coordinate in local i coordinate system (i = 2,3).
Y	Indicates x coordinate in global coordinate system.
y_{m}	The amplitudes of vibration corresponding to the time points t_{m}.
^{i}y	Indicates y coordinate in local i coordinate system (i = 2,3).
Z	Indicates x coordinate in global coordinate system.
^{i}z	Indicates z coordinate in local i coordinate system (i = 2,3).

Greek Symbols

α	Angle shown (figure 3.5).
β	Coefficient used to approximate the damping effect.
γ	Shearing strain.
$^{i}\gamma_{xz}$	Torsional shearing strain in local xz plane (i = 2,3).
Δ	General bending displacement for a cantilever beam.
Δt	Time increment between data readings.
δ	Logarithmic decrement.
$^{i}\bar{\epsilon}_{x}$	Axial strains for link i in the local ^{i}x direction (i = 2,3).
$^{i}\{\epsilon\}$	Column matrix of strain values (i = 2,3).
$^{i}\epsilon_{j}$	Strain values (i = 2,3) (j = 1,2,3).
ϵ_{xmax}	Maximum axial strain at extreme fiber of the cross section.

$^{i}\epsilon_{jk}$	Strain gage reading strain gage sets, where one set is made up of four single element strain gages. (i = 2,3) (j = 1,2,3) (k = 1,2,3,4).
ζ	Damping ratio.
$\otimes_x$	Angle of rotation about the global X–axis.
$\otimes_y$	Angle of rotation about the global Y–axis.
$\otimes_z$	Angle of rotation about the global Z–axis.
$^{i}\theta_j$	Axial strain from rosette element at angle j (i = 2,3) (j = 1,2,3).
$^{i}\theta_x$	angle of rotation about the local ^{i}x–axis (i = 2,3).
$^{i}\theta_y$	angle of rotation about the local ^{i}y–axis (i = 2,3).
$^{i}\theta_z$	Angle of rotation about the local ^{i}z–axis (i = 2,3).
λ	Angle at joint number 2 set at 126.87 degrees (figure 3.0).
μ	Poisson's ratio (for steel $\approx$ 0.30).
π	Archimedes' number 3.14159265.....
ρ	Normal distance from the center the tube to the midpoint of the face.
σ	bending stress.
σ_{max}	Maximum bending stress at extreme fiber of the cross section.
σ_j	maximum bending stress in beam at strain gage set j (j = 1,2,3).
τ	Shearing stress.
φ	Angle shown (figure 3.5).
Ψ	Is an integer equal to the number of amplitudes minus one.
ϕ_j	Angle (j = 1, 2, 3) shown (figure 3.1).
$^{i}\psi$	An arbitrary angle measured from the ^{i}x axis (figure 3.10).
$^{i}\psi_j$	The corresponding angle from the ^{i}x axis for link i for each of three gages in the three element rectangular rosettes (j = 1,2,3).
$^{i}\psi_1$	Angle 1 = 0^{o}.
$^{i}\psi_2$	Angle 2 = 45^{o}.

$^{i}\psi_3$ Angle 3 = 90^{o}.

ω_o The natural frequency of vibration.

ω_d The frequency of damped vibration.

Graphic Symbols


Fixed support which resists all forces and moments.


Pinned connection which resists all forces but not moments.


Nodal point connection which resists all forces and moments.


Center line.


Dimensional limits.


Angle designation.

LIST OF FIGURES

TABLE OF CONTENTS

CHAPTER ONE

Introduction

The objective of the *Army Research Office* (ARO) robotics project is to design and control a relatively lightweight elastic three–link robot (figure 1.1) capable of supporting and moving along defined paths of motion an object load at least equal to its own weight. This study is supported at the *University of Nevada, Las Vegas* (UNLV) by the U.S.ARO under grant No.DAAL03–87–G–0004. A static and quasi dynamic mathematical model of the robot manipulator was derived [Ladkany, S.G. and Bonnoura, T.M., 1989] using the theory of structures and the fourth order differential equations of slender beams. The model gives the three displacements and the three rotations of the end effector due to static and quasi dynamic load vectors and moment vectors applied to the end effector and the centers of gravities of the links. The model was used in the design of the steel manipulator, the study of which is the subject of this thesis. It is believed that the results presented in this thesis will expand existing robot kinematics and dynamic theory to include the effects of elasticity and active damping.

The definition of the term *robot* as used in this thesis is to be that as defined by the Robotics International Division of the Society of Manufacturing Engineers (RI/SME) as "a reprogrammable multi–functional manipulator designed to move material, parts, tools, or specialized devices through variable programmed motions for the performance of a variety of tasks" [Koren 1985]. The term *manipulator* is defined as the mechanical unit consisting of a series of mechanical links and joints capable of producing various movements in different directions within the

three–dimensional workspace [Koren 1985]. The robot studied here is also equipped at the end with a work device called an *end effector*. The end effector is manipulated by a servo motor drive connected at joint 3 (figure 1.1).

The reason for designing a relatively lightweight elastic robot is to increase the load–to–weight ratio, where the *load* is the weight of the object transported and the *weight* is the weight of the manipulator. Most industrial robots are constructed of very stiff link members which move by heavy servo motor drive devices located at the joints. By using very stiff link members, the amplitudes of vibration are greatly reduced, therefore, robots designed in this manner do not have major vibrational problems. However, the joint servo motor devices are limited in the object loads they can manipulate, and the load–to–weight ratio is usually much less than one. In order to increase the load–to–weight ratio hydraulic actuators, which have greater load resistance capabilities than servo motor joint drive devices, are used in this research study to move the link members (figure 3.1). A major disadvantage in designing an elastic lightweight manipulator is the vibrational problems associated with the flexibility of the link members. In this research model link 2 & 3 are elastic and, therefore, subject to various modes of vibration due to imposed loads. Because of the possible large amplitudes of vibration which may occur, active damping methods and/or path motion studies are necessary for proper control of the manipulator. To solve the vibrational problems, the use of active damping methods in conjunction with path motion studies are under consideration in the design of the controller.

The control technique concentrated on in this thesis will be that of positioning strain gages at certain defined locations on each link in conjunction with angular encoder sensors at each joint to ultimately define kinematically the position of the end effector in space and time. The strain gages are connected to Wheatstone

bridge amplification circuitry, which are connected in turn through an A–D board to micro–computers. The strain gage data and angular encoder sensor data are read into a FORTRAN program code [Appendix–B] utilizing Lagrange polynomials and shape functions developed to convert the strain gage readings and the angular encoder sensor readings into joint displacements. The axial, flexural, and rotational Lagrange polynomial displacement equations describe the defected shape of each link in its local coordinate system as a function of the strain gage readings, their location x along the link, and time t. From the rotational displacement at a rigid joint, the rigid body rotation of the connected link is determined. Torsional displacements are determined from multiple strain gage elements known as rosettes. The rosettes are located on each link of the robotic model, and measure torsional shearing strain in the links caused by an external torque in the direction of the local axis of the link. A slight twist or torsional strain in one link will result in a rotational displacement of the joint connecting the two links. This, in turn, results in a rigid body out of plane rotation of the next link affecting the final location of the end effector. Once the local displacements are known, they are transformed into global displacements to be used by the controller.

A Fourier series representation using numerical methods is developed to approximate the response of the end effector for defined positions within the workspace. The Fourier series representation utilizes the displacements at the end effector calculated in the FORTRAN program code at predetermined time intervals. These displacements represent amplitudes of vibration of the end effector as a function of time. The dynamic response of the robotic mechanism is also studied by a finite element analysis. The finite element program GIFTS is used to determine the theoretical response as a function of the configuration of the robot within the workspace. The natural frequency for both the manipulator with a

lumped mass at the end effector and without are under study.

The control of the robotic mechanism depends upon knowledge of the position of the end effector at any instant in time within the defined workspace. The robotic mechanism moves along a variety of paths of motion and is subject to a variety of forces. Due to the flexibility of the robotic mechanism, any variation in the motion of the arm will result in a dynamic vibrational response. This thesis is mainly interested in the response of the end effector at or near the *end* of the path of motion. This vibrational response can be approximated experimentally with the use of a Fourier series representation as noted above. From the determination of the approximate response of the end effector for different robotic arm configurations and different paths of motion, more advanced methods of control can be developed.

CHAPTER TWO

Literature survey and discussion of Robot Applications

2.1 Discussion

The term *robot* comes from the Czech dialect and originally meant "forced labor" [Koren, 1985]. As defined by Robotics International Division of the Society of Manufacturing Engineers (RI/SME) in chapter one, the term *robot* covers a variety of possible manipulator types. At present, robots which utilize computers as an integral part of their control, and can be programmed to do a variety of difficult tasks accurately and quickly, are popular in today's very competitive industrial arena. The majority of tasks currently being performed by robots in industrial applications are in the areas of spot welding, arc welding, product assembly, material handling, loading and unloading of machines, inspection, laser–beam cutting, spray painting, die–casting and forging operations, and drilling and deburring of metal parts [Koren, 1985]. Current literature dealing with arc welding control techniques on scheduling are discussed in a paper by Tonkay, G.L. and Knott, K. (1989). The advances in automated robotic control systems in industrial applications are actually a new phase in the industrial revolution which began in Europe two centuries ago. In addition to industrial uses, non–industrial uses are becoming increasingly more interesting to the general public. In a paper by Osborn, J.F. (1989), the applications of robotics in hazardous waste management is discussed with emphasis on using robots in place of humans to reduce human exposure to hazardous materials. Robots are also under development for exploration of other

planets [Bares, J.E. and Whittaker, W.L., 1989]. Some non–industrial applications of robots range from the shearing of sheep in Australia, to the operation of a robotic arm aboard the space shuttle Colombia, to decorating chocolates at a local confectionary shop to mention a few. The boundary of possible uses of robots appears to be limited only by the human imagination.

The majority of robots used in industrial applications are designed with stiff link members in order to eliminate the vibrational problems associated with flexible manipulators. The stiffness requirement leads to heavier and bulkier manipulators. Depending upon the task, this may or may not present a serious problem. However, the trend in future robot design is that of lightweight, flexible robots which are easier to transport, take up less space, and require less energy to operate.

2.2 Literature Survey

The end–effector deviation from a desired path of motion presents a general problem in the design and use of light–weight robot manipulators with flexible links. Implementing a measure of the position error requires the development of an accurate dynamic model. Developing a dynamic model for a three–link hydraulically activated robot manipulator is under study at the University of Nevada, Las Vegas. *Lagrangian mechanics* principles with numerical solutions of these pertinent equations using the *assumed modes method* are being used to develop the dynamic model through which the equations of motion can be obtained [Trabia, M.B. and Yim, W., 1988]. The structural design of the three–link hydraulically activated arm under static and quasi dynamic loading was developed by Ladkany and Bannoura (1989), while computer simulation of the three–link robotic arm was developed by Culbreth and Krueger (1989). Control algorithms are under development [Nathan,

J., and Singh, N.] to remove unwanted oscillations of the hydraulically activated three–link robot manipulator segments.

An experimental four foot long flexible single link direct drive manipulator model was studied by Hastings & Book (1986) utilizing a separable formulation of assumed modes to represent the transverse bending displacements. The kinetic and potential energies were determined using Lagrangian dynamics. Both a clamped and pinned mass payload type attached to the free end of the flexible arm were studied. The input into the system was that of a torque applied by the DC motor at the base joint. Strain gages were used in the experiment to measure the frequencies. Data acquisition was accomplished through signal conditioning with an A/D converter. A 16 bit computer system was used to implement the control algorithms and a D/A conversion for the torque signal output. The flexible beam used in the experimental model was constructed of Aluminum 6061–t6 and was rectangular in form. This experiment presented a linear model for use in controlling a flexible manipulator, which agreed favorably with the measured response for a selection of a clamped–mass and assumed modes.

One study underway for damping out vibrations associated with light–weight robotic arms, used in high–speed operations, is the vibratory effects produced by varying the length of one arm with time [Wang, P.K.C., and Wei, Jin–Duo]. This paper focused on the rectilinear motion of the arm and found that extending the length of the arm produced a destabilizing effect while contracting the length of the arm produced a stabilizing effect. The laboratory model was made up of a long flexible thin walled slender prismatic beam set within and allowed to move through a prismatic joint attached to a base.

A computational scheme was developed by Tang, S.C., and Wang, C., (1987) to predict the actual positions of the robot end effector under the influence of link

deformations for static loads. Classical beam theory equations were used to determine the displacements for a hypothetical two–link robot. The results were verified by analytical solutions with less than 1% variation.

A method for dynamic modeling of manipulators with flexible links was presented in a paper by Geradin, M., Robert, G., Bernardin, C., (1984). The finite element concept was used to describe the structural behavior of individual links and was based on the assumption that the linear elastic deformation of the links occurs around the nonlinear rigid body motion of the kinematic chains.

CHAPTER THREE

Robot Manipulator Displacements

3.1 Displacement Equations Using Strain Gages and Lagrange Polynomials

The deflected and rotated position of the end effector in the global coordinate system required for ultimate control of the robot will be determined from the local deflections and rotations of links 2 & 3 and all associated rigid body motions of the manipulator arm (figures 3.5, 3.6, 3.7, 3.8, 3.9, 3.10 & 3.11). Strain gages are used to measure experimentally the maximum axial strains on all four orthogonal surfaces at three specific locations in the direction of the local ^{i}x–axes of link 2 and link 3. It is to be noted that strains measured along the faces of links 2 and 3, due to flexural bending alone, are of opposite signs, while the strains due to the axial deformations of the links are of the same signs. By using the Lagrange interpolation formula, a shape function is developed from these strain measurements which directly describes the strain $^{i}\bar{\epsilon}_{x}$ at any point ^{i}x along the local ^{i}x–axis of each link. The bar $\bar{}$ notation above the strain symbol ϵ, defines a typical individual strain value at a face of a particular link member. The superscript i in the notation throughout this thesis defines the link number as shown below:

$$i = 2 \text{ for link 2 and 3 for link 3.} \qquad (3.1)$$

Note: *All strain values in this thesis are considered positive if tensile in nature and negative if compressive in nature.*

The intention of this chapter is first to develop Lagrange polynomials to describe the axial strain ${}^{i}\bar{\epsilon}_{x}$ and then to use these polynomials to develop displacement equations to describe the deflected shape of link 2 and link 3 in their respective local coordinate systems. From these displacement equations, the displacements at the jointed ends of link 2 and link 3 are determined. The displacements of interest to be determined in this thesis are: three translational ${}^{i}u$, ${}^{i}v$ and ${}^{i}w$, three rotational ${}^{i}\theta_{x}$, ${}^{i}\theta_{y}$ and ${}^{i}\theta_{z}$ and all rigid body motion effects associated with these displacements. The three translational displacements are in the direction of the ${}^{i}x$, ${}^{i}y$ and ${}^{i}z$ local axes respectively (figure 3.5 & 3.6). The three rotational displacements are defined by the subscripts x, y, and z which indicate the local axes about which the rotational displacements occur (figure 3.5 & 3.6). After all local displacements for links 2 and 3 are determined, the position of the end effector in global coordinates X,Y, and Z are found by coordinate transformation.

It is to be noted that the strain and displacement polynomials developed here are a function of ${}^{i}x$ and time t, where ${}^{i}x$ is the dimension along the local ${}^{i}x$–axis from the clamped end of the link, and t is a time parameter relative to a set initial time. *In order to simplify all further notation, it is to be understood from this point on in this thesis that all equations developed are a function of x and t.*

The structural design of the robotic links [Ladkany/Bannoura, 1988] limited the maximum allowable stresses calculated, for the worst loading condition, to a value below the yield stress of the material. Therefore, all stress–strain beam equations which apply within the elastic range of the material will be valid here. The stress–strain beam equations developed in this chapter are based upon linearized theory and the following assumptions:

$$\epsilon = \frac{\sigma}{E}, \ (\textit{Hooke's law}) \qquad (3.2)$$

$$\gamma = \frac{\tau}{G}, \text{ (\textit{Hooke's law for shearing strain})} \qquad (3.3)$$

$$\epsilon = \frac{F}{AE}, \text{ (axial strain)} \qquad (3.4)$$

$$\epsilon_{max} = \frac{Mc}{EI}, \text{ (bending strain)} \qquad (3.5)$$

$$\gamma_{max} = \frac{M_x c}{JG}, \text{ (torsional strain)} \qquad (3.6)$$

where:

ϵ Indicates axial strain.

ϵ_{max} Indicates maximum strain at the extreme fiber.

σ Indicates axial stress.

γ Indicates shear strain.

γ_{max} Indicates maximum shearing strain at the extreme fiber.

τ Indicates shear stress.

A Cross–sectional Area.

c Distance from the neutral axis to the extreme fiber of the beam.

E Defines the Modulus of Elasticity.

F Axial force.

G Defines the Shearing Modulus of Elasticity.

I Defines the Moment of Inertia of the beam cross section.

J Defines the polar Moment of Inertia.

M Defines the moment value about the y and z axes at the point under consideration.

M_x Torsional Moment about local x–axis.

Link 2 and link 3 are connected to the manipulator via rigid joints; they deflect under loading in the orthogonal planes as cantilever beams clamped at one end in their respective local coordinate systems. As shown in (figure 1.1) link 2 is considered clamped at joint B and link 3 is considered clamped at joint 2 ,however, link 2 and 3 are hinged together in the ${}^{i}x{}^{i}y$ plane and rigidly attached together in the ${}^{i}x{}^{i}z$ plane. The local ${}^{i}x$ axis has an origin at joint B for link 2 and an origin at joint 2 for link 3. Based on this assumption the local boundary conditions at ${}^{i}x = 0$ for link 2 and link 3 are noted below:

$$@\ {}^{i}x = 0 \tag{3.7}$$

$$\begin{aligned} {}^{i}u_o &= 0 \\ {}^{i}v_o &= 0 \\ {}^{i}w_o &= 0 \\ {}^{i}\theta_{x_o} &= 0 \\ {}^{i}\theta_{y_o} &= 0 \\ {}^{i}\theta_{z_o} &= 0 \end{aligned}$$

The proper interfacing of the pertinent strain gage sets is imperative for calculation of the correct displacements at any point ${}^{i}x$ along link 2 and link 3. Therefore, the first part of this section is devoted to clarification of the locations and orientations of the strain gages employed. On each link (link 2 & 3) there are four sets of strain gages mounted (figure 3.2 and 3.3a & b). The first three sets on each link are made up of four single element gages, and the fourth set is made up of two three element rosette strain gages.

The first three sets have one gage mounted on each face of the steel tube at the same location ${}^{i}\{x_j\}$ from the clamped end. The general notation used in this thesis to define the first three strain gage sets is shown below:

$$ {}^{i}_{\ell}\{\epsilon_j\} = {}^{i}\begin{Bmatrix} \epsilon_1 \\ \epsilon_2 \\ \epsilon_3 \end{Bmatrix}_{\ell} \qquad (3.8) $$

where:

i Defines the link number (i = 2 or 3).

j Refers to the strain gage sets 1, 2, and 3 (figure 3.2 and 3.3a), where set 1 is at location ${}^{i}x_1$, set 2 is at location ${}^{i}x_2$, and set three is at location ${}^{i}x_3$.

ℓ Is an integer which refers to the correct strain gage combination from the positions noted (figure 3.3b).

Note:

$\ell = 1$ Combined strain gages readings from positions 1, 2, 3, and 4.

$\ell = 2$ Combined strain gage readings from positions 1 and 3.

$\ell = 3$ Combined strain gage readings from positions 2 and 4.

The fourth set on each link has one rosette on the positive ${}^{i}y$–face and negative ${}^{i}y$–face of link 2 and 3 at an arbitrary location ${}^{i}x_4$ (figure 3.2 and 3.2a). The exact location of the fourth set is not required since the torsion strain is constant throughout the length of each link. The general notation used in this thesis to define the fourth strain gage set for link 2 and 3 is shown below:

$$ {}^{i}\{\epsilon_{\psi_{\S}}\} = {}^{i}\begin{Bmatrix} \epsilon_{\psi_1} \\ \epsilon_{\psi_2} \\ \epsilon_{\psi_3} \end{Bmatrix} \tag{3.9} $$

Where:

ψ Is an angle in the plane of the rosette (figure 3.4).

§ Refers to the strain gage combinations required for temperature compensation to be defined more clearly in section 3.1.4.

A *general* polynomial which describes the axial strain along the local x–axis is:

$$ {}^{i}\bar{\epsilon}(x,t) \equiv {}^{i}\bar{\epsilon}_x = a_1 + a_2{}^{i}x + a_3{}^{i}x^2 + \ldots + a_n{}^{i}x^{n-1} \tag{3.10} $$

In the analysis, *Lagrange* polynomials will be used to describe the deformed shape of the manipulator links 2 and 3 using the strain gages. If these polynomials are to describe the static deformed shape of the links *exactly*, the polynomials must have an order at least equal to the highest order in ${}^{i}x$ required for the theoretical deflection equations associated with the desired loading condition. It is assumed that the highest degree loading condition the link members may experience is that of a uniform load q (such as their own weight per linear ${}^{i}x$ dimension), which leads to a fourth order polynomial. In general, from beam theory for a uniform load condition, the displacement equation which results in the highest order in ${}^{i}x$ is the bending displacement equation, which is termed Δ. The theoretical bending displacement equation from beam theory for a cantilever beam, where x is measured from the clamped end, is noted below [AISC, 1980]:

$$\Delta = \frac{q\,(\,4\,{}^{i}x L^{3} - 6\,{}^{i}x^{2} L^{2} + 4\,{}^{i}x^{3} L - {}^{i}x^{4}\,)}{24\,E\,I} \qquad (3.11)$$

where:

L Defines the length of a typical cantilever beam.

q Defines a uniform distributed loading.

From the equation above it can be seen that a *fourth* order Lagrange polynomial in ${}^{i}x$ is required to *exactly* describe the static bending deformation of link No.2 and link No.3 for this type of loading condition. Beam curvature is defined as the second derivative of the displacement equation ${}^{i}\Delta$ with respect to ${}^{i}x$. The beam curvature is related to the maximum axial strain ${}^{i}\epsilon_{xmax}$ along the local ${}^{i}x$–axis at the extreme fiber of the link member as shown below:

$$\frac{d^{2\,i}\Delta}{d\,{}^{i}x^{2}} = \frac{M}{E\,I} = \frac{2\,\sigma_{max}}{E\,h} = \frac{2\,\epsilon_{xmax}}{h} \qquad (3.12)$$

where:

h Defines the out–to–out dimension of the link member cross section.

σ_{max} Defines the maximum stress along the local x–axis at the extreme fiber of the steel tube.

In order to determine the *exact* static displacement equation ${}^{i}\Delta$, a Lagrange polynomial which describes the strain must be at least second order in ${}^{i}x$ (n=3). By integrating twice, the second order strain polynomial in ${}^{i}x$ becomes a fourth order polynomial in ${}^{i}x$ and thus defines the displacement equation ${}^{i}\Delta$. The Lagrange polynomial required to develop all of the displacement equations desired here is:

$$ {}^{i}\bar{\epsilon}_x = {}^{i}a_1 + {}^{i}a_2\,{}^{i}x + {}^{i}a_3\,{}^{i}x^2 \qquad (3.13) $$

To derive a second order polynomial in ${}^{i}x$, that defines the strain as a shape function, a *Lagrange* polynomial is used in terms of the strain values. Lagrange's interpolation formula [Cook, 1981] used to define the axial strain ${}^{i}\bar{\epsilon}_x$ as a polynomial in terms of a shape function ${}^{i}\lfloor N \rfloor$ is noted below:

$$ {}^{i}\bar{\epsilon}_x = {}^{i}\lfloor N \rfloor\, {}^{i}_{\ell}\{\epsilon_j\} \qquad (3.14) $$

where:

The strain values ${}^{i}_{\ell}\{\epsilon_j\}$ as defined above in equation (3.8) are strain measurements determined experimentally by placing three single element strain gages orientated along the local ${}^{i}x$–axis of each link (figure 3.2 and 3.3a) and located at ${}^{i}x_1$, ${}^{i}x_2$ and ${}^{i}x_3$ respectively. The values ${}^{i}x_1$, ${}^{i}x_2$ and ${}^{i}x_3$ are set dimensions, measured from the clamped end of each link (figure 3.2 and 3.3a). By using the *Lagrange* polynomial (3.14) in conjunction with the equations defining the small deflection theory of beams, other polynomials are derived which describe the axial, rotational, torsional and flexural displacements of each link. The shape function ${}^{i}\lfloor N \rfloor = {}^{i}\lfloor N_1\ N_2\ N_3 \rfloor$ used in the Lagrange polynomials are formulated below:

$$ {}^{i}N_1 = \frac{({}^{i}x - {}^{i}x_2)\,({}^{i}x - {}^{i}x_3)}{({}^{i}x_1 - {}^{i}x_2)\,({}^{i}x_1 - {}^{i}x_3)} \qquad (3.15) $$

$$ {}^{i}N_2 = \frac{({}^{i}x - {}^{i}x_1)\,({}^{i}x - {}^{i}x_3)}{({}^{i}x_2 - {}^{i}x_1)\,({}^{i}x_2 - {}^{i}x_3)} $$

$$ {}^{i}N_3 = \frac{({}^{i}x - {}^{i}x_1)({}^{i}x - {}^{i}x_2)}{({}^{i}x_3 - {}^{i}x_1)({}^{i}x_3 - {}^{i}x_2)} $$

3.1.1 Axial Displacements In Local ${}^{i}x$ Direction

The required combination of strain gage readings (ℓ=1), for the determination of the axial displacement ${}^{i}u$ are shown below:

$$ {}^{i}_{1}\{\epsilon_j\} = {}^{i}_{1}\left[\frac{\bar{\epsilon}_1 + \bar{\epsilon}_2 + \bar{\epsilon}_3 + \bar{\epsilon}_4}{4}\right]_j \qquad (3.16) $$

$$ (i = 2, 3) $$

$$ (j = 1, 2, 3) $$

In this equation, the individual single element strain gage values which make up the strain gage set at location ${}^{i}\{x_j\}$ are further described as:

- ${}^{i}\bar{\epsilon}_1$ [positive y face position 1 (figure 3.3b)]
- ${}^{i}\bar{\epsilon}_2$ [positive z face position 2 (figure 3.3b)]
- ${}^{i}\bar{\epsilon}_3$ [negative y face position 3 (figure 3.3b)]
- ${}^{i}\bar{\epsilon}_4$ [negative z face position 4 (figure 3.3b)]

From equation (3.15) the axial displacement ${}^{i}u$, determined from the strain measurements ${}^{i}_{1}\{\epsilon_j\}$, is obtained by integration:

$$ {}^{i}\bar{\epsilon}_x = \frac{d\,{}^{i}u}{d\,{}^{i}x} = {}^{i}\lfloor N \rfloor \, {}^{i}_{1}\{\epsilon_j\} \qquad (3.17) $$

Therefore:

$$ {}^{i}u = {}^{i}_{1}\{\epsilon_j\} \int_x {}^{i}\lfloor N \rfloor \, dx = {}^{i}b_1 + {}^{i}b_2\,{}^{i}x + {}^{i}b_3\,{}^{i}x^2 + {}^{i}b_4\,{}^{i}x^3 $$

or

$$ {}^{i}u = \left[\frac{{}^{i}x^3 - \frac{{}^{i}x^2}{2}({}^{i}x_2 + {}^{i}x_3) + {}^{i}x_2\,{}^{i}x_3\,{}^{i}x}{({}^{i}x_1 - {}^{i}x_2)({}^{i}x_1 - {}^{i}x_3)} \right] {}^{i}_{1}\epsilon_1 \qquad (3.18) $$

$$ + \left[\frac{{}^{i}x^3 - \frac{{}^{i}x^2}{2}({}^{i}x_1 + {}^{i}x_3) + {}^{i}x_1\,{}^{i}x_3\,{}^{i}x}{({}^{i}x_2 - {}^{i}x_1)({}^{i}x_2 - {}^{i}x_3)} \right] {}^{i}_{1}\epsilon_2 $$

$$ + \left[\frac{{}^{i}x^3 - \frac{{}^{i}x^2}{2}({}^{i}x_1 + {}^{i}x_2) + {}^{i}x_1\,{}^{i}x_2\,{}^{i}x}{({}^{i}x_3 - {}^{i}x_1)({}^{i}x_3 - {}^{i}x_2)} \right] {}^{i}_{1}\epsilon_3 + C_1 $$

From the boundary conditions at ${}^{i}x = 0$, the constant of integration ($C_1 = 0$) is obtained.

3.1.2 Flexural Displacements In Local ${}^{i}y$ Direction

The required combination of strain gage readings (ℓ=2) for the determination of the flexural ${}^{i}v$ displacements is shown below:

$$ {}^{i}_{2}\{\epsilon_j\} = {}^{i}_{2}\left[\frac{\bar{\epsilon}_3 - \bar{\epsilon}_1}{2}\right]_j \qquad (3.19) $$

$$ (i = 2,3) $$

$$ (j = 1,2,3) $$

where:

${}^{i}\bar{\epsilon}_1$ [positive y face position 1 (figure 3.3b)]

${}^{i}\bar{\epsilon}_3$ [negative y face position 3 (figure 3.3b)]

The bending strain varies with the bending moment which varies along the length of the link, therefore, the bending strain is determined at each ${}^{i}\{x_j\}$ from the strain gages. From equation (3.15) the flexural displacements ${}^{i}v$ are obtained by integration:

$$ \frac{d^2\ {}^{i}v}{d\ {}^{i}x^2} = \frac{2}{h}\ {}^{i}\lfloor N \rfloor\ {}^{i}_{2}\{\epsilon_j\} \qquad (3.20) $$

where:

$$ {}^{i}v = \frac{2}{h}\ {}^{i}_{2}\{\epsilon_j\} \int_x \int_x {}^{i}\lfloor N \rfloor\, dx\, dx = {}^{i}c_1 + {}^{i}c_2\,{}^{i}x + {}^{i}c_3\,{}^{i}x^2 + {}^{i}c_4\,{}^{i}x^3 + {}^{i}c_5\,{}^{i}x^4 $$

or

$$ {}^{i}v = \frac{2}{h}\left[\frac{\frac{{}^{i}x^4}{12} - \frac{{}^{i}x^3}{6}({}^{i}x_2 + {}^{i}x_3) + {}^{i}x_2\,{}^{i}x_3\,\frac{{}^{i}x^2}{2}}{({}^{i}x_1 - {}^{i}x_2)({}^{i}x_1 - {}^{i}x_3)}\right] {}^{i}_{2}\epsilon_1 $$

$$+\left[\frac{{}^{i}x^{4}/12 - {}^{i}x^{3}/6\,({}^{i}x_1 + {}^{i}x_3) + {}^{i}x_1\,{}^{i}x_3\,{}^{i}x^{2}/2}{({}^{i}x_2 - {}^{i}x_1)({}^{i}x_2 - {}^{i}x_3)}\right]{}^{i}_{2}\epsilon_2$$

$$+\left[\frac{{}^{i}x^{4}/12 - {}^{i}x^{3}/6\,({}^{i}x_1 + {}^{i}x_2) + {}^{i}x_1\,{}^{i}x_2\,{}^{i}x^{2}/2}{({}^{i}x_3 - {}^{i}x_1)({}^{i}x_3 - {}^{i}x_2)}\right]{}^{i}_{2}\epsilon_3\Bigg]$$

$$+ C_3\,{}^{i}x + C_4 \qquad (3.21)$$

From the boundary conditions at x = 0, the constants of integration ($C_3 = C_4 = 0$) are obtained.

It should be again noted that the fourth order polynomial derived above will *exactly* describe the static deflected shape of each robotic link with applied concentrated loads and reaction couples as well as uniformly distributed loadings.

3.1.3 Flexural Displacements In Local ${}^{i}z$ Direction

The required combination of strain gage readings (ℓ=3), for the determination of the bending ${}^{i}w$ displacement, is shown below:

$${}^{i}_{3}\{\epsilon_j\} = {}^{i}_{3}\left[\frac{\bar{\epsilon}_4 - \bar{\epsilon}_2}{2}\right]_j \qquad (3.22)$$

$$(i = 2, 3)$$

$$(j = 1, 2, 3)$$

where:

$^{i}\bar{\epsilon}_2$ [positive z face position 2 (figure 3.3b)]

$^{i}\bar{\epsilon}_4$ [negative z face position 4 (figure 3.3b)]

The bending strain varies with the bending moment, which varies along the link therefore, the bending strain is determined at each $^{i}\{x_j\}$ from the strain gages. From equation (3.12) the flexural displacements ^{i}w are obtained by integration:

$$\frac{d^2\ {}^{i}w}{d\ {}^{i}x^2} = \frac{2}{h}\ {}^{i}\lfloor N \rfloor\ {}^{i}_{3}\{\epsilon_j\} \tag{3.23}$$

where:

$$^{i}w = \frac{2}{h}\ {}^{i}_{3}\{\epsilon_j\} \int_x \int_x {}^{i}\lfloor N \rfloor\, dx\, dx = {}^{i}d_1 + {}^{i}d_2\,{}^{i}x + {}^{i}d_3\,{}^{i}x^2 + {}^{i}d_4\,{}^{i}x^3 + {}^{i}d_5\,{}^{i}x^4$$

or

$$^{i}w = \frac{2}{h}\left[\left[\frac{\frac{{}^{i}x^4}{12} - \frac{{}^{i}x^3}{6}({}^{i}x_2 + {}^{i}x_3) + {}^{i}x_2\,{}^{i}x_3\,\frac{{}^{i}x^2}{2}}{({}^{i}x_1 - {}^{i}x_2)({}^{i}x_1 - {}^{i}x_3)}\right]\ {}^{i}_{3}\epsilon_1\right.$$

$$+\left[\frac{\frac{{}^{i}x^4}{12} - \frac{{}^{i}x^3}{6}({}^{i}x_1 + {}^{i}x_3) + {}^{i}x_1\,{}^{i}x_3\,\frac{{}^{i}x^2}{2}}{({}^{i}x_2 - {}^{i}x_1)({}^{i}x_2 - {}^{i}x_3)}\right]\ {}^{i}_{3}\epsilon_2$$

$$\left.+\left[\frac{\frac{{}^{i}x^4}{12} - \frac{{}^{i}x^3}{6}({}^{i}x_1 + {}^{i}x_2) + {}^{i}x_1\,{}^{i}x_2\,\frac{{}^{i}x^2}{2}}{({}^{i}x_3 - {}^{i}x_1)({}^{i}x_3 - {}^{i}x_2)}\right]\ {}^{i}_{3}\epsilon_3\right]$$

$$+ C_5 {}^{i}x + C_6 \tag{3.24}$$

From the boundary conditions at x = 0, the constants of integration ($C_5 = C_6 = 0$) are obtained.

It should be again noted that the fourth order polynomial derived above will *exactly* describe the static deflected shape of each robotic link with applied concentrated loads and reaction couples as well as uniformly distributed loadings.

3.1.4 Torsional Rotational Displacements In Local ${}^{i}x$ Direction

A torque applied to a link will induce a shearing strain in that link. The links, made of structural steel tubing, are considered thin walled tubes. For thin walled tubes of constant thickness, the shearing strain due to applied concentrated torques is constant for the full length of each link. To determine the shearing strain, two rosette strain gages are mounted, one on the positive y–face and one on the negative y–face of each link at location ${}^{i}x_4$ (figure 3.2 & 3.3a). It should be noted that mounting rosettes on the positive and negative z–faces would also give the same results. Each rosette is a cluster of three single element strain gages oriented in the local ${}^{i}x{}^{i}z$ plane at angles ${}^{i}\psi_1, {}^{i}\psi_2$, and ${}^{i}\psi_3$ (figure 3.4). Opposite face single element strain gages in each rosette are oriented in the same directions. Two rosettes per link i are necessary to temperature compensate and properly determine the torsional shearing strain. The strain at *any* arbitrary angle in two dimensional space on the surface of the steel tube is defined in terms of the local cartesian strains as shown below [Popov, 1952]:

$${}^{i}\epsilon_{\psi} = {}^{i}\epsilon_x \cos^2({}^{i}\psi) + {}^{i}\epsilon_z \sin^2({}^{i}\psi) + {}^{i}\gamma_{xz} \sin {}^{i}\psi \cos {}^{i}\psi \tag{3.25}$$

$$(i = 2, 3)$$

where:

${}^{i}\psi$ Is defined as an arbitrary angle measured from the ${}^{i}x$ axis (figure 3.4).

For a three element strain gage cluster or *rosette*, three simultaneous equations may be written to describe the strain in each strain gage element for each corresponding angle ${}^{i}\psi_1$, ${}^{i}\psi_2$, and ${}^{i}\psi_3$ as shown below:

$${}^{i}\epsilon_{\psi_1} = {}^{i}\epsilon_x \cos^2({}^{i}\psi_1) + {}^{i}\epsilon_z \sin^2({}^{i}\psi_1) + {}^{i}\gamma_{xz} \sin{}^{i}\psi_1 \cos{}^{i}\psi_1 \qquad (3.26a)$$

$${}^{i}\epsilon_{\psi_2} = {}^{i}\epsilon_x \cos^2({}^{i}\psi_2) + {}^{i}\epsilon_z \sin^2({}^{i}\psi_2) + {}^{i}\gamma_{xz} \sin{}^{i}\psi_2 \cos{}^{i}\psi_2 \qquad (3.26b)$$

$${}^{i}\epsilon_{\psi_3} = {}^{i}\epsilon_x \cos^2({}^{i}\psi_3) + {}^{i}\epsilon_z \sin^2({}^{i}\psi_3) + {}^{i}\gamma_{xz} \sin{}^{i}\psi_3 \cos{}^{i}\psi_3 \qquad (3.26c)$$

The strain values ${}^{i}\epsilon_{\psi_1}$, ${}^{i}\epsilon_{\psi_2}$, and ${}^{i}\epsilon_{\psi_3}$ are determined experimentally from the strain gages and, therefore, are known values. To minimize computational work, three element rosette gages with ${}^{i}\psi_1 = 0^o$, ${}^{i}\psi_2 = 45^o$, and ${}^{i}\psi_3 = 90^o$ were chosen for the laboratory model. This type of rosette is also known as a *rectangular* or *45° strain rosette* [Popov, 1952]. By direct substitution of ${}^{i}\psi_1 = 0^o$, ${}^{i}\psi_2 = 45^o$, and ${}^{i}\psi_3 = 90^o$ into the three equations above ${}^{i}\epsilon_x$, ${}^{i}\epsilon_z$, and ${}^{i}\gamma_{xz}$ are determined as shown below for a *rectangular rosette* [Popov, 1952]:

$${}^{i}\epsilon_{\psi_1} = {}^{i}\epsilon_x \qquad (3.27)$$

$${}^{i}\epsilon_{\psi_3} = {}^{i}\epsilon_z \qquad (3.28)$$

$$ {}^{i}\gamma_{xz} = 2\,{}^{i}\epsilon_{\psi_2} - ({}^{i}\epsilon_{\psi_1} + {}^{i}\epsilon_{\psi_3}) \tag{3.29} $$

Strains ${}^{i}\{\epsilon_{\psi_\S}\}$ (§ = 1, 2, 3) are defined in order to temperature compensate as noted below (figure 3.4):

$$ {}^{i}\epsilon_{\psi_1} = {}^{i}\left[\frac{\bar{\epsilon}_1 - \bar{\epsilon}_4}{2}\right] \tag{3.30} $$

$$ {}^{i}\epsilon_{\psi_2} = {}^{i}\left[\frac{\bar{\epsilon}_5 - \bar{\epsilon}_2}{2}\right] \tag{3.31} $$

$$ {}^{i}\epsilon_{\psi_3} = {}^{i}\left[\frac{\bar{\epsilon}_6 - \bar{\epsilon}_3}{2}\right] \tag{3.32} $$

The individual strain values, for each of the single element strain gages which make up each rosette, are explained in detail below:

${}^{i}\bar{\epsilon}_1$ [positive y face position 1 (${}^{i}\psi_1 = 0^{o}$) (figure 3.4)]
${}^{i}\bar{\epsilon}_2$ [positive y face position 2 (${}^{i}\psi_2 = 45^{o}$) (figure 3.4)]
${}^{i}\bar{\epsilon}_3$ [positive y face position 3 (${}^{i}\psi_3 = 90^{o}$) (figure 3.4)]
${}^{i}\bar{\epsilon}_4$ [negative y face position 4 (${}^{i}\psi_1 = 0^{o}$) (figure 3.4)]
${}^{i}\bar{\epsilon}_5$ [negative y face position 5 (${}^{i}\psi_2 = 45^{o}$) (figure 3.4)]
${}^{i}\bar{\epsilon}_6$ [negative y face position 6 (${}^{i}\psi_1 = 90^{o}$) (figure 3.4)]

From the torsional shear strain ${}^{i}\gamma_{xz}$, the rotational displacements ${}^{i}\theta_x$ are

determined in the local coordinate system as shown below:

$$ {}^{i}\theta_{x} = \frac{2L_{i}\,{}^{i}\gamma_{xz}}{h} = \frac{2L_{i}}{h}\left[2\,{}^{i}\epsilon_{\psi_2} - ({}^{i}\epsilon_{\psi_1} + {}^{i}\epsilon_{\psi_3})\right] \qquad (3.33) $$

3.1.5 Rotational Bending Displacements In Local ${}^{i}y$ Direction

The required combination of strain gage readings (ℓ=3), for the determination of the rotational $-{}^{i}\theta_{y}$ and ${}^{i}w$ displacement is shown below:

$$ {}^{i}_{3}\{\epsilon_{j}\} = {}^{i}_{3}\left[\frac{\bar{\epsilon}_4 - \bar{\epsilon}_2}{2}\right]_{j} \qquad (3.34) $$

$$ (i = 2, 3) $$

$$ (j = 1, 2, 3) $$

where:

${}^{i}\bar{\epsilon}_{2}$ [positive z face position 2 (figure 3.3b)]

${}^{i}\bar{\epsilon}_{4}$ [negative z face position 4 (figure 3.3b)]

The rotational displacements $-{}^{i}\theta_{y}$ derived from the strain measurements ${}^{i}_{3}\{\epsilon_{j}\}$ are defined below. The negative sign in front is required for consistency with the right–hand rule sign convention used throughout this thesis.

$$ -{}^{i}\theta_{y} = \frac{d\,{}^{i}w}{d\,{}^{i}x} = {}^{i}_{3}\{\epsilon_{j}\}\int_{x} {}^{i}\lfloor N \rfloor\, dx \qquad (3.35) $$

where:

$$-{}^{i}\theta_{y} = {}^{i}f_{1} + {}^{i}f_{2}\,{}^{i}x + {}^{i}f_{3}\,{}^{i}x^{2} + {}^{i}f_{4}\,{}^{i}x^{3}$$

or

$$-{}^{i}\theta_{y} = \frac{2}{h}\left[\left[\frac{{}^{i}x^{3} - {}^{i}x^{2}\left(\frac{{}^{i}x_{2} + {}^{i}x_{3}}{2}\right) + {}^{i}x_{2}\,{}^{i}x_{3}\,{}^{i}x}{({}^{i}x_{1} - {}^{i}x_{2})({}^{i}x_{1} - {}^{i}x_{3})}\right]{}^{i}_{3}\epsilon_{1}\right. \qquad (3.36)$$

$$+\left[\frac{{}^{i}x^{3} - {}^{i}x^{2}\left(\frac{{}^{i}x_{1} + {}^{i}x_{3}}{2}\right) + {}^{i}x_{1}\,{}^{i}x_{3}\,{}^{i}x}{({}^{i}x_{2} - {}^{i}x_{1})({}^{i}x_{2} - {}^{i}x_{3})}\right]{}^{i}_{3}\epsilon_{2}$$

$$\left.+\left[\frac{{}^{i}x^{3} - {}^{i}x^{2}\left(\frac{{}^{i}x_{1} + {}^{i}x_{2}}{2}\right) + {}^{i}x_{1}\,{}^{i}x_{2}\,{}^{i}x}{({}^{i}x_{3} - {}^{i}x_{1})({}^{i}x_{3} - {}^{i}x_{2})}\right]{}^{i}_{3}\epsilon_{3}\right] + C_{2}$$

From the boundary conditions at x = 0, the constant of integration ($C_2 = 0$) is obtained.

3.1.6 Rotational Bending Displacements In Local ${}^{i}z$ Direction

The required combination of strain gage readings (ℓ=2), for the determination of the rotational ${}^{i}\theta_{z}$ displacements, is shown below:

$$ {}^{i}_{2}\{\epsilon_j\} = {}^{i}_{2}\left[\frac{\bar{\epsilon}_3 - \bar{\epsilon}_1}{2} \right]_j \qquad (3.37) $$

$$ (i = 2, 3) $$

$$ (j = 1, 2, 3) $$

where:

${}^{i}\bar{\epsilon}_1$ [positive y face position 1 (figure 3.3b)]

${}^{i}\bar{\epsilon}_3$ [negative y face position 3 (figure 3.3b)]

The rotational displacements ${}^{i}\theta_z$ derived from the strain measurements ${}^{i}_{2}\{\epsilon_j\}$ are defined below:

$$ {}^{i}\theta_z = \frac{d\,{}^{i}v}{d\,{}^{i}x} = {}^{i}_{2}\{\epsilon_j\} \int_x {}^{i}\lfloor N \rfloor \, dx \qquad (3.38) $$

where:

$$ {}^{i}\theta_z = {}^{i}g_1 + {}^{i}g_2\,{}^{i}x + {}^{i}g_3\,{}^{i}x^2 + {}^{i}g_4\,{}^{i}x^3 $$

or

$$ {}^{i}\theta_z = \frac{2}{h}\left[\left[\frac{{}^{i}x^3 - {}^{i}x^2\left({}^{i}x_2 + {}^{i}x_3\right) + {}^{i}x_2\,{}^{i}x_3\,{}^{i}x}{\left({}^{i}x_1 - {}^{i}x_2\right)\left({}^{i}x_1 - {}^{i}x_3\right)} \right] {}^{i}_{2}\epsilon_1 \right. \qquad (3.39) $$

$$ \left. + \left[\frac{{}^{i}x^3 - {}^{i}x^2\left({}^{i}x_1 + {}^{i}x_3\right) + {}^{i}x_1\,{}^{i}x_3\,{}^{i}x}{\left({}^{i}x_2 - {}^{i}x_1\right)\left({}^{i}x_2 - {}^{i}x_3\right)} \right] {}^{i}_{2}\epsilon_2 \right] $$

$$+\left[\frac{{}^{i}x^{3}-\frac{{}^{i}x^{2}}{2}({}^{i}x_1+{}^{i}x_2)+{}^{i}x_1\,{}^{i}x_2\,{}^{i}x}{({}^{i}x_3-{}^{i}x_1)({}^{i}x_3-{}^{i}x_2)}\right]{}^{i}_{2}\epsilon_3\Bigg]+C_2$$

From the boundary conditions at x = 0, the constant of integration ($C_2 = 0$) is obtained.

3.1.7 Summary of Displacement Equations

In summary, the displacement equations for link 2 and link 3 developed in subsections 3.1.1 through 3.1.6 are noted below with their corresponding equation reference numbers:

${}^{i}u$	(3.18)
${}^{i}v$	(3.21)
${}^{i}w$	(3.24)
${}^{i}\theta_x$	(3.33)
$-{}^{i}\theta_y$	(3.36)
${}^{i}\theta_z$	(3.39)

3.2 Joint Displacements

3.2.1 Joint Displacement Notations

The displacement equations developed using the Lagrange polynomials in subsections 3.1.1 through 3.1.6 *exactly* describe the static deflected shape of link 2

and 3, as previously noted. In order to determine the deflected and rotated position of the end effector, all joint displacements and all rigid body motion displacements must be determined. The joint displacements at the ends of link 2 and 3 in the local coordinate systems can be determined from the displacement equations developed in subsections 3.1.1 through 3.1.6.

Special notations are required to help clarify the many local displacements at each joint analyzed in this and the following subsections. The local joint displacement notations for the six joint displacements considered in this thesis are:

$$ {}^{i}_{\iota}u_{s} $$

$$ {}^{i}_{\iota}v_{s} $$

$$ {}^{i}_{\iota}w_{s} $$

$$ {}^{i}_{\iota}\theta_{xs} $$

$$ {}^{i}_{\iota}\theta_{ys} $$

$$ {}^{i}_{\iota}\theta_{zs} $$

Where, for example, ${}^{i}_{\iota}v_{s}$ corresponds to the displacement in the ${}^{i}y$ direction at joint i for condition s (s = 1, 2, 3...6).

i Defines the link number.

ι Defines the joint number at which the displacements are determined (ι = 2, 3, or 4).

s Is a displacement designation developed to simplify programming notation and to allow for a method of separately calculating displacements due to rigid body motions where:

s = 1 For the displacements determined from the strain gage values.

s = 2 For the displacements from rigid body motions in the ${}^{i}x{}^{i}y$ plane.

s = 3 For the displacements from rigid body motions in the ${}^{i}x{}^{i}z$ place.

s = 4 For the displacements from rigid body motions from rotational displacements equations ${}^{i}\theta_{x}$, ${}^{i}\theta_{y}$, and ${}^{i}\theta_{z}$

s = 5 For the displacements from rigid body motions from actuator fluctuations.

In order to find joint displacements ${}^{i}_{\iota}u_{1}$, ${}^{i}_{\iota}v_{1}$, ${}^{i}_{\iota}w_{1}$, ${}^{i}_{\iota}\theta_{y1}$, ${}^{i}_{\iota}\theta_{z1}$ the length L_i of link i must be substituted for the ${}^{i}x$ terms in the displacements equations (3.18), (3.21), (3.24), (3.36), and (3.39) in addition to inputting the set location values ${}^{i}\{x_j\}$ and the strain gage combination values ${}^{i}_{\ell}\{\epsilon_j\}$. To find the remaining joint displacements ${}^{i}_{\iota}\theta_{x1}$ the length L_i of link i, the out to out dimension of the link h, and the strain values ${}^{i}\{\epsilon_{\psi_{\S}}\}$ are substituted into equation (3.33).

3.2.2 Rigid Body Motion From Joint Displacements

Rigid body motion effects (RBME) are translational displacements and rigid body rotational displacements resulting from adjoining link joint displacements. All

articulated robot manipulators of more than one link experience rigid body motions which are a function of the number of degrees of freedom of each joint. *It is to be understood that the rigid body effects are first determined in the local coordinate system and then transformed to the global coordinate system before being combined with other global displacements.*

Normally the "Denavit–Hartenberg" method presented in a matrix format is used to solve the arm kinematics due to RBME for each joint of a *rigid* robot with non–flexible links [Koren, 1985]. This is accomplished by successive multiplications of appropriate transformation matrices for every link. The angles used in the transformation matrices are the local angles between the adjoining links. In this thesis a straightforward geometric technique proved to be simpler and more applicable, since the analysis is that of a flexible robot subject to bending, twisting, and axial deformations of the flexible links leading to three dimensional displacements and rotations at the joints. It is seen from the analysis presented in the following subsections 3.2.3 through 3.2.5 that a similar approach to that used by Koren is used in this thesis, even though the equations are not presented in matrix format.

3.2.3 Rigid Body Motion Effects In The Local $^{i}x^{i}y$ Plane.

The RBME in the local xy plane result from the joint displacements ${}^{2}_{2}v_{1}$, ${}^{3}_{3}v_{1}$, and ${}^{3}_{3}\theta_{z1}$ at joint 2 and 3. Joint 2 is considered pinned in the local and global XY plane. Therefore, any flexural displacement ${}^{2}_{2}v_{1}$ at joint 2 results in only a rigid body translation of joint 3 and *end effector center point* (EECP) 4 (figure 3.7). Similarly, a flexural displacement ${}^{3}_{3}v_{1}$ at joint 3 will result in a rigid body translation of EECP 4. However, since joint 3 is rigid in the global XY plane, the

rotational displacement ${}^{3}_{3}\theta_{z1}$ which accompanies the flexural displacement ${}^{3}_{3}v_1$ at joint 3 results in an additional rotation of the end effector link and ultimately a change in the position of EECP 4. It is to be noted that there are no out of plane RBME associated with these particular displacements. Therefore, the displacements in the ${}^{i}z$ direction are not indicated in this section.

A positive flexural joint displacement ${}^{2}_{2}v_1$ at the end of link 2 at joint 2 causes joint 2 to move to $2'$, joint 3 to move to $3'$, and joint 4 to move to $4,'$ (figure 3.7). This represents RBME in translation of joint 3 and joint 4 as defined below:

$$ {}_{3}u' = {}^{2}_{2}v_1 \sin(\phi_2 - \phi_1) \tag{3.40} $$

$$ {}_{3}v' = {}^{2}_{2}v_1 \cos(\phi_2 - \phi_1) \tag{3.41} $$

$$ {}_{4}u' = {}^{2}_{2}v_1 \sin(\phi_3 - \phi_1) \tag{3.42} $$

$$ {}_{4}v' = {}^{2}_{2}v_1 \cos(\phi_3 - \phi_1) \tag{3.43} $$

where the superscript 4 indicates the local rigid body displacements at the EECP 4.

A positive flexural displacement ${}^{3}_{3}v_1$ at the end of link 3 at joint 3 causes the joint at $3'$ to move to $3''$ and the EECP $4'$ to move to $4''$ (figure 3.7). This represents RBME in translation of EECP 4 as defined below:

$$ {}_{4}u'' = {}^{3}_{3}v_1 \sin(\phi_3 - \phi_2) \tag{3.44} $$

$$ {}_{4}v'' = {}^{3}_{3}v_1 \cos(\phi_3 - \phi_2) \tag{3.45} $$

Since joint 3 is considered rigid in the ${}^{i}x{}^{i}y$ plane, a rotational displacement ${}^{3}_{3}\theta_{z1}$ at the end of link 3 at joint 3 results in RBME in rotation of the end effector link (figure 3.7). As joint 3 rotates an angle ${}^{3}_{3}\theta_{z1}$ EECP $4''$ moves to $4'''$ (figure 3.7) and a rigid body rotation of the EECP 4 also occurs. These displacements are defined below:

$$ {}_{4}u''' = -L_4 \, {}^{3}_{3}\theta_{z1} \sin({}^{3}_{3}\theta_{z1}/2) \tag{3.46} $$

$$ {}_{4}v''' = L_4 \, {}^{3}_{3}\theta_{z1} \cos({}^{3}_{3}\theta_{z1}/2) \tag{3.47} $$

$$ {}_{4}\theta_{z}''' = {}^{3}_{3}\theta_{z1} \tag{3.48} $$

The total net RBME which result at joint 3 and EECP 4 from the displacements ${}^{2}_{2}v_1$, ${}^{3}_{3}v_1$, and ${}^{3}_{3}\theta_{z1}$ are combined below:

$$ {}^{3}_{3}u_2 = {}_{3}u' \tag{3.49} $$

$$ {}^{3}_{3}v_2 = {}_{3}v' \tag{3.50} $$

$$ {}^{4}_{4}u_2 = {}_{4}u' + {}_{4}u'' + {}_{4}u''' \tag{3.51} $$

$$ {}^{4}_{4}v_2 = {}_{4}v' + {}_{4}v'' + {}_{4}v''' \tag{3.52} $$

$$ {}^{4}_{4}\theta_{z2} = {}_{4}\theta_{z}''' \tag{3.53} $$

3.2.4 Rigid Body Motion Effects In The Local ${}^{i}x{}^{i}z$ Plane.

A positive flexural displacement ${}^{2}_{2}w_{1}$ at the end of link 2 at joint 2 results in RBME at joint 3 and at the *end effector center point* (EECP) 4. As Joint 2 moves to $2'$ joint 3 moves to $3'$ and EECP 4 moves to $4'$ (figure 3.8). This represents RBME in translation of joint 3 and EECP 4 equal to the displacement ${}^{2}_{2}w_{1}$ as shown below (figure 3.8):

$$ {}_{3}u' = 0.0 \tag{3.54} $$

$$ {}_{3}w' = {}^{2}_{2}w_{1} \tag{3.55} $$

$$ {}_{4}u' = 0.0 \tag{3.56} $$

$$ {}_{4}w' = {}^{2}_{2}w_{1} \tag{3.57} $$

It is to be noted that joint 2 is considered rigid in the xz plane, therefore, a negative rotational displacement $-{}^{2}_{2}\theta_{y1}$ at the end of link 2 at joint 2 results in RBME in rotation of link 3 together with the end effector link (figure 3.8). As joint 2 rotates an angle $-{}^{2}_{2}\theta_{y1}$ joint $3'$ moves to $3''$, joint $4'$ moves to $4''$ (figure 3.8) and a rigid body rotation of joint 3 and the EECP 4 also occurs. The net effect at joint 3 and EECP 4 is a displacement ${}_{4}w''$ in the z–direction and a displacement ${}_{4}u''$ in the x–direction as defined below:

$$ {}_{3}u'' = -L_{3}\,{}^{2}_{2}\theta_{y1}\,\sin({}^{2}_{2}\theta_{y1}/2) \tag{3.58} $$

$$ {}_3w'' = -L_3\, {}^2_2\theta_{y1} \cos({}^2_2\theta_{y1}/2) \tag{3.59} $$

$$ {}_3\theta_y'' = -{}^2_2\theta_{y1} \tag{3.60} $$

$$ {}_4u'' = -(L_3+L_4)\, {}^2_2\theta_{y1} \sin({}^2_2\theta_{y1}/2) \tag{3.61} $$

$$ {}_4w'' = -(L_3+L_4)\, {}^2_2\theta_{y1} \cos({}^2_2\theta_{y1}/2) \tag{3.62} $$

$$ {}_4\theta_y'' = -{}^2_2\theta_{y1} \tag{3.63} $$

A positive bending displacement ${}^3_3w_1$ at the end of link 3 at joint 3 results in RBME at joint 3 and at the EECP 4. As Joint $3''$ moves to $3'''$ the EECP $4''$ moves to $4'''$(figure 3.8). This represents RBME in translation of the EECP 4 as defined below:

$$ {}_3u''' = {}^3_3w_1 \sin({}^2_2\theta_{y1}) \tag{3.64} $$

$$ {}_3w''' = {}^3_3w_1 \cos({}^2_2\theta_{y1}) \tag{3.65} $$

$$ {}_4u''' = {}^3_3w_1 \sin({}^2_2\theta_{y1}) \tag{3.66} $$

$$ {}_4w''' = {}^3_3w_1 \cos({}^2_2\theta_{y1}) \tag{3.67} $$

It is to be noted that joint 3 is also considered rigid in the xz plane, therefore, a negative rotational displacement $-{}^3_3\theta_{y1}$ at the end of link 3 at joint 3 results in RBME in rotation of the end effector link (figure 3.8). As joint 3 rotates

an angle $-{}^{3}_{3}\theta_{y1}$ EECP $4'''$ moves to $4''''$ (figure 3.8) and a rigid body rotation of the EECP 4 also occurs. The net effect at EECP 4 is a displacement ${}_{4}w''''$ in the z–direction and a displacement ${}_{4}u''''$ in the x–direction as defined below:

$$ {}_{4}u'''' = -L_4\, {}^{3}_{3}\theta_{y1} \sin({}^{2}_{2}\theta_{y1} + {}^{3}_{3}\theta_{y1}/2) \tag{3.68} $$

$$ {}_{4}w'''' = -L_4\, {}^{3}_{3}\theta_{y1} \cos({}^{2}_{2}\theta_{y1} + {}^{3}_{3}\theta_{y1}/2) \tag{3.69} $$

$$ {}_{4}\theta_{y}'''' = -{}^{3}_{3}\theta_{y1} \tag{3.70} $$

The total net RBME which results from the displacements ${}^{2}_{2}w_1$, ${}^{3}_{3}w_1$, $-{}^{2}_{2}\theta_{y1}$ and $-{}^{3}_{3}\theta_{y1}$ are combined as shown below:

$$ {}^{3}_{3}u_3 = {}_{3}u'' + {}_{3}u''' \tag{3.71} $$

$$ {}^{3}_{3}w_3 = {}_{3}w' + {}_{3}w'' + {}_{3}w''' \tag{3.72} $$

$$ {}^{3}_{3}\theta_{y3} = {}_{3}\theta_{y}'' \tag{3.73} $$

$$ {}^{4}_{4}u_3 = {}_{4}u'' + {}_{4}u''' + {}_{4}u'''' \tag{3.74} $$

$$ {}^{4}_{4}w_3 = {}_{4}w' + {}_{4}w'' + {}_{4}w''' + {}_{4}w'''' \tag{3.75} $$

$$ {}^{4}_{4}\theta_{y3} = {}_{4}\theta_{y}'' + {}_{4}\theta_{y}'''' \tag{3.76} $$

3.2.5 Rigid Body Motion Effects From Rotational Displacements ${}^{i}_{\ell}\theta_{xs}$

The local rotational displacements ${}^{i}_{\ell}\theta_{x}$ result from torsional moments and all components of those moments and forces which cause a twisting deformation in link 2 and 3. A local rotational displacement ${}^{2}_{2}\theta_{x1}$ or twist in link 2 at joint 2 will result in a rotational RBME in link 3 and also in the end effector link. A local rotational displacement ${}^{3}_{3}\theta_{x1}$ or twist in link 3, by the same reasoning, will result in a rotational RBME in the end effector link. The RBME associated with these rotational displacements are described separately below:

As joint 2 rotates the angular displacement ${}^{2}_{2}\theta_{x1}$ joint 3 moves to 3', which results in the displacements ${}_{3}u'$, ${}_{3}v'$, and ${}_{3}w'$ at joint 3 and a rigid body rotation ${}_{3}\theta_{x}'$ (figure 3.9). In addition, as joint 2 rotates the angular displacement ${}^{2}_{2}\theta_{x1}$ *end effector center point* (EECP) 4 moves to 4', which results in the displacements ${}_{4}u'$, ${}_{4}v'$, and ${}_{4}w'$ at EECP 6 and a rigid body rotation ${}_{4}\theta_{x}'$ (figure 3.9). The displacements relating to this motion are described below:

$$ {}_{3}u' = R_2 \sin(\phi_2 - \phi_1) \tag{3.77} $$

$$ {}_{3}v' = R_2 \cos(\phi_2 - \phi_1) \tag{3.78} $$

$$ {}_{3}w' = R_1 \sin({}^{2}_{2}\theta_{x1}) \tag{3.79} $$

$$ {}_{3}\theta_{x}' = {}^{2}_{2}\theta_{x1} \cos(\phi_2 - \phi_1) \tag{3.80} $$

$$ {}_{4}u' = R_4 \sin(\phi_3 - \phi_2) \tag{3.81} $$

$$ {}_4v' = R_4 \cos(\phi_3 - \phi_2) \tag{3.82} $$

$$ {}_4w' = R_3 \sin({}^2_2\theta_{x1}) \tag{3.83} $$

$$ {}_4\theta'_x = {}^2_2\theta_{x1} \cos(\phi_2 - \phi_1)\cos(\phi_3 - \phi_2) \tag{3.84} $$

where:

R_r Are constants defined below used to simplify the RBME equations above and to make programming simpler and faster (r = 1,2,3,4).

$$ R_1 = L_3 \sin(\phi_2 - \phi_1) \tag{3.85} $$

$$ R_2 = R_1(\cos({}^2_2\theta_{x1}) - 1.0) \tag{3.86} $$

$$ R_3 = R_1 + L_4 \sin(\phi_3 - \phi_1) \tag{3.87} $$

$$ R_4 = R_3(\cos({}^2_2\theta_{x1}) - 1.0) \tag{3.88} $$

As joint 3 rotates the angular displacement ${}^3_3\theta_{x1}$ EECP 6' moves to 6'' which results in the displacements ${}_4u''$, ${}_4v''$, and ${}_4w''$ in addition to a rigid body rotation ${}_4\theta''_x$ at EECP 4 (figure 3.10). The displacements relating to this motion are described below:

$$ {}_4u'' = R_6 \sin(\phi_3 - \phi_2) \tag{3.89} $$

$$ {}_4v'' = R_6 \cos(\phi_3 - \phi_2) \tag{3.90} $$

$$ {}_4w'' = R_5 \sin({}^3_3\theta_{x1}) \tag{3.91} $$

$$ {}_4\theta_x'' = {}^3_3\theta_{x1} \cos(\phi_3 - \phi_2) \tag{3.92} $$

where:

R_r Are constants similar to those noted above (r = 5,6).

$$ R_5 = L_4 \sin(\phi_3 - \phi_2) \tag{3.93} $$

$$ R_6 = R_5(\cos({}^3_3\theta_{x1}) - 1.0) \tag{3.94} $$

In summary, the net effect at the end effector in local coordinates at the EECP 4 from the RBME associated with the rotational displacements ${}^i\theta_x$ are:

$$ {}^3_3u_4 = {}_3u' \tag{3.95} $$

$$ {}^3_3v_4 = {}_3v' \tag{3.96} $$

$$ {}^3_3w_4 = {}_3w' \tag{3.97} $$

$$ {}^3_3\theta_{x4} = {}_3\theta_x' \tag{3.98} $$

$$ {}^4_4u_4 = {}_4u' + {}_4u'' \tag{3.99} $$

$$ {}^4_4v_4 = {}_4v' + {}_4v'' \tag{3.100} $$

$$ {}^{4}_{4}w_4 = {}_4w' + {}_4w'' \tag{3.101} $$

$$ {}^{4}_{4}\theta_{x4} = {}_4\theta_x' + {}_4\theta_x'' \tag{3.102} $$

3.2.6 Rigid Body Motion Effects From Actuator Fluctuations

Any fluid displacement in the hydraulic actuators ab and de on the model (figure 1.1) will induce a rigid body motion effect at joints 2,3 and the *end effector center point* (EECP) 4. Any fluid displacement in the hydraulic actuator at the base link 1 is neglected here, therefore, all out–of–plane displacements ${}^{i}_{\iota}w_s$ are zero and not shown.

The displacements from actuator ab are determined and defined as displacements ${}^{i}_{\iota}u_s$ and ${}^{i}_{\iota}v_s$ at joints 2,3,and EECP 4. This derivation is shown below (figure 3.11):

$$ d\varphi = \frac{C_1 \quad ERR_1}{A_1 B_1 \sin\varphi} = d\phi_1 \tag{3.103} $$

where:

$$ \varphi = \frac{\pi}{2} + \phi_1 - \phi \tag{3.104} $$

$$ C_1 = [\, A_1{}^2 + B_1{}^2 - 2\, A_1\, B_1\, \mathrm{Cos}\, \varphi \,]^{1/2} \tag{3.105} $$

$$ {}_2u' = B_2\, d\varphi \sin(d\varphi/2) \tag{3.106} $$

$$ {}_2v' = B_2\, d\varphi \cos(d\varphi/2) \tag{3.107} $$

$$ {}_3u' = B_2\, d\varphi \sin(\phi_2 - \phi_1 + d\varphi/2) \tag{3.108} $$

$$ {}_3v' = B_2\, d\varphi \cos(\phi_2 - \phi_1 + d\varphi/2) \tag{3.109} $$

$$ {}_4u' = B_2\, d\varphi \sin(\phi_3 - \phi_1 + d\varphi/2) \tag{3.110} $$

$$ {}_4v' = B_2\, d\varphi \cos(\phi_3 - \phi_1 + d\varphi/2) \tag{3.111} $$

where:

ERR_1 Fluid displacements in units of strain in actuator ab.

B1 Dimension (figure 3.11).

ϕ Set angle equal to $\tan^{-1}(6''/22'') = .26625$ radians (figure 3.11).

The fluid displacements from actuator de are determined and defined as displacements ${}^{i}_{\iota}u_s$ and ${}^{i}_{\iota}v_s$ at joints 2,3,and EECP 4. This derivation is shown below (figure 3.11)

$$ d\alpha = \frac{C_2 \quad ERR_2}{A_2 B_2 \sin\alpha} = d\phi_2 \tag{3.112} $$

$$ \alpha = 180 + \phi_1 - \phi_2 - \lambda \tag{3.113} $$

$$ C_2 = [\, A_2^{\,2} + B_2^{\,2} - 2\, A_2\, B_2\, \mathrm{Cos}\ \alpha\,]^{1/2} \tag{3.114} $$

$$ {}_3u'' = L_3\, d\alpha \sin(d\alpha/2) \tag{3.115} $$

$$ {}_3v'' = L_3\, d\alpha \cos(d\alpha/2) \tag{3.116} $$

$$ {}_4u'' = L_3\, d\alpha \sin(\phi_3 - \phi_2 + d\alpha/2) \tag{3.117} $$

$$ {}_4v'' = L_3\, d\alpha \cos(\phi_3 - \phi_2 + d\alpha/2) \tag{3.118} $$

where:

ERR_2 Fluid displacements in units of strain in actuator de.

λ Angle at joint 2 set at $126.87^0 = 2.214$ radians (figure 3.11).

The combined displacements due to the fluid displacements in actuators ab and de at joints 2 and 3 and the EECP 4 are:

$$ {}^2_2u_5 = {}_2u' \tag{3.119} $$

$$ {}^2_2v_5 = {}_2v' \tag{3.120} $$

$$ {}^3_3u_5 = {}_3u' + {}_3u'' \tag{3.121} $$

$$ {}^3_3v_5 = {}_3v' + {}_3v'' \tag{3.122} $$

$$ {}^4_4u_5 = {}_4u' + {}_4u'' \tag{3.123} $$

$$ {}^4_4v_5 = {}_4v' + {}_4v'' \tag{3.124} $$

3.2.7 Summary of Joint Displacements

In summary, the joint displacements at the ends of link 2 and 3 in the local

coordinate systems can combined with all additional local joint displacements due to rigid body motion effects as shown below:

$$ {}^{i}_{\iota}u = \sum_{s=1}^{6} {}^{i}_{\iota}u_s \tag{3.125} $$

$$ {}^{i}_{\iota}v = \sum_{s=1}^{6} {}^{i}_{\iota}v_s \tag{3.126} $$

$$ {}^{i}_{\iota}w = \sum_{s=1}^{6} {}^{i}_{\iota}w_s \tag{3.127} $$

$$ {}^{i}_{\iota}\theta_x = \sum_{s=1}^{6} {}^{i}_{\iota}\theta_{xs} \tag{3.128} $$

$$ {}^{i}_{\iota}\theta_y = \sum_{s=1}^{6} {}^{i}_{\iota}\theta_{ys} \tag{3.129} $$

$$ {}^{i}_{\iota}\theta_z = \sum_{s=1}^{6} {}^{i}_{\iota}\theta_{zs} \tag{3.130} $$

$$ (\iota = 2, 3, 4) $$

3.3 Local to Global Coordinate Transformations

To be of use to the controller, the local displacements determined in the

above discussion need to be combined and then transformed from the local coordinate systems to the global coordinate systems, before combining with any additional global displacements, in order to determine the location of the end effector. Upper case notation is used to define the *global* displacements and lower case notation is used to define the *local* displacements (figure 3.5 & 3.6).

$$\begin{bmatrix} U \\ V \\ W \\ \otimes_X \\ \otimes_Y \\ \otimes_Z \end{bmatrix} = \begin{bmatrix} C & -S & 0 & 0 & 0 & 0 \\ S & C & 0 & 0 & 0 & 0 \\ 0 & 0 & 1 & 0 & 0 & 0 \\ 0 & 0 & 0 & C & -S & 0 \\ 0 & 0 & 0 & S & C & 0 \\ 0 & 0 & 0 & 0 & 0 & 1 \end{bmatrix} {}^{i}_{\iota}\begin{bmatrix} u \\ v \\ w \\ \theta_x \\ \theta_y \\ \theta_z \end{bmatrix} \qquad (3.131)$$

where:

C Cosine of joint angle ϕ_ι [$\cos(\phi_\iota)$].

S Sine of joint angle ϕ_ι [$\mathrm{Sin}(\phi_\iota)$].

ι Defines the joint number (2, 3, or 4).

CHAPTER FOUR

Dynamic Response Study

4.1 Periodic Steady State Response Of The Manipulator

The robot is designed to move within a defined workspace (figure 4.1 & 4.2) where it is subject, due to its flexibility, to a variety of forced vibrations. The workspace in the XY plane (figure 4.1) is extended in three dimensional space by rotating the base around its own vertical y–axis through an angle of approximately 208 degrees (figure 4.2). There are a variety of parameters which will influence the dynamic response of the robot end effector as it moves throughout the workspace. The main parameters are the path of motion of the end effector, the velocity variation and the acceleration variation of the end effector throughout the path of motion, the mass and inertia of the object or objects being moved, and the natural passive damping of the manipulator and its hydraulic actuators. The ideal motion of the robot under the direction of the controller is that motion which would result in the smallest amplitude of vibration.

This thesis is mainly concerned with the response of the end effector at and near the end of its path of motion. Once the response of the end effector is determined experimentally and equations developed to describe the response, a prediction can be made by the controller as to when the amplitude of vibration would damp to an acceptable level. It would be desirable to quickly damp out the vibration at the end effector by using the hydraulic actuators in such a way as to apply forced active damping. This damping technique applies to the vibrations in

the XY plane via the two hydraulic actuators which function only in this plane (figure 1.1) and the rotary horizontal actuator which rotates the base around its vertical axis.

From the shape functions and Lagrange polynomials developed in Chapter 3, the deformations of link 2 and 3 are determined for the first four modes of vibration. The deformations of link 2 and 3 are a function of the spacial parameter ${}^{i}x$, the time parameter t, and the strain gage readings at predetermined time intervals (Δt). Due to data acquisition time and computer on line processing time limitations, the time intervals regulated by the analog digitizer (A/D) boards must be set at approximately one tenth of one period of vibration. This criteria is determined in order to prevent possible response misrepresentation as shown (figure 4.3). The strain values are read continuously at these time intervals into a FORTRAN program code, where they are transformed into *six* generalized global displacements U, V, W, $\otimes_X$, $\otimes_Y$, and $\otimes_Z$ at the end effector. From these *six* generalized displacements *six* equations describing the vibrational response at the end effector can be determined as shown later in this chapter. Since the strain gages are read continuously, the displacement equations are continuously being updated periodically for various periods of vibration. Therefore, an accurate prediction of the response can be made by the controller at any time t. From this prediction control techniques can be developed.

Since the strain gages give strain values at predetermined time intervals, the amplitudes of vibration of the end effector are calculated as a set of discrete points. The *six* displacements at the end effector are the discrete amplitudes ${}^{r}D_m$ (r = 1, 2, 3...6) of vibration at discrete time points t_m (m = 1, 2, 3...N). Assuming the response is periodic, a Fourier series representation can be described where the Fourier series coefficients ${}^{r}a_0$, ${}^{r}a_n$ and ${}^{r}b_n$ [Rao,S.S.,1986] can be evaluated by using

a numerical integration method like the *Trapezoidal rule* [Gerald,C.F.,1984] as shown below:

$$ {}^{r}\{D\} = e^{-\beta t}\left[\frac{{}^{r}a_{o}}{2} + \sum_{n=1}^{\infty}\left[{}^{r}a_{n}\cos(n\omega_{d}t) + {}^{r}b_{n}\sin(n\omega_{d}t)\right]\right] \qquad (4.1) $$

$$ (r = 1, 2, 3, 4, 5, 6) $$

Where ${}^{r}\{D\}$ is defined as the global displacements in matrix form as:

$$ {}^{r}\{D\} = \begin{Bmatrix} {}^{1}D \\ {}^{2}D \\ {}^{3}D \\ {}^{4}D \\ {}^{5}D \\ {}^{6}D \end{Bmatrix} = \begin{Bmatrix} U \\ V \\ W \\ \otimes_{x} \\ \otimes_{y} \\ \otimes_{z} \end{Bmatrix} \qquad (4.2) $$

and where:

$$ {}^{r}a_{o} = \frac{2}{T_{d}}\int_{o}^{T_{d}} {}^{r}D\, dt \cong \frac{2}{N}\sum_{m=1}^{N} {}^{r}D_{m} \qquad (4.3) $$

$$ {}^{r}a_{n} = \frac{2}{T_{d}}\int_{o}^{T_{d}} {}^{r}D\cos(n\omega_{d}t)dt \cong \frac{2}{N}\sum_{m=1}^{N} {}^{r}D_{m}\cos\left[\frac{2n\pi t_{m}}{T_{d}}\right] \qquad (4.4) $$

$$ {}^{r}b_{n} = \frac{2}{T_{d}}\int_{o}^{T_{d}} {}^{r}D\sin(n\omega_{d}t)dt \cong \frac{2}{N}\sum_{m=1}^{N} {}^{r}D_{m}\sin\left[\frac{2n\pi t_{m}}{T_{d}}\right] \qquad (4.5) $$

$$\omega_d = \frac{2\pi}{T_d} \tag{4.6}$$

$$T_d = N\,\Delta t \tag{4.7}$$

$$\Delta t = t_{m+1} - t_m \tag{4.8}$$

$$(m=1, 2, 3,...N)$$

where:

β Damping coefficient determined in section 4.3.

ω_d The circular frequency of damped vibration [radians/sec].

T_d The period of damped vibration [sec].

t_m Are a number of equidistant time points over the period T_d.

y_m Are the amplitudes of vibration corresponding to the time points t_m.

Δt Time increment between data readings.

n An integer which depicts the number of terms in the Fourier series.

N Is an integer relating to the number of data points t_m and y_m for one period of vibration.

π Archimedes' number pi = 3.14159265.....

The final equation to describe the amplitude response of the end effector is approximated as shown below, where K is an integer replacing the infinity symbol ∞ set large enough to maintain the required accuracy.

$$^{r}\{D\} = e^{-\beta t}\left[\frac{1}{N}\sum_{m=1}^{N} {}^{r}D_m + \sum_{n=1}^{K}\left[\frac{2}{N}\sum_{m=1}^{N}\left[{}^{r}D_m \cos\left[\frac{2\,n\,\pi\,t_m}{T_d}\right]\right]\cos(n\omega_d t)\right.\right.$$

$$+ {}^{r}D_{m}\sin\left[\frac{2\,n\,\pi\,t_{m}}{T_{d}}\right]\sin(n\omega_{d}t)\Bigg]\Bigg]\Bigg] \qquad (4.9)$$

$$(r = 1, 2, 3, 4, 5, 6)$$

It should be noted that since the acquisition of strain data is continuous, this equation is periodically updated and always gives the most current representation of the dynamic response of the end effector under steady state conditions.

4.2 On Line Determination of the System Frequencies

In order to determine the system frequencies of damped vibration the damped period of vibration for each response must be determined. Since the manipulator changes shape and stiffness within its workspace, the damped period of vibration at the end effector is always a function of the position of link 2 and 3 in space and time. The position of link 2 and 3 is a function of the joint angles ϕ_1 and ϕ_2, therefore, the damped period of vibration can be defined as a function of the angles ϕ_1, and ϕ_2. By placing the manipulator arms in certain static positions and subjecting the end effector to a forced vibration, a series of frequencies can be determined experimentally for each position analyzed.

Computer programming methods are used here to determine the damped periods of vibration as a function of the joint angles. Equation (4.9) is programmed to read the damped amplitudes of vibration at discrete time points. By comparing each amplitude value with the previous value determined, key time points

associated with points of zero velocity of the end effector can be tagged (figure 4.3). The key time points where the velocities are zero are associated with amplitude peaks. These peaks can be noted as changes in amplitudes from continuously increasing to decreasing values or from continuously decreasing to increasing values. Basically, when the differences in the absolute value of the amplitudes $\Delta^{r}D_{m} = \left|{}^{r}D_{m+1}\right| - \left|{}^{r}D_{m}\right|$ changes its value from positive to negative or is equal to zero, a time point t_{m+1} is tagged which relates to a peak amplitude value. The incremental time value associated with these tagged points of zero velocity are the damped periods of vibration T_d. By inputting T_d into equation (4.9) the frequency of damped vibration ω_d is determined.

4.3 Determination Of Velocities And Accelerations

Once the equation for the end effector displacements ${}^{r}\{D\}$ is determined by equation (4.1), the velocities and accelerations could be obtained by differentiation, keeping in mind that ${}^{r}a_{n}$ and ${}^{r}b_{n}$ are constants. The velocity is developed by differentiating equation (4.9) as shown below:

$$ {}^{r}\{\dot{D}\} = \frac{\partial \ {}^{r}\{D\}}{\partial t} \qquad (4.10) $$

$$ {}^{r}\{\dot{D}\} = e^{-\beta t}\left[\sum_{n=1}^{K}\left[\frac{2}{N}\sum_{m=1}^{N}\left[-{}^{r}D_{m} n\omega_{d}\cos\left[\frac{2 n \pi t_{m}}{T_{d}}\right]\sin(n\omega_{d}t)\right.\right.\right. $$

$$+ {}^{r}D_m n\omega_d \sin\left[\frac{2\,n\,\pi\,t_m}{T_d}\right]\cos(n\omega_d t)\Bigg]\Bigg]\Bigg]$$

$$-\beta e^{-\beta t}\Bigg[\frac{1}{N}\sum_{m=1}^{N} {}^{r}D_m + \sum_{n=1}^{K}\Bigg[\frac{2}{N}\sum_{m=1}^{N}\Bigg[{}^{r}D_m \cos\left[\frac{2\,n\,\pi\,t_m}{T_d}\right]\cos(n\omega_d t)$$

$$+ {}^{r}D_m \sin\left[\frac{2\,n\,\pi\,t_m}{T_d}\right]\sin(n\omega_d t)\Bigg]\Bigg]\Bigg] \qquad (4.11)$$

$$(r = 1, 2, 3, 4, 5, 6)$$

$${}^{r}\{\dot{D}\} = \begin{Bmatrix} {}^{1}\dot{D} \\ {}^{2}\dot{D} \\ {}^{3}\dot{D} \\ {}^{4}\dot{D} \\ {}^{5}\dot{D} \\ {}^{6}\dot{D} \end{Bmatrix} = \begin{Bmatrix} \dot{U} \\ \dot{V} \\ \dot{W} \\ \dot{\otimes}_x \\ \dot{\otimes}_y \\ \dot{\otimes}_z \end{Bmatrix} \qquad (4.12)$$

The acceleration is developed by differentiating equation (4.10) as shown below:

$${}^{r}\{\ddot{D}\} = \frac{\partial^2 {}^{r}\{D\}}{\partial^2 t} = \frac{\partial {}^{r}\{\dot{D}\}}{\partial t} \qquad (4.13)$$

$$
{}^{r}\{\ddot{D}\} = e^{-\beta t}\left[\sum_{n=1}^{K}\left[\frac{2}{N}\sum_{m=1}^{N}\left[-{}^{r}D_m(n\omega_d)^2\cos\left[\frac{2n\pi t_m}{T_d}\right]\cos(n\omega_d t)\right.\right.\right.
$$

$$
\left.\left.\left.-{}^{r}D_m(n\omega_d)^2\sin\left[\frac{2n\pi t_m}{T_d}\right]\sin(n\omega_d t)\right]\right]\right]
$$

$$
-2\beta e^{-\beta t}\left[\sum_{n=1}^{K}\left[\frac{2}{N}\sum_{m=1}^{N}\left[-{}^{r}D_m n\omega_d\cos\left[\frac{2n\pi t_m}{T_d}\right]\sin(n\omega_d t)\right.\right.\right.
$$

$$
\left.\left.\left.+{}^{r}D_m n\omega_d\sin\left[\frac{2n\pi t_m}{T_d}\right]\cos(n\omega_d t)\right]\right]\right]
$$

$$
+\beta^2 e^{-\beta t}\left[\frac{1}{N}\sum_{m=1}^{N}{}^{r}D_m+\sum_{n=1}^{K}\left[\frac{2}{N}\sum_{m=1}^{N}\left[{}^{r}D_m\cos\left[\frac{2n\pi t_m}{T_d}\right]\cos(n\omega_d t)\right.\right.\right.
$$

$$
\left.\left.\left.+{}^{r}D_m\sin\left[\frac{2n\pi t_m}{T_d}\right]\sin(n\omega_d t)\right]\right]\right] \qquad (4.14)
$$

$$(r = 1, 2, 3, 4, 5, 6)$$

$$ {}^{r}\{\ddot{D}\} = \begin{Bmatrix} {}^{1}\ddot{D} \\ {}^{2}\ddot{D} \\ {}^{3}\ddot{D} \\ {}^{4}\ddot{D} \\ {}^{5}\ddot{D} \\ {}^{6}\ddot{D} \end{Bmatrix} = \begin{Bmatrix} \ddot{U} \\ \ddot{V} \\ \ddot{W} \\ \ddot{\otimes}_{x} \\ \ddot{\otimes}_{y} \\ \ddot{\otimes}_{z} \end{Bmatrix} \tag{4.15} $$

As noted earlier, equations (4.11) and (4.14) are periodically updated to give the most current dynamic response of the end effector.

4.4 Determination Of The Damping Coefficient β

From experimental observation, the response at the end effector appears to damp out after a certain number of cycles. Since there are no passive damping devices installed, the cause of the damping may be from the looseness of the joints, the effect of the surrounding air, minor fluctuations in the flow rate and compressibility of the fluid in the hydraulic actuators. In order to approximate this damping effect, the Fourier series response equations noted above are multiplied by a function $e^{-\beta t}$, where β is an arbitrary coefficient used to approximate the damping effect noted above. β is determined as shown below [Rao,S.S.,1986]:

$$ \frac{{}^{r}D_{1}}{{}^{r}D_{\Psi+1}} = \frac{e^{-\beta t_{m}}}{e^{-\beta (t_{m}+T_{d})}} = e^{\beta T_{d}} \tag{4.16} $$

The logarithmic decrement δ is defined below, where ${}^{r}D_{1}$ and ${}^{r}D_{\Psi+1}$ are two successive amplitudes of vibration separated in time by a number of equal periods of damped vibration T_d:

$$\delta = \frac{1}{\Psi} \ln \left[\frac{{}^{r}D_{1}}{{}^{r}D_{\Psi+1}} \right] = \beta T_d \tag{4.17}$$

$$\beta = \frac{1}{\Psi} \ln \left[\frac{{}^{r}D_{1}}{{}^{r}D_{\Psi+1}} \right] \frac{1}{T_d} \tag{4.18}$$

where:

Ψ Is an integer equal to the number of amplitudes read minus one.

From off–line experimentation with the manipulator, a set of damping coefficients β can be determined at specified locations in the defined workspace (figure 4.1 & 4.2) at specified joint angles ϕ_1 and ϕ_2 (figure 3.1). At each of these specified locations, the value of β is determined from equations (4.17) and (4.18) over the span of several cycles of vibration, using an oscilloscope attached to the Wheatstone bridge amplification circuitry. These values for the damping coefficients can be determined at certain grid locations throughout the workspace for use in equations (4.9), (4.11), and (4.14), which could in turn be used by the controller to predict the vibration response of the end effector.

CHAPTER FIVE

Finite Element Model

5.1 Finite Element Analysis of The Manipulator

The finite element method of analysis is used here to determine the static and free natural vibrational response of the end effector of the robot manipulator. It was decided to find the solutions to the static and vibrational response of the end effector by the use of a versatile numerical method such as finite element analysis. A finite element analysis, using a finite element system program [CASA/GIFTS, 1986] lends itself very nicely to complex structural problems and provides results acceptable in standard engineering practice.

The program GIFTS is one of a variety of finite element programs available which can handle dynamic as well as static analysis. The GIFTS program can perform static analysis, free and forced vibration analyses, and thermal stress analysis. Of main interest here are the static analysis, and free and forced vibration analyses capabilities. By modeling the robot manipulator and subjecting it to static and dynamic forces, the response of the end effector could be simulated and studied.

The GIFTS program first requires that a finite element model be generated. It is to be noted that no active damping is considered in the GIFTS finite element model generated. It was decided to use rod elements, also known as truss elements, for actuator ab and de (figure 1.1) and beam elements for the remaining manipulator segments. Beam elements transfer bending moments, shear

forces, and axial forces at each node, whereas rod elements transfer only axial forces at the nodes. The actuators are pin connected on the actual robot model in the xy–plane at each end and, therefore, it is assumed in the modeling that the actuator rods feel only axial forces. This assumption is based on the laboratory observation that the actuator rods do not appear to bend significantly under different loading conditions, since any significant bending would effect their proper operation. In order to simulate the actual laboratory robot model, which is constructed with a two dimensional pin at joints 1 and 2, the moments about the z–axis were released with a RELP command at nodes 1 and 2 (figure 5.1).

The first part of the model generation required is to define the beam and rod elements which make up the robot structure. Beam elements and rod elements are sections of the structure defined by a node number at each end and connected to other elements at these nodes (figure 5.1). The processor BEAMCS is used to define the beam element cross sections (figures 5.3 to 5.8). To generate the finite element model for this thesis, an input generator called MODEL.FOR (Appendix–C) was developed using the FORTRAN programing language. The only input information required is the angles ϕ_1, ϕ_2, and ϕ_3 which set the robot configuration (figure 4.1). The GIFTS data file created by MODEL.FOR is ROB.DAT. The data file ROB.DAT is then copied as ROBx.SRC where the x is an integer relating to the robot position (figure 4.1). For example: ROB3.SRC will define the model for position 3 (figure 4.1). The generation file must have the extension .SRC in order to be used by the on–line–batch file command OLB. Once the model has been generated, a standard GIFTS procedure is followed to run the static or dynamic cases as noted in the following sections 5.1.1 and 5.1.2.

5.1.1 Finite Element Procedure "STATIC"

The GIFTS program is made up of a series of *procedures*, each of which requires the execution of several *processors* in a specific sequence. The procedure used for the static analysis presented in this thesis is defined and shown in order below:

BEAMCS
EDITM
LOADBC
MSTATIC { BULKF, OPTIM, ADSTIF, ELSTFF, STASS, DECOM, DEFL, STRESS } (macro)
RESULT

BEAMCS Is used to define the thickness groups for use in generating the elements of the model. Each thickness group defines the cross–sectional properties of the different beam and rod elements used in the model (figures 5.3 to 5.9). An on–line–batch file (OLB) called NEW1BC.SRC (Appendix–C) was created to be called upon in the BEAMCS processor in order to eliminate the recreation of all beam element properties each time they are required.

EDITM Is used for model generation and editing. To eliminate the time

consuming repetitive creation of the model for different configurations of angles ϕ_1,ϕ_2 and ϕ_3 (figure 4.1), a FORTRAN program called MODEL.FOR was developed (Appendix–C). The program MODEL.FOR creates source (SRC) files for generating the model for each specific configuration defined by the ϕ_1, ϕ_2, and ϕ_3 manipulator angles (figure 5.2).

LOADBC Is used to apply loads and boundary conditions to the models generated in EDITM. An on–line–batch file (OLB) called NEW1LD.SRC (Appendix–C) was created to be called upon in the LOADBC processor so as to eliminate the recreation of each load and boundary condition each time they are required.

MSTATIC A macro used to execute computational procedures without the need to call the processors individually. The processors executed with this macro are defined below in the order they are executed:

- BULKF Assigns the basic freedom pattern to the structural points, based on element type and orientation.
- OPTIM Computes a half bandwidth of the symmetric structural stiffness matrix by rearranging point and element numbers internally without affecting the user point numbers, and selects the wave front which produces the minimum bandwidth.
- ADSTIF Computes disk allocation for the assembled stiffness matrix.
- ELSTFF Computes all element stiffness matrices.
- STASS Assembles all the element stiffness matrices into the structural stiffness matrix.
- DECOM Decomposes the assembled stiffness matrix using a generalized hypermatrix Cholesky scheme.

DEFL Computes point deflections.

STRESS Computes all element stresses.

RESULT Displays computational results using the information commands.

The GIFTS static procedure noted above was used to process results for positions 1, 3, and 5 with a one hundred pound force applied in the negative y direction at the end effector center point 4. The GIFTS files generated for positions 1, 3, and 5 are called NEW1ROB, NEW3ROB, and NEW5ROB respectively and the results are given in appendix–C.

5.1.2 Finite Element Procedure "MODES"

The GIFTS program procedure "Modes" is used to compute the first ten vibrational modes for the robot manipulator under its own weight without any additional masses applied at the joints. It is defined and noted in the order below:

BEAMCS
EDITM
LOADBC
BULKF
OPTIM
STIFF { ADSTIF, ELSTFF, STASS } (macro)
SUBS
STRESS
RESULT

SUBS Given a specified number of modes to determine, this processor performs iterations to determine the lowest natural modes of vibration.

STIFF A macro similar in function to MSTATIC noted above, and is used to execute computational procedures without the need to call the processors individually.

The natural frequencies are printed out using the command INFFREQ while in the processor RESULT. A summary of these modes is noted in appendix–C. It should be noted that the frequency variations for the different robot manipulator configurations at the extreme ends of the workspace (figure 4.1) are less than 15% in magnitude.

The GIFTS modes procedure noted above was used to process results for positions 1, 3, 5, 7, 8, and 11 without any additional masses applied at the joints. The GIFTS files generated for positions 1, 3, 5, 7, 8, and 11 are called NEW1ROB, NEW3ROB, NEW5ROB, NEW7ROB, NEW8ROB, and NEW11ROB, respectively, and the results are given in appendix–C. A plot of the mode shapes is obtained via the command PLOT,1. Examples are shown in Appendix–C.

CHAPTER SIX

Laboratory Experimentation

6.1 Cantilever Beam Lab Experiment No.1

6.1.1 Cantilever Beam Experiment No.1 [Static]

The purpose of experiment No.1 is to determine if the theory previously developed, using strain gage readings and Lagrange polynomials, will give acceptable results when applied to a cantilever beam. To test this theory, a controlled experiment is devised which is in strict accordance with all assumptions made in the development of the theory.

A flexible steel beam is clamped at one end to an unyielding support. The beam is 1/4 inch thick by 2.0 inches wide of ASTM A36 steel, with a yield strength of 36,000 psi., and a modulus of elasticity of 29,000,000.psi. The length of the unclamped portion, from the face of the support to the point of the applied concentrated loads, is 40.56 inches. Three strain gage sets, made up of two single element strain gages per set, are placed at three specific locations X_1, X_2, and X_3 along the cantilever beam from the face of the support at X_1=2.56", X_2=18.0", and X_3=37.19". One gage in each gage set is placed on the top or positive y–face, and one is placed on the bottom or negative y–face. The single element strain gages used are type EA–06–125AD–120 manufactured by Measurements Group, Inc. of Raleigh, North Carolina. The single element gage is one–eighth inch in length, madeof an alloy called constantan, and has an unstrained gage resistance of 120

ohms plus or minus 0.15%. The gage factor at 75 degrees fahrenheit is 2.055 plus or minus 0.5%.

The free end of the cantilever beam is loaded in the vertical direction with calibrated weights. Nine different weights are applied in 500 gram increments from 500 grams to 4500 grams (approximately 1.1 to 9.92 pounds–force in English units). The vertical deflection of the beam due to its own weight is not considered since all displacement measurements are taken from the static equilibrium position.

The strain values are documented for each load condition and for each strain gage set using strain indicator Model P–3500 by Measurements Group, Inc. of Raleigh, North Carolina. The strain values from the strain indicator are then input into a FORTRAN program code [Appendix–B], which utilizes the Lagrange polynomials defined earlier, to calculate the theoretical free end displacement. In order to confirm the displacements calculated, the results are compared with two analytical methods noted below:

1) The first method is to calculate the theoretical vertical displacements at the free end of the cantilever beam for each load condition using the standard beam theory formulas noted below:

$$v(L) = \frac{P L^3}{3 E I} \tag{6.1}$$

$$\sigma(j) = \pm \frac{P L_j c}{I} \tag{6.2}$$

where:

v(L) Vertical displacement at free end of cantilever beam.

P Load applied at the free end which varies from 1.10 lbs to 9.92 lbs.

L Unsupported length of the beam (40.565 in).

E Modulus of Elasticity (29,000,000 psi).

I Moment of inertia of the beam (.002604 in^4).

$\sigma(j)$ Maximum bending stress in beam at strain gage set j.

j An integer which refers to the strain gage set locations at X_1,X_2, or X_3.

L_j Length in inches from P load to strain gage set at X_j.

c Distance from the neutral axis of the beam cross–section to the extreme fiber on the y–face (0.125").

2) The second method is to measure mechanically with a micrometer the static displacement at the free end of the beam. The micrometer is set to measure additional displacement starting from the static equilibrium deflected position, thereby ignoring any initial displacement at the free end due to the beam weight. The micrometer used is Model C81S–001 manufactured by Federal and is considered accurate to one–thousandth of one inch.

6.1.2 Results of Lab Experiment No. 1 [Static]

Location X_1:

Initial strain indicator reading in micro–strains = 4800.

Location of P load from gage set X_1 (L_{p1}= 38.0 inches).

P Load (grams)	P Load (lbs.)	Indicator readings	Strain (in/in)	Stress (psi)
500	1.10	4660	7.000E–05	2011
1000	2.20	4520	1.400E–04	4021
1500	3.31	4380	2.100E–04	6032
2000	4.41	4240	2.800E–04	8042
2500	5.51	4100	3.500E–04	10053
3000	6.61	3960	4.200E–04	12064
3500	7.72	3820	4.900E–04	14074
4000	8.82	3680	5.600E–04	16085
4500	9.92	3542	6.290E–04	18095

Location X_2:

Initial strain indicator reading in micro–strains = 770.

Location of P load from gage set X_2 (L_{p2}= 22.56 inches).

P Load (grams)	P Load (lbs.)	Indicator readings	Strain (in/in)	Stress (psi)
500	1.10	686	4.200E–05	1194
1000	2.20	604	8.300E–05	2387
1500	3.31	522	1.240E–04	3581
2000	4.41	439	1.655E–04	4775
2500	5.51	357	2.065E–04	5968
3000	6.61	274	2.480E–04	7162
3500	7.72	191	2.895E–04	8356
4000	8.82	110	3.300E–04	9549
4500	9.92	29	3.705E–04	10743

Location X_3:

Initial strain indicator reading in micro–strains = 2800.

Location of P load from gage set X_3 (L_{p3}= 3.375 inches).

P Load (grams)	P Load (lbs.)	Indicator readings	Strain (in/in)	Stress (psi)
500	1.10	2788	6.000E–06	179
1000	2.20	2776	1.200E–05	357
1500	3.31	2764	1.800E–05	536
2000	4.41	2751	2.450E–05	714
2500	5.51	2739	3.050E–05	893
3000	6.61	2726	3.700E–05	1071
3500	7.72	2713	4.350E–05	1250
4000	8.82	2701	4.950E–05	1429
4500	9.92	2690	5.500E–05	1607

Displacements at Free End of Cantilever Beam:

P Load (grams)	P Load (lbs.)	Theory (inch)	Method 1. (inch)	Method 2. (inch)
500	1.10	0.3293	0.3248	0.3340
1000	2.20	0.6550	0.6495	0.6660
1500	3.31	0.9806	0.9743	0.9960
2000	4.41	1.3082	1.2990	1.3270
2500	5.51	1.6338	1.6238	1.6550
3000	6.61	1.9615	1.9486	1.9840
3500	7.72	2.2911	2.2734	2.3120
4000	8.82	2.6130	2.5981	2.6520
4500	9.92	2.9340	2.9229	2.9770

where:

Theory: Implies displacements calculated from equation (6.1).

Method 1: Implies displacements calculated using strain gage readings and Lagrange polynomials from chapter 3.

Method 2: Implies displacements measured by the micrometer measuring device.

By comparing the results of the theoretical analysis with the two analytical methods noted, it can be concluded that the displacement functions derived previously from Lagrange polynomials are satisfactory in determining the displacement at the free end of a cantilever beam. It should be noted that if the robotic links act as true cantilever beams, then an accurate determination of the location of joints No. 2 and 3 can be achieved.

6.1.3 Cantilever Beam Lab Experiment No.1 [Dynamic]

The second goal of Experiment No.1 is to determine the natural damped

frequency of the beam for the first mode of vibration, using the strain gages noted above, and compare this experimental frequency with the calculated theoretical value given by the equation noted below [Meirovitch,L., 1986]:

$$f_d = \frac{(1.875)^2}{2\pi}\left[\frac{E\ I}{m_s L^4}\right]^{\frac{1}{2}} \qquad (6.3)$$

where:

f_d Natural frequency of vibration in hertz.

m_s Mass of the beam per unit length (.00367 slugs/in^2).

The strain gage set X_1 is connected to the strain indicator Model P–3500 and the output signal is connected to a 60 mega hertz digital storage oscilloscope, model 2220 by Tektronix Inc., which can save the response over a specified time increment. The cantilever beam is given an initial vertical displacement of approximately one half inch at the free end and then released. From the response curve saved on the oscilloscope, the damped period of vibration is read to the nearest one hundredth of one second. The period of damped vibration was read as 0.21 seconds. This damped period of vibration converts to a natural frequency of 4.76 hertz. The theoretical frequency calculated from equation (6.3) is 4.86 hertz, which is a difference of approximately 2% from the measured frequency. Therefore, it can be noted that the strain gages are accurately measuring the response of the cantilever beam as expected.

As discussed in chapter four, the damping coefficient β is to be determined based on successive amplitude measurements separated by a specified number of periods of damped vibration. Equation (4.17) from chapter four is repeated below:

$$\delta = \frac{1}{\Psi} \ln \left[\frac{{}^{r}D_{1}}{{}^{r}D_{\Psi+1}} \right] \tag{6.4}$$

$$\beta = \frac{\delta}{T_d} \tag{6.5}$$

where:

${}^{r}D_{m}$ Displacement amplitudes (m = 1,2,3,....N).

Ψ An integer equal to the number of amplitudes read minus one.

T_d Damped period of vibration.

6.1.4 Results of Lab Experiment No. 1 [Dynamic]

First response reading:

$T_d = 0.21$

${}^{r}D_{1} = 5.80$

${}^{r}D_{1} = 5.60$

${}^{r}D_{1} = 5.35$

${}^{r}D_{1} = 5.15$

Therefore: $\beta = 0.189$

Second response reading:

$T_d = 0.21$

${}^{r}D_{1} = 3.60$

${}^{r}D_{2} = 3.50$

${}^{r}D_{3} = 3.40$

${}^{r}D_{4} = 3.35$

Therefore: $\beta = 0.114$

The difference in the two calculated values of β is within the visual accuracy of the oscilloscope screen. The damping coefficient β calculated above is very small which is to be expected since the only damping in the system is that from the surrounding air. There may also be a very slight damping contribution from hysteresis damping, otherwise known as structural damping. However, this damping effect in structural steel is usually considered negligible due to the high modulus of elasticity and toughness of steel.

6.2 Robot Manipulator Lab Model Experiment No.2

The purpose of experiment No.2 is to confirm the theory previously developed, using strain gage readings and Lagrange polynomials on the actual robotic model. A static vertical load is to be applied to the end effector (node No. 4 figure 3.1). Four sets of strain gages are mounted on links No. 2 and No. 3. The strain gage readings are input into the FORTRAN program code [Appendix–B] and the theoretical vertical displacement of the end effector is determined. The vertical displacement results are compared with the finite element results and those obtained by the micrometer readings taken in the lab.

The lab model is a *robot* manipulator one–third the scale of the intended full scale version, it is supported and powered by a PRAB hydraulic base. The first link is constructed of standard steel pipe ASTM A53 grade 'B', eight inches in diameter and two inches thick, with a yield strength of 35,000 psi. The first link is constructed in the global Y–axis and is able to rotate about this vertical axis through a total angle of approximately 208 degrees (figure 4.2). The length of link 1

is 39.37 inches. The second and third links are constructed out of ASTM A500 Grade 'B' cold formed tube steel (TS $1^1/2"$ x $1^1/2"$ x $^1/4$ ") with a yield strength of 46,000 psi. and are able to move in the global XY plane with the help of hydraulically driven actuators, mounted as shown (figure 1.1). Link 2 is 45.375 inches in length and link 3 is 31.5 inches in length. All remaining parts are made of plate steel grade ASTM A36 of one inch stock with a yield strength of 36,000 psi. In comparison to the other link members, the first link is considerably stiffer and, therefore, is considered to be rigid in this analysis. The stiffness ratio of link 1 and link 2 is $(I_1/L_1)/(I_2/L_2) = 7590$, which is three orders of magnitude. Refer to figure 3.1 for a detailed description of the actual dimensions of the lab model.

All joint angles are measured from the global coordinate system (figure 3.1). To measure the joint angles, the robot manipulator is equipped with an angular encoder sensor at each joint. The joint angles are used to locate the end effector in the X,Y and Z global axes.

The strain gages used are type EA–06–125AD–120 manufactured by Measurements Group, Inc. of Raleigh, North Carolina. The single element gage is one–eighth inch in length made of an alloy called constantan and has an unstrained gage resistance of 120 ohms plus or minus 0.15%. The gage factor at 75 degrees fahrenheit is 2.055 plus or minus 0.5%. During operation all strain gages are electrically wired to a series of strain indicator and amplification circuits, otherwise known as Wheatstone bridge circuitry. Each Wheatstone bridge channel would be connected in a half bridge configuration, utilizing the reading of two strain gages located on opposite faces of each link. Due to the action of flexural bending and due to the fact that links 2 & 3 are square in cross section and of uniform thickness, the strains at the extreme fiber on opposite faces would be equal in magnitude but opposite in sign. This configuration would temperature compensate for any errors

associated with changes in temperature during experimentation. Signal conditioning is through an A/D converter for data acquisition into a 25 megahertz micro–computer utilizing a 32 bit bus.

It was decided to neglect axial displacements in all experimentation in this thesis for two reasons:

1) The axial strains and displacements due to the axial deformation of the links are relatively minor in comparison to those due to bending and twist and, therefore, will not cause any appreciable error in predicting the location of the end effector.

2) In order to determine the axial displacements in addition to any rotational and bending displacements, each strain gage must be connected to a separate Wheatstone bridge channel as a quarter bridge. This would require many more channels to be read by the computer, thereby reducing the response time available to control the robot dynamically.

6.2.1 Robot Manipulator Lab Model Experiment No. 2 [Static]

A static experiment is performed using the strain gage sets mounted on links 2 and 3 as previously noted. Eight different weights are applied in five pound increments from 5 lbs to 40 lbs at the end effector center point 4 in the vertical direction for robot manipulator configuration 3 (figure 4.1). The strain values are documented for each load and for each strain gage set using a switch and balance unit, model SB–10, connected to a strain indicator, Model P–3500, both by Measurements Group, Inc. of Raleigh, North Carolina. The strain values from the strain indicator are then input into a FORTRAN program code [Appendix–B],

which utilizes the Lagrange polynomials defined earlier to calculate the theoretical free end vertical displacement at the end effector center point 4. An attempt was made to confirm the displacements calculated by taking actual lab measurements with a micrometer positioned at the end effector center point 4. Due to constant drift experienced at the end effector, the displacement measurements using the micrometer were not obtained.

6.2.2 Results of Lab Experiment No.2 [Static]

The strain gage results are read into the FORTRAN program STRAIN.FOR (Appendix–B) where the displacements at the end effector center point 4 as well as joints 2 and 3 are computed. These displacements are for robot manipulator configuration 3 (figure 4.1) and the results are given in appendix–B in order from the 5 lb load to the forty pound load.

It is to be noted that the vertical loading does not cause out–of–plane bending and twisting. Thus, all strain gage readings corresponding to these deformations are zero.

6.2.3 Robot Manipulator Model Experiment No.2 [Dynamic]

The second part of Experiment No.2 is to determine the natural damped frequency of the beam for the first mode of vibration, using the strain gages noted above, and compare this experimental frequency with the values calculated in the finite element analysis of chapter five.

The strain gage set X_1 is connected to the strain indicator Model P–3500 and the output signal is connected to a 60 mega hertz Digital Storage Oscilloscope

model 2220, manufactured by Tektronix Inc., similar to experiment No.1 noted earlier. The end effector is given an initial vertical displacement of approximately one inch at the free end and then released. From the response curve saved on the oscilloscope, the damped period of vibration is read to the nearest one hundredth of one second. The period of damped vibration was read as 0.23 seconds. This damped period of vibration converts to a natural frequency of 4.35 hertz. The frequency calculated from the finite element analysis for the same configuration is 5.31 hertz which is a difference of approximately 22% from the frequency measured.

As discussed in chapter four, the damping coefficient β is to be determined based on successive amplitude readings separated by periods of damped vibration. Equation (4.17) from chapter four is repeated below:

$$\delta = \frac{1}{\Psi} \ln \left[\frac{{}^{r}D_{1}}{{}^{r}D_{\Psi+1}} \right] \tag{6.6}$$

$$\beta = \frac{\delta}{T_{d}} \tag{6.7}$$

where:

${}^{r}D_{m}$ Displacement amplitudes (m = 1,2,3,....N).

Ψ An integer equal to the number of amplitudes read minus one.

T_{d} Damped period of vibration.

6.2.4 Results of Lab Experiment No. 2 [Dynamic]

First response reading:

$T_{d} = 0.23$

$^{r}D_1 = 4.10$

$^{r}D_2 = 3.60$

$^{r}D_3 = 3.10$

$^{r}D_4 = 2.80$

$^{r}D_5 = 2.30$

Therefore: $\beta = 0.628$

Second response reading:

$T_d = 0.23$

$^{r}D_1 = 3.40$

$^{r}D_2 = 2.90$

$^{r}D_3 = 2.50$

$^{r}D_4 = 2.20$

$^{r}D_5 = 1.90$

Therefore $\beta = 0.632$

The damping coefficient β calculated above is relatively large which is also visually obvious and may be due to energy dissipation from looseness of the joints, the effect of flow rate fluctuations and fluid compressibility in the hydraulic actuators, and the resistance of the surrounding air. Since there are no passive damping devices installed on the robot manipulator, the damping coefficient β can be accepted as a built in parameter of the robot to be determined experimentally for consideration in the design of the control system and for use in equations (4.9, 4.11, and 4.14).

CHAPTER SEVEN

Conclusions and Recommendations

7.1 Conclusions

The displacement equations developed in chapter three using strain gages and Lagrange polynomials represent the exact deformations of elastic links 2 and 3 when subjected to static forces, and a close approximation to the exact deformation when subjected to moderate dynamic forces. By inputting the strain gage values from the strain gages mounted on each link and the angular encoder readings from the angular encoders mounted at each joint, the FORTRAN program "STRAIN.FOR" calculates the joint displacements, self weight displacements, and rigid body motion effects associated with the elastic link deformations. The joint displacements calculated from the FORTRAN program "STRAIN.FOR" were in close agreement with the measured static displacements from static forces applied at the end effector. The dynamic displacements as discussed in chapter four are yet to be verified.

The free end vertical displacement results of the static cantilever beam, experiment No.1 of chapter six, are within 0.6% of the displacements calculated from beam theory formulas. This experiment proves that by substituting experimentally measured strain values from strain gages mounted at three defined locations on a cantilever beam into the displacement functions derived previously as Lagrange polynomials, the free end static displacements of a cantilever beam can be accurately determined. It can be concluded that the strain gages and

electronic equipment are working properly and the results given are acceptable.

The frequency of vibration of the cantilever beam in the cantilever beam experiment No.1 found from the digital storage oscilloscope agreed to within 2% of the theoretical calculated value from dynamic theory. The calculation of the damping coefficient β for the two exercises shown in chapter six is done for the purpose of obtaining a rough estimate of this damping coefficient. The accuracy of β is limited by the accuracy of the oscilloscope screen.

The vertical displacement of the *end effector center point* (EECP) 4 for position 3 (figure 4.1) calculated from the strain gage readings for a forty pound load is 0.36 inches as shown in section 6.2.1. The static displacement of the EECP 4 given in the results of the finite element GIFTS program section 5.1.1 for position 3 (figure 4.1) is approximately 0.30 inches. The variation in results from the program results and the finite element analysis is approximately 20% . Attempts were made to determine the actual vertical displacements at the EECP 4 with the use of a micrometer measuring device placed at EECP 4. However, the vertical displacements could not be obtained since the end effector would constantly drift vertically during the experiment.

The frequency calculation from GIFTS for position 3 for the mode of vibration in the vertical direction is approximately 22% higher than the value read from the oscilloscope. This discrepancy may be due to a possible damping of the robot model due to the drift phenomena noted above. The higher frequency given in the finite element analysis implies a stiffer robot model than the actual laboratory model, which is logically correct since the finite element analysis does not include any active damping. However, the robot manipulator laboratory model may be experiencing active damping from fluctuations in the hydraulic actuator valves, which may also be causing the drift phenomena noted above.

It is to be noted that the periods of vibration measured with the oscilloscope by switching from strain gages connected at set 1 to set 2 and to set 3 (figure 3.2 & 3.3a), for both link 2 and 3, produced the same values. This implies that any of the strain gage sets can by used to measure the natural frequency of vibration. This is a good indication that the vibration studied is harmonic in nature.

7.2 Recommendations

In order to accurately compare the theoretical results obtained from laboratory experiment No.2 [Static] described in section 6.2.1 with the actual laboratory model displacements, the drift phenomena noted above should be investigated and prevented in order to allow acceptable measurements to be obtained. The assumption that the link members act as cantilever beams can be verified by comparing the actual displacements of the end effector center point 4 with the output from the FORTRAN program STRAIN.FOR.

It is recommended that a series of tests be run to determine the damping coefficient as discussed in chapter four for use in the equations developed in chapter four. A series of experiments are needed in order to determine the damping coefficients for each of the first six different modes of free vibration. An accurate calculation of the damping coefficient β is to be determined off line with the amplitudes coming directly from the FORTRAN program code developed for this purpose, as discussed in chapter four. It was observed that the damping coefficient also varies with the load applied at the end effector. Therefore, experiments should be performed to determine β for different loads as well.

Since the natural frequency of the laboratory robot model was observed to

change when different masses were placed at the end effector center point (EECP) 4, an experiment should be conducted to measure the different frequencies of the laboratory model for a number of different masses placed at the EECP 4 and for different robot manipulator positions in the XY plane workspace (figure 4.1). The results of this type of experiment will prove to be very useful in the development of the control system.

REFERENCES:

AISC, 1980, Manual of Steel Construction, Eighth Edition, Chicago, Illinois.

Anderson, J.S. and Bratos–Anderson M., 1987, Solving Problems in Vibrations, First Edition, Longman Scientific Technical, Singapore.

Bannoura. T.M., 1988, "Structural Analysis and Design of a Flexible Three–Link Hydraulically Actuated Robotic Arm", Masters Dissertation, Department of Civil and Mechanical Engineering, University of Nevada, Las Vegas.

Bares, J.E. and Whittaker, W.L., 1989, "Configuration of an Autonomous Robot for Mars Exploration", *Society of Manufacturing Engineers Transaction, May* 7–11.

CASA/GIFTS INC., 1986, "Computer Aided Structural Analysis Graphical Interactive Finite Element Total System", University of Arizona.

Cook, R. D., 1981, Concepts and Application of Finite Element Analysis, Second Edition, John Wiley and Sons, Inc., New York.

Culbreth, W.G., and Krueger, A., 1989, "Computer Simulation of a Three–Link Hydraulically Actuated Robotic Arm", *Society of Manufacturing Engineers Transaction, May* 7–11.

Dally, J. W. and Riley, W. F., 1965, Experimental Stress Analysis, McGraw–Hill Book Company, Inc., New York.

Geradin, M., Rober, G., Bernardin, C., 1984, "Dynamic Modelling of Manipulators With Flexible Members", *Advanced Software in Robotics*, Elsevier Science Publishers B.V. (North Holland), pp. 27–39.

Gerald, C.F. and Wheatley, P.O., 1984, Applied Numerical Analysis, Third Edition, Addison–Wesley, Reading, Mass.

Hastings, G.G., and Book, W.J., 1986, "Verification of a Linear Dynamic Model for Flexible Robotic Manipulators", *Proceedings IEEE International Conference on Robotics and Automation, pp. 1024–1029.*

Koren, Yoram., 1985, Robotics For Engineers, McGraw–Hill Book Company, Inc., New York.

Ladkany, S.G. and Bannoura, T.M., 1989, "Structural Design of a Flexible Three–Link Hydraulically Activated Robotic Arm", *Society of Manufacturing Engineers Transaction, May* 7–11.

Meirovitch, Leonard, 1986, Elements of Vibration Analysis, Second Edition, McGraw–Hill Book Company, Inc., New York.

Nathan, P.J., and Singh, S.N., 1989, "Sliding Mode Control and Elastic Mode Stabilization Of A Robotic Arm With Flexible Links", *American Society of*

Mechanical Engineers (ASME), Journal Of Dynamic Systems, Measurement and Control. Report No. EER–89–008.

Osborn, J.F., 1989, "Applications of Robotics in Hazardous Waste Management", *Society of Manufacturing Engineers Transaction, May* 7–11.

Popov, E.P., 1952, Mechanics of Materials, Prentice–Hall, Inc., New Jersey.

Rao, S.S., 1986, Mechanical Vibrations, First Edition, Addison–Wesley Publishing Company, Massachusetts.

Salmon, Charles G., and Johnson, John E., 1980, Steel Structures: Design and Behavior, Second Edition, Harper & Row, New York.

Tanaka,M., Seguchi,Y., Yamaguchi, T., 1989, "Structural Kinematics and Incremental Sequence of Truss–type Parallel Robotic Mechanism with Highly Multiple DOFs", *Society of Manufacturing Engineers Transaction, May* 7–11.

Tang, S.C. and Wang, C., 1987, "Computation Of The Effects Of Link Deflections And Joint Compliance On Robot Positioning", *Proceedings IEEE International Conference on Robotics and Automation*, pp. 910–915.

Timoshenko, Stephen, Young, D. H., and Weaver, W., 1974, Vibration Problems in Engineering, Fourth Edition, John Wiley & Sons, New York, London, Sydney, Toronto.

Tonkay, G.L., and Knott, K., 1989, "Intelligent Process Specification for Robotic Arc Welding", *Society of Manufacturing Engineers Transaction, May* 7–11.

Trabia, M.B. and Yim, W., 1989, "Dynamic Simulation of a Three Degrees of Freedom Hydraulically Activated Robotic Arm with Flexible Links, *Society of Manufacturing Engineers Transaction, May* 7–11.

Wang, P.K.C. and Wei, Jin–Duo, 1987, "Vibrations In A Moving Flexible Robot Arm", Journal Of Sound and Vibration, Vol. 116, No.1, pp. 149–160.

Wylie, C. R. Jr, 1951, Advanced Engineering Mathematics, First Edition, McGraw–Hill Book Company, Inc., New York, Toronto, London.

APPENDIX–A

Figures Corresponding to Chapters One, Two, Three, Four, Five, and Six.

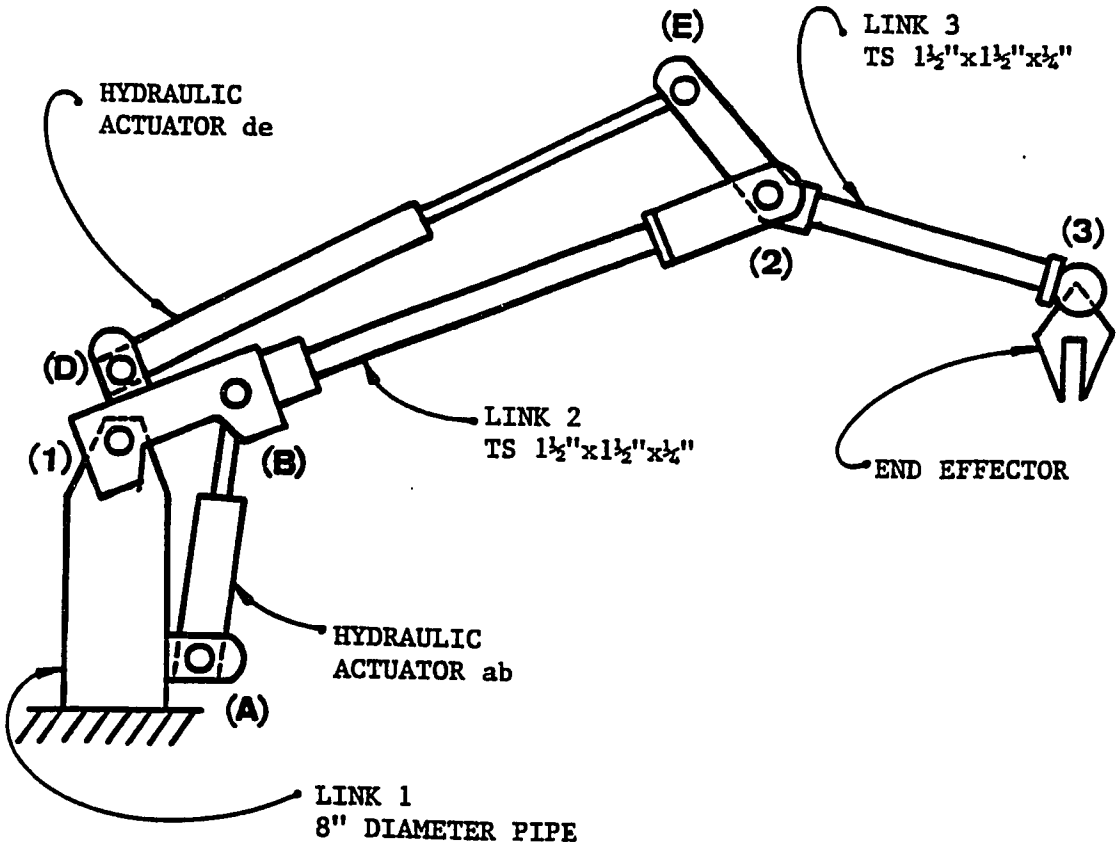

FIGURE 1.1 SCHEMATIC OF THREE-LINK ROBOT MANIPULATOR

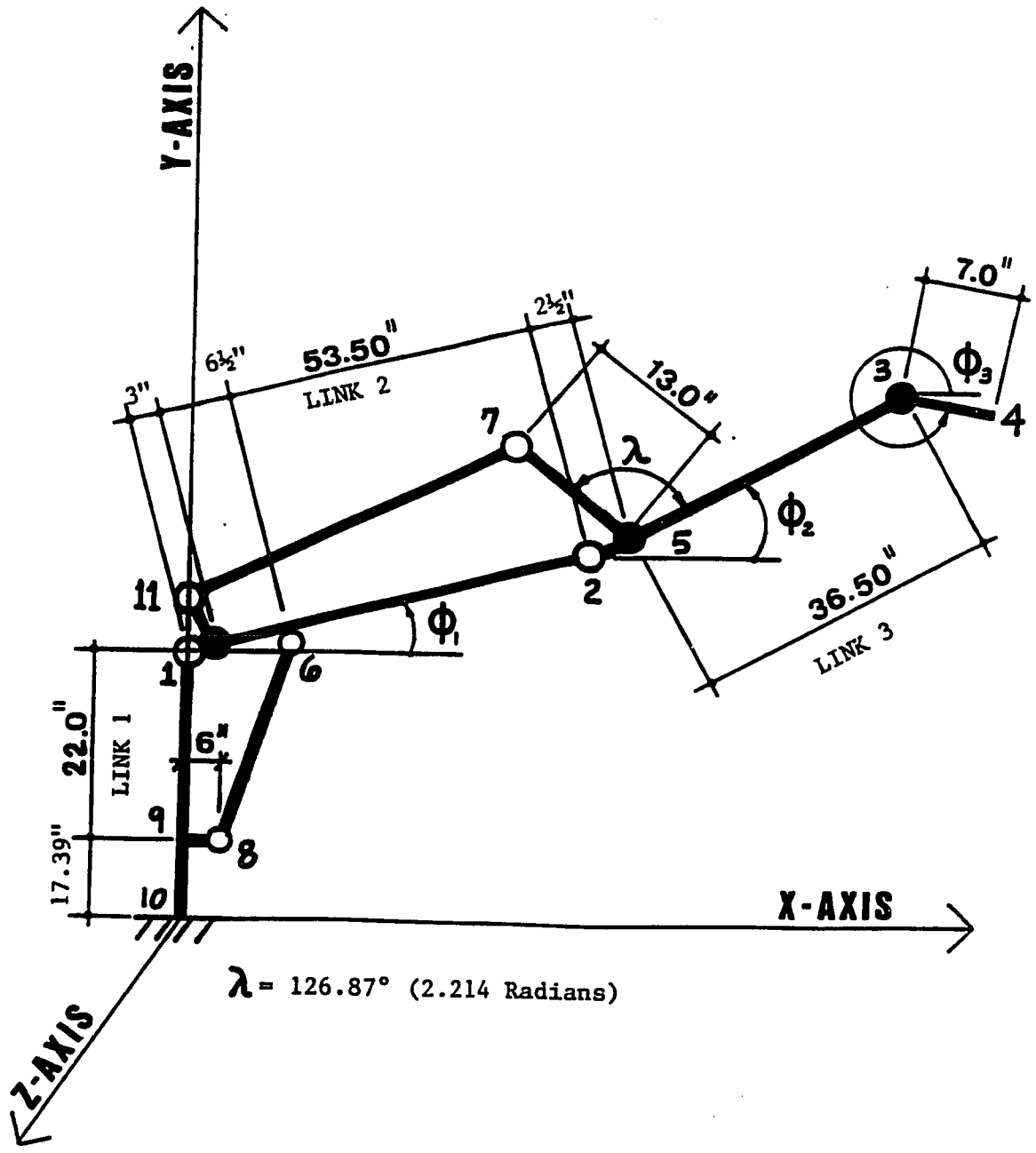

FIGURE 3.1 DIMENSIONAL SCHEMATIC OF ROBOT MANIPULATOR

X1 = 7.0"

X2 = 22.0"

X3 = 43.0"

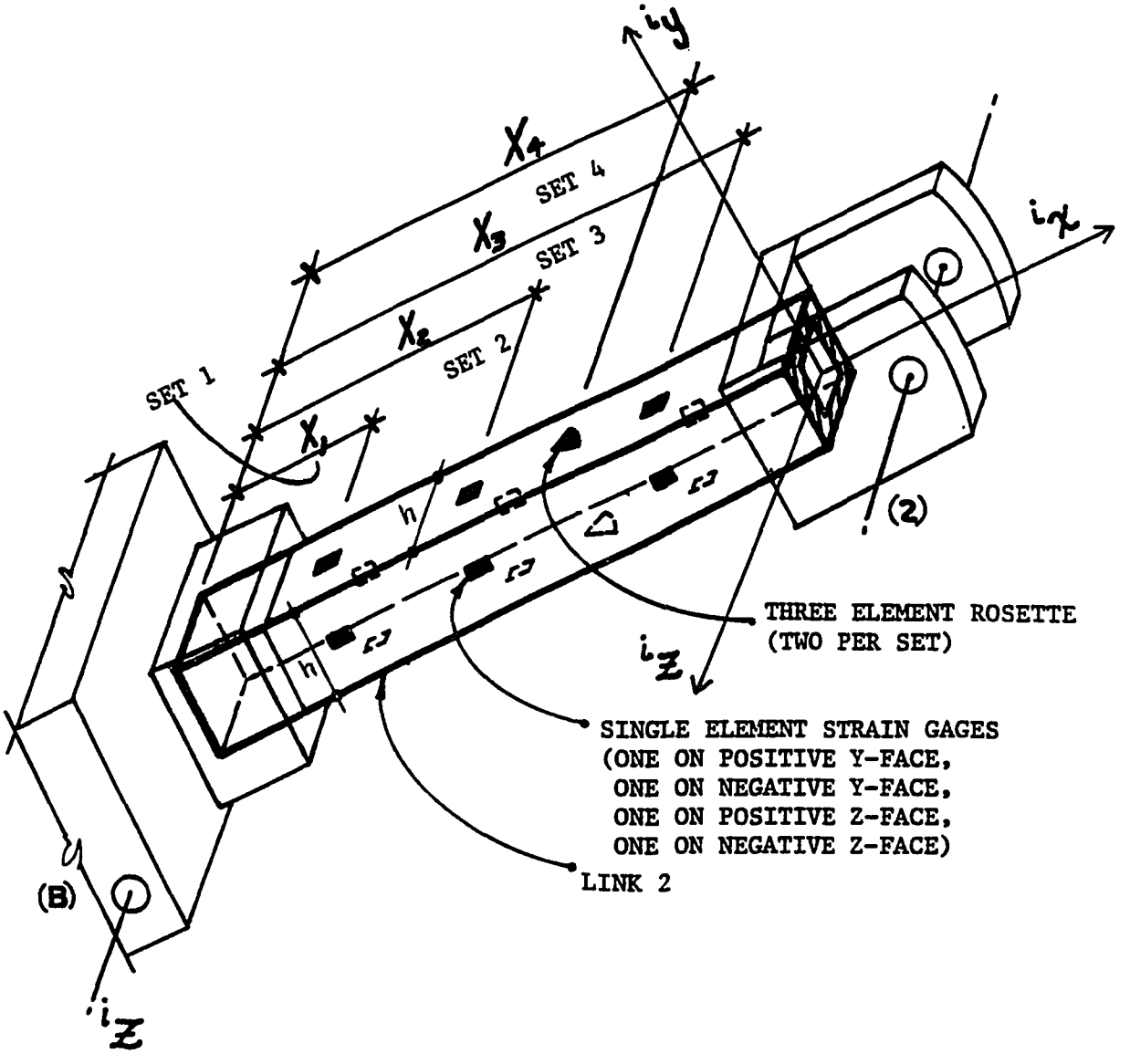

FIGURE 3.2 LINK 2 STRAIN GAGE SET LOCATIONS

X1 = 2.5"

X2 = 15.0"

X3 = 29.0"

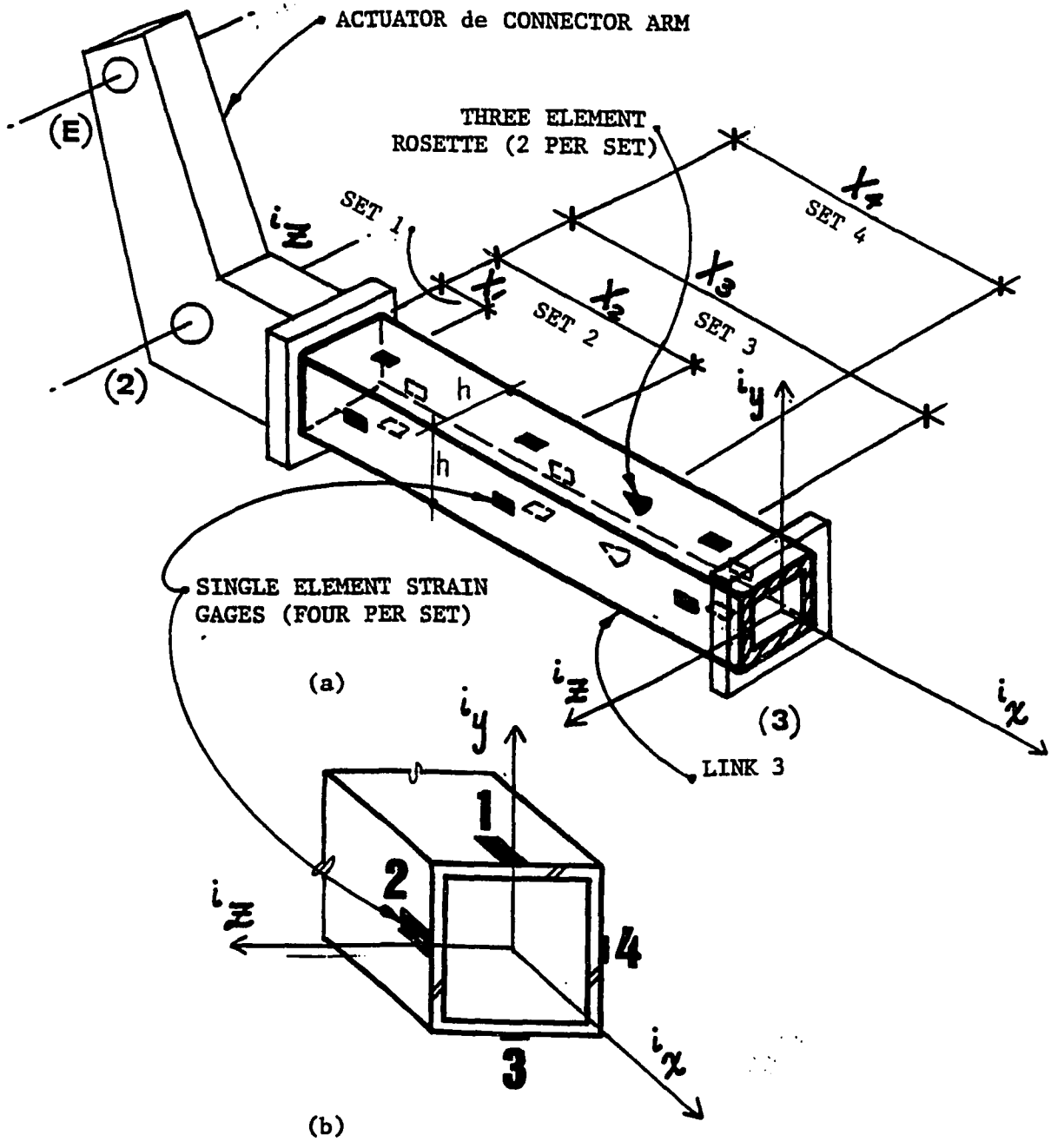

FIGURE 3.3a LINK 3 STRAIN GAGE SET LOCATIONS

FIGURE 3.3b SINGLE ELEMENT STRAIN GAGE POSITIONS

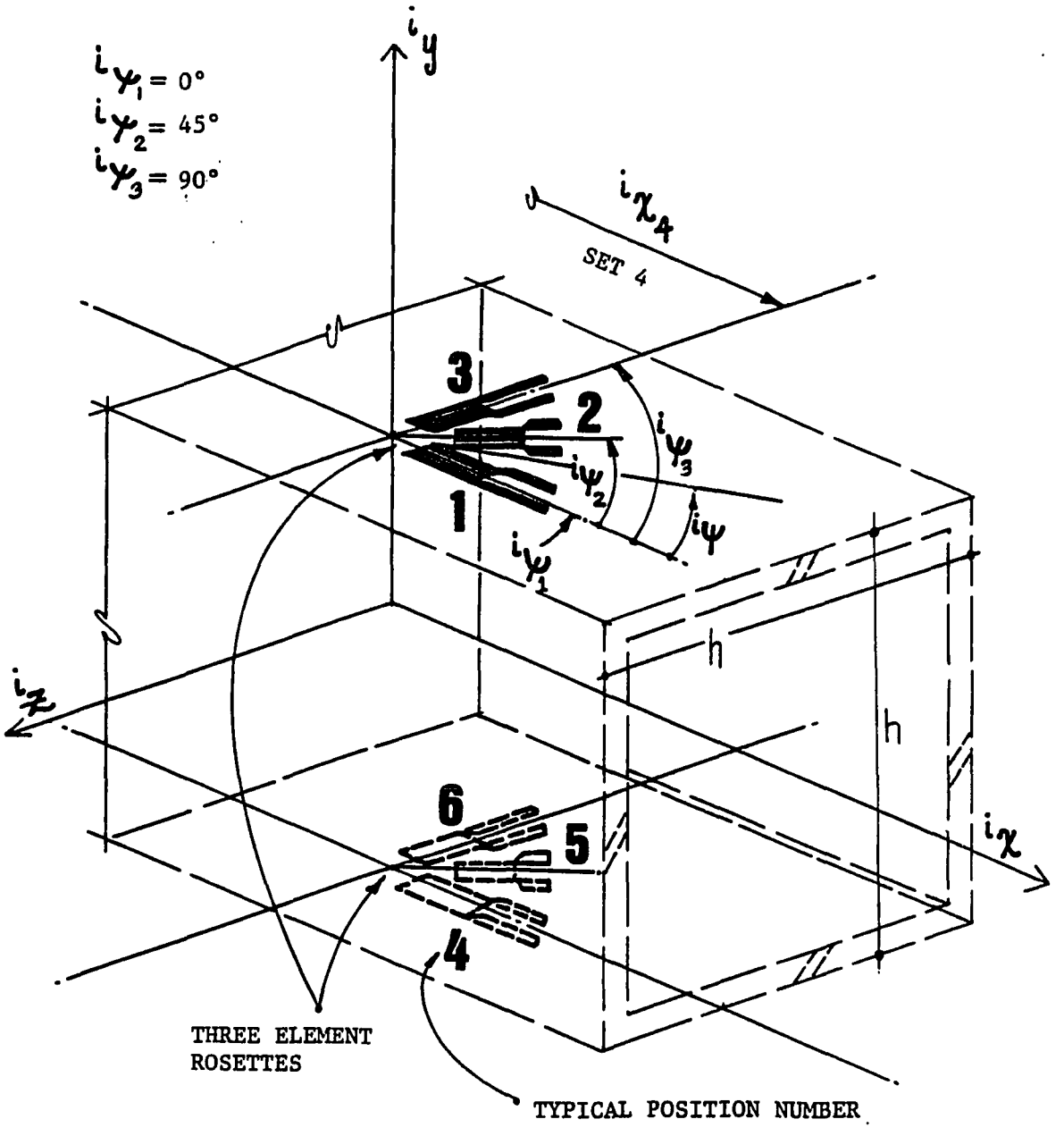

FIGURE 3.4 THREE ELEMENT ROSETTE ORIENTATION

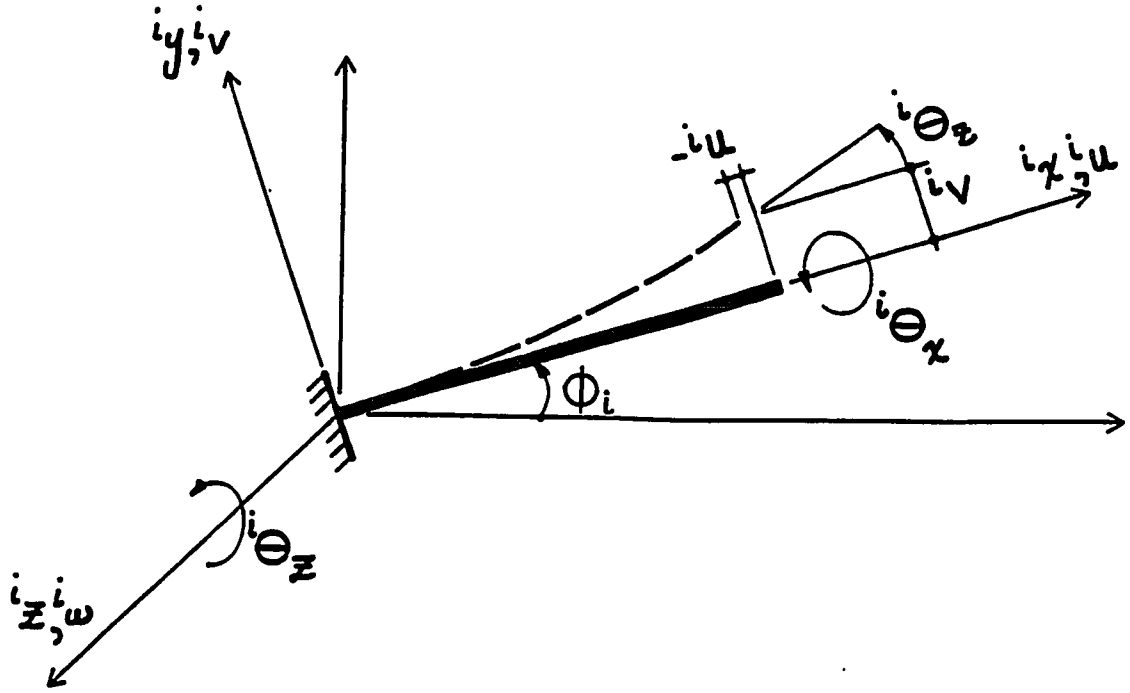

FIGURE 3.5 LINK ELEVATION VIEW AS A CANTILEVER BEAM

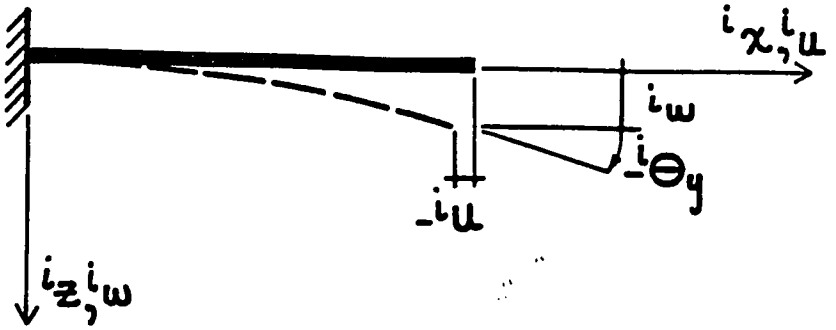

FIGURE 3.6 LINK PLAN VIEW AS A CANTILEVER BEAM

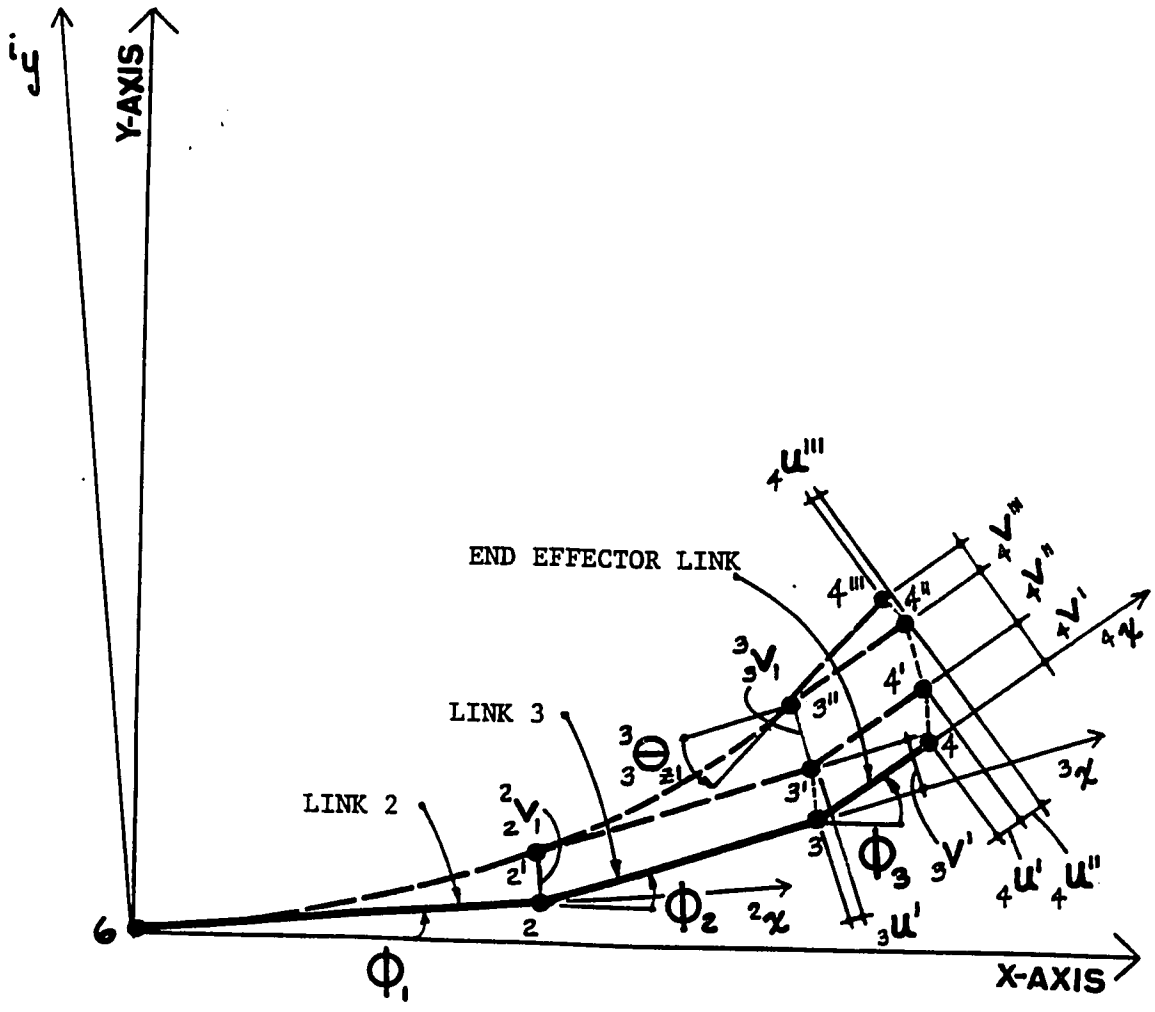

FIGURE 3.7 RIGID BODY MOTION EFFECTS IN $^{i}_{x}{}^{i}_{y}$ PLANE
(REFER TO EQUATIONS 3.48 THROUGH 3.51)

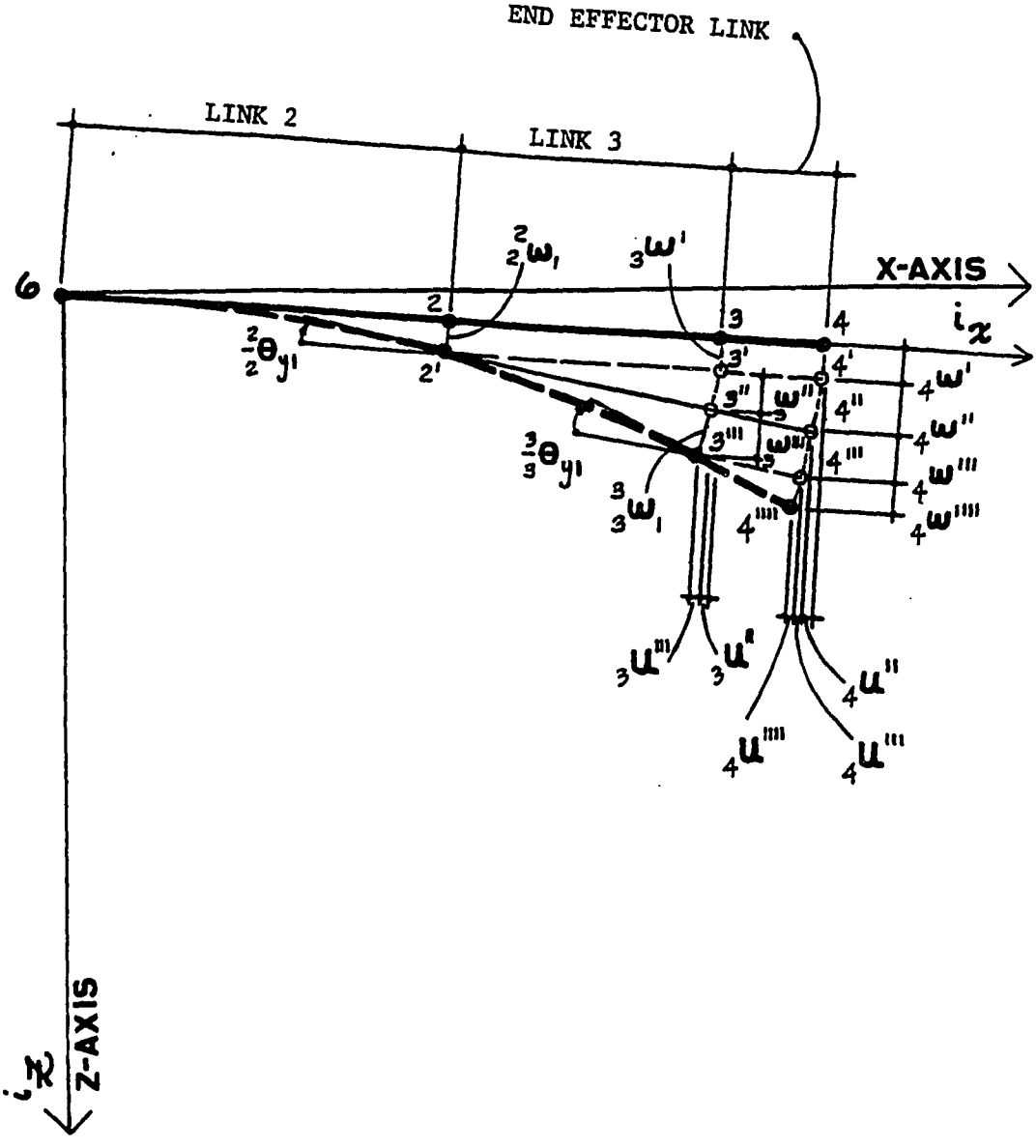

FIGURE 3.8 RIGID BODY MOTION EFFECTS IN $^{i}x^{i}z$ PLANE
(REFER TO EQUATIONS 3.66 THROUGH 3.69)

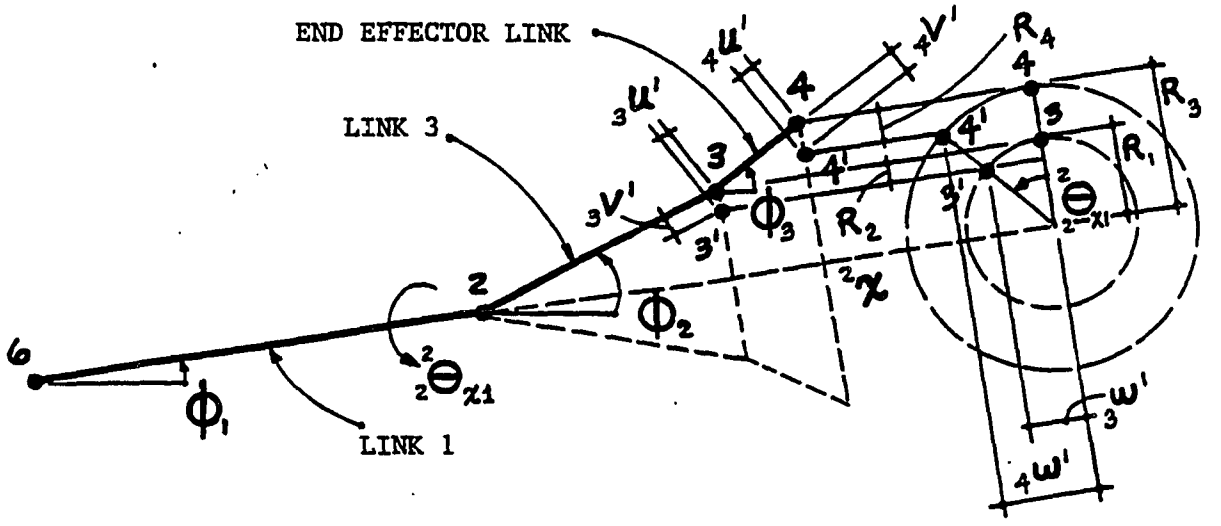

FIGURE 3.9 RIGID BODY MOTION EFFECTS FROM ROTATIONAL DISPLACEMENT ${}^{2}_{2}\Theta_{\chi 1}$
(REFER TO EQUATIONS 3.88 THROUGH 3.95)

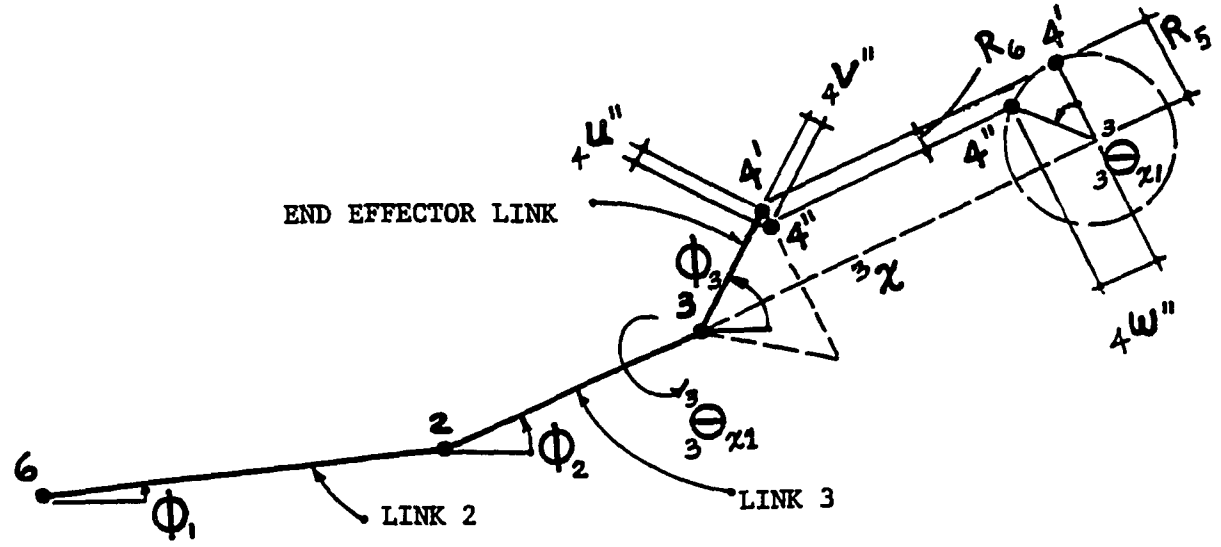

FIGURE 3.10 RIGID BODY MOTION EFFECTS FROM ROTATIONAL DISPLACEMENT ${}^{3}_{3}\Theta_{\chi 1}$
(REFER TO EQUATIONS 3.88 THROUGH 3.95)

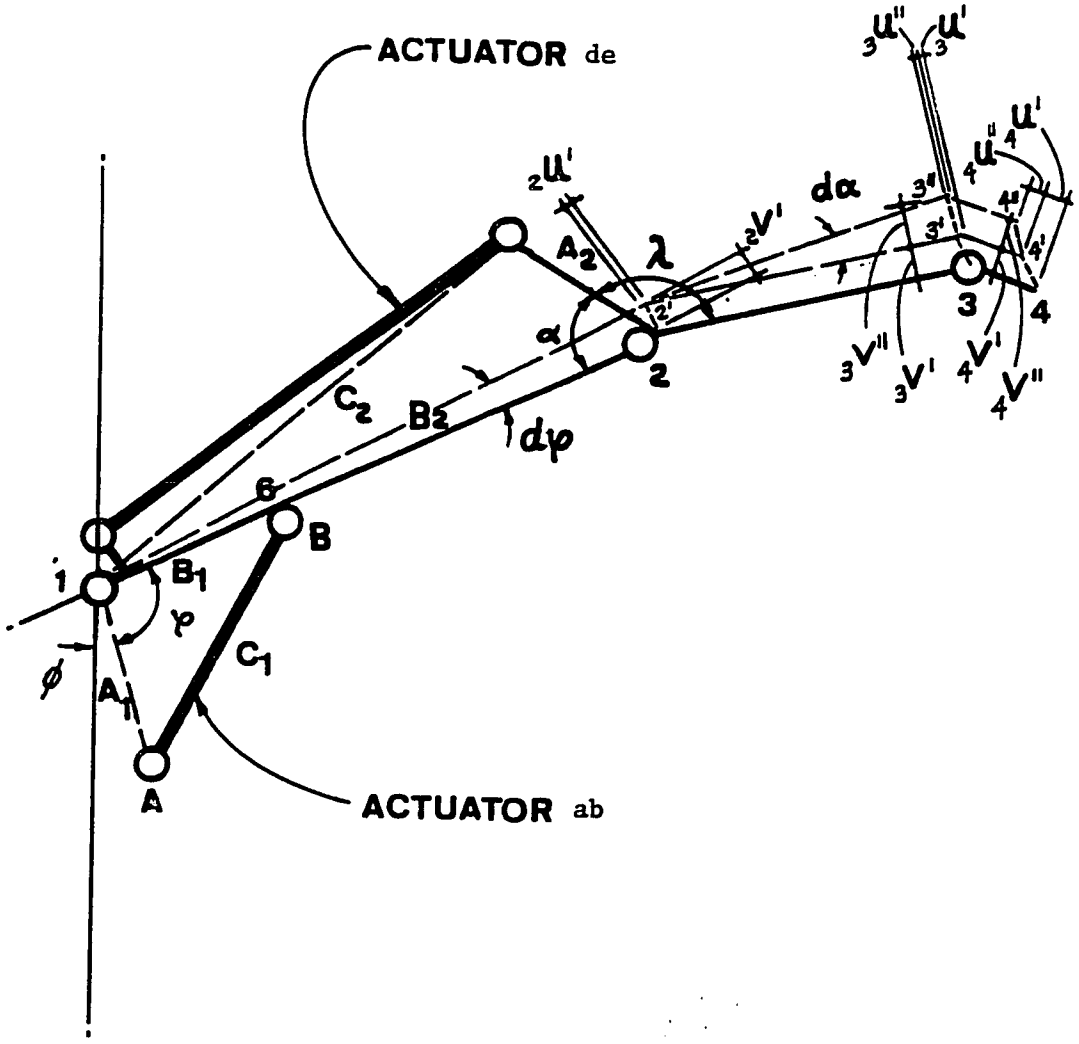

FIGURE 3.11 RIGID BODY MOTION EFFECTS FROM ACTUATOR FLUCTUATIONS
(REFER TO EQUATIONS 3.112 THROUGH 3.117)

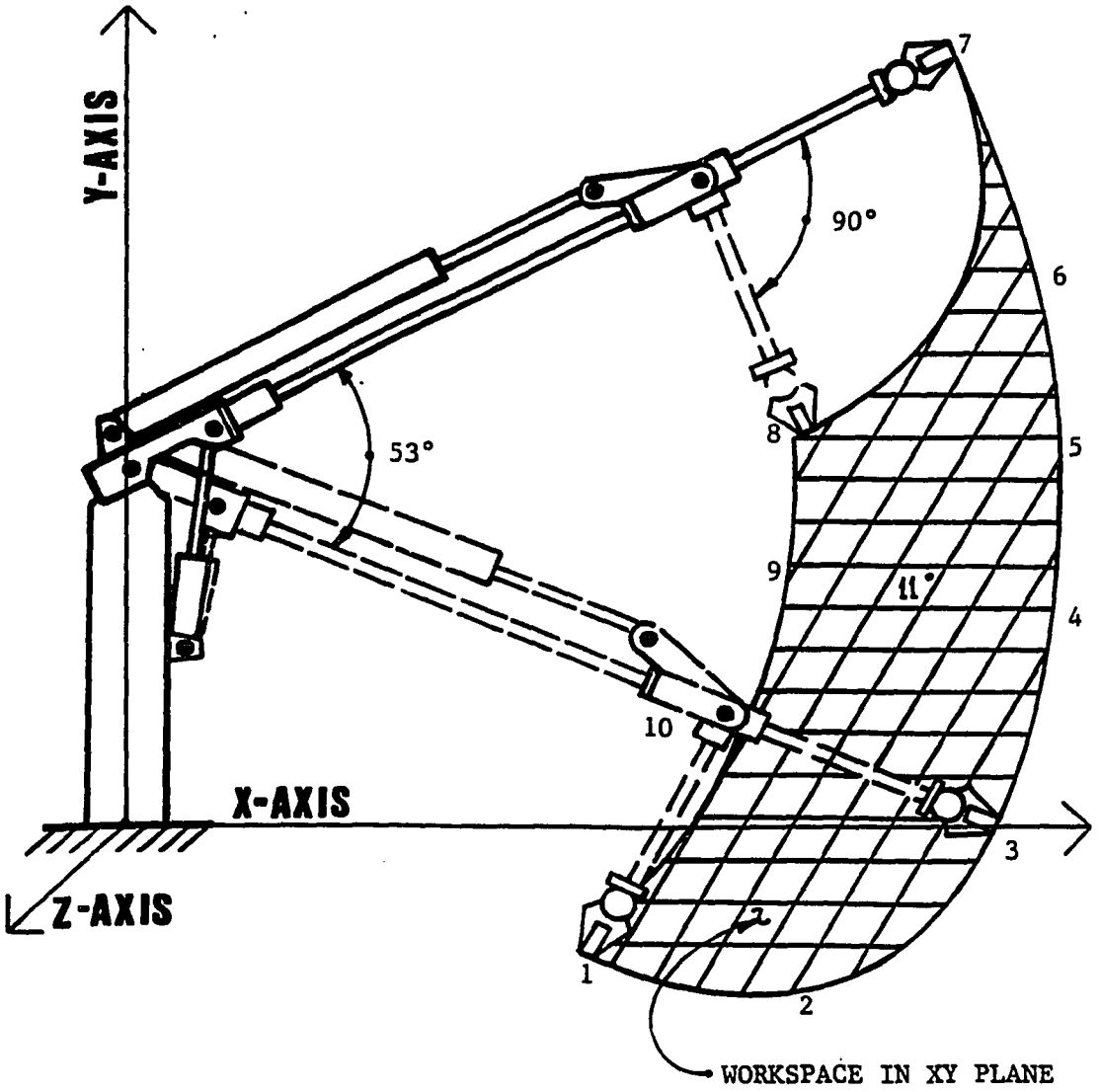

FIGURE 4.1 ELEVATION VIEW SHOWING WORKSPACE ENVELOPE IN XY PLANE

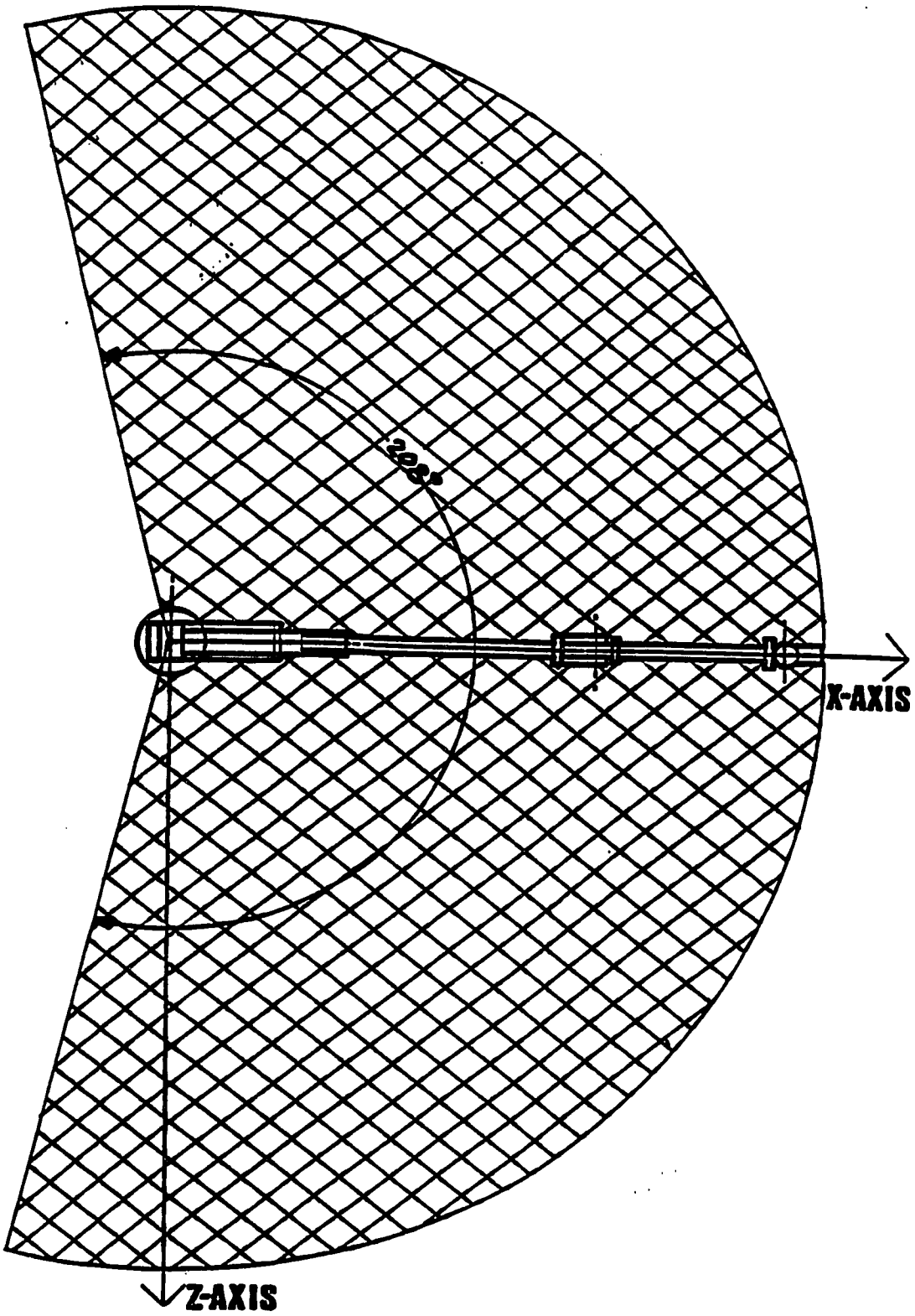

FIGURE 4.2 PLAN VIEW SHOWING WORKSPACE ENVELOPE IN XZ PLANE

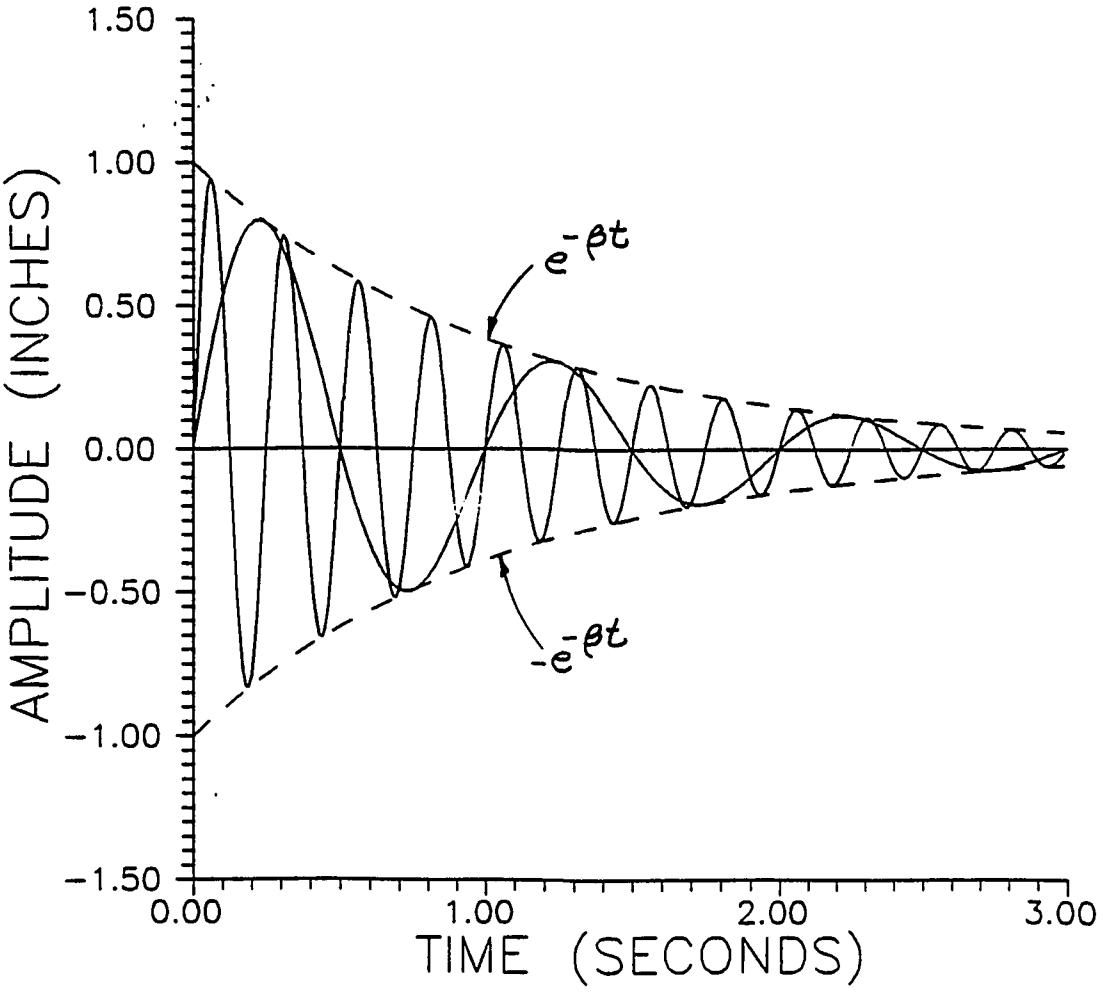

FIGURE 4.3 TWO CURVE FITS HAVING DIFFERENT FREQUENCIES AND THE SAME DAMPING CONSTANT, PASSING THROUGH THE SAME DATA POINTS.

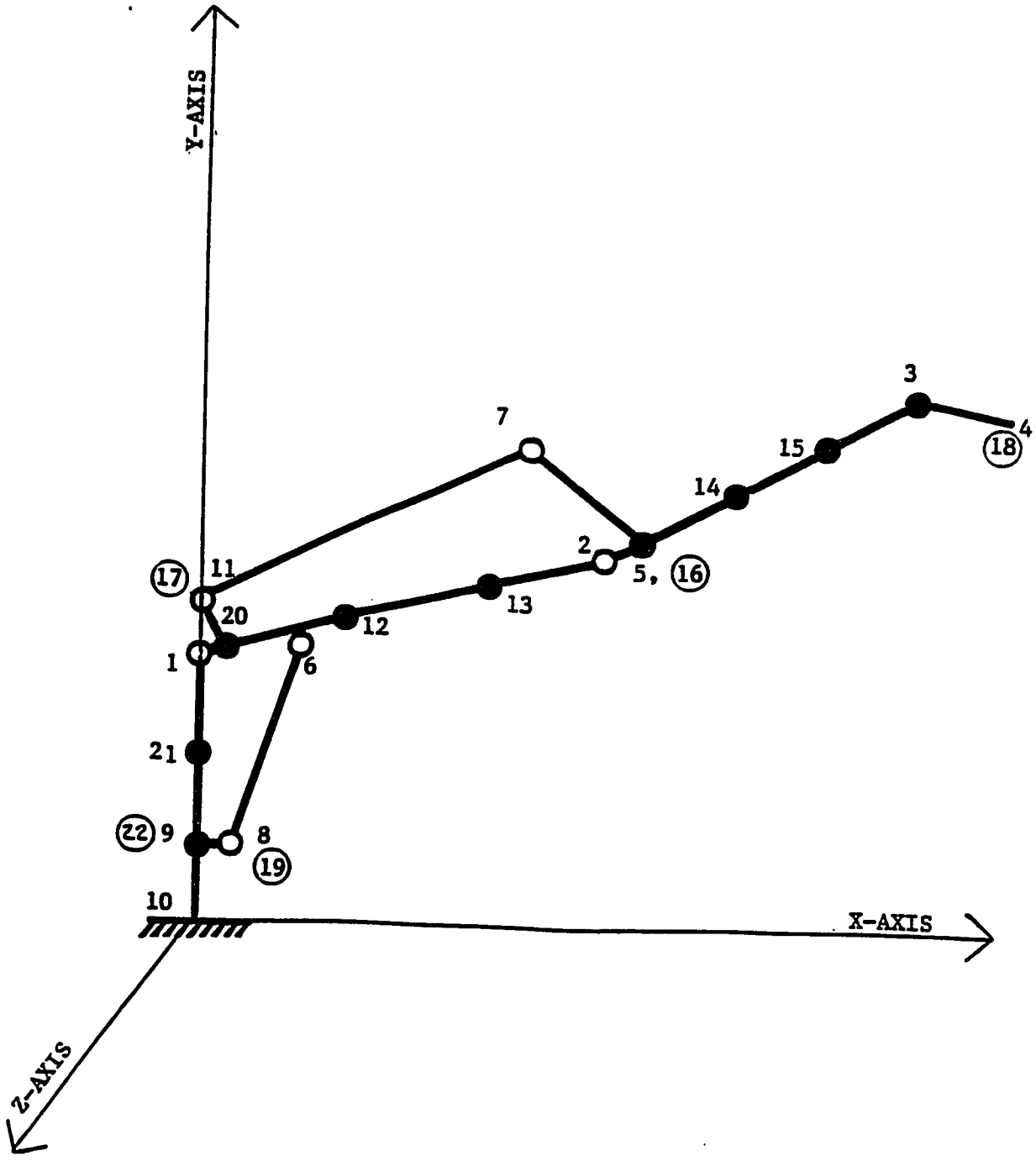

FIGURE 5.1 FINITE ELEMENT MODEL USED IN "GIFTS" PROGRAM

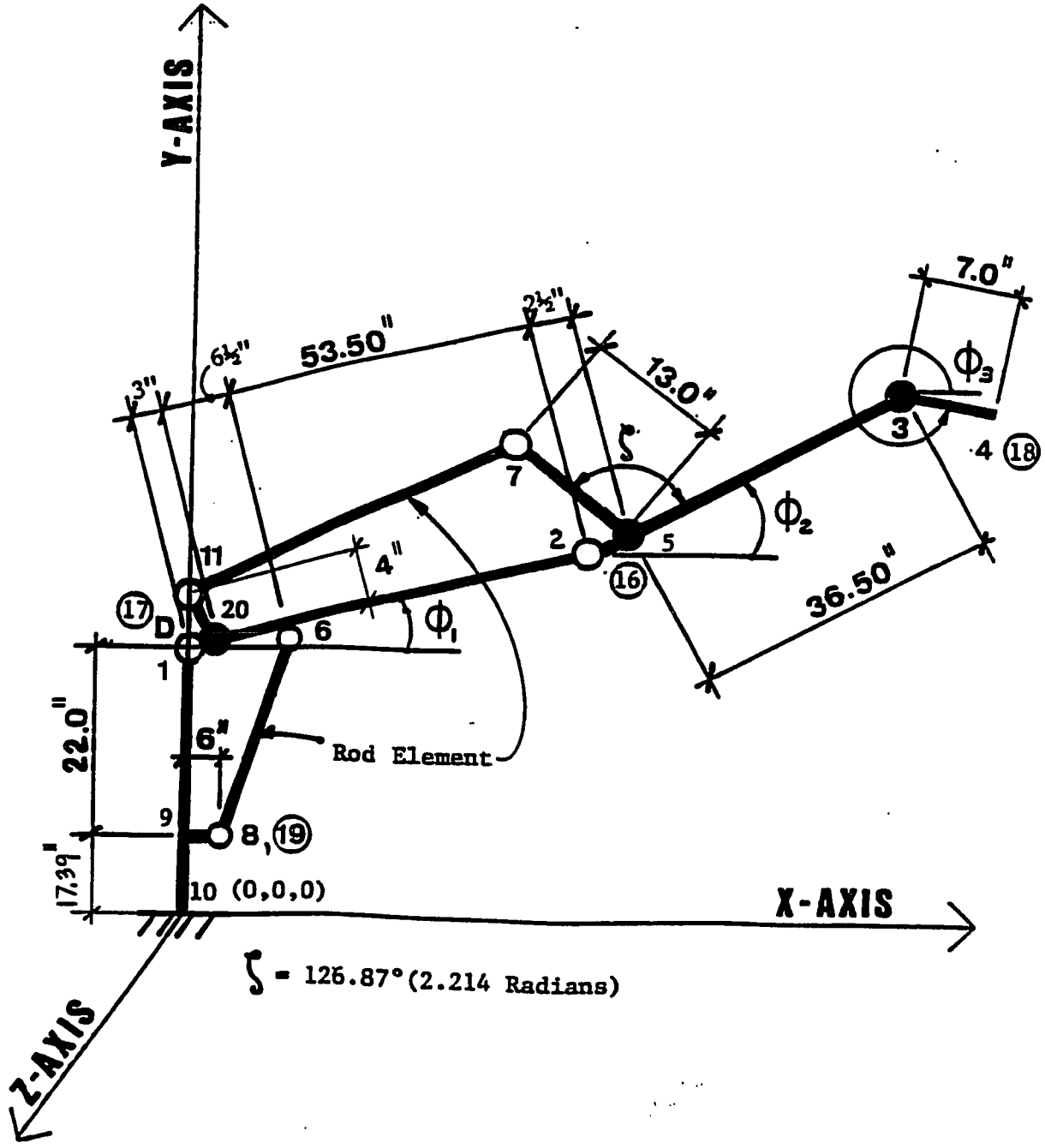

FIGURE 5.2 FINITE ELEMENT GEOMETRY

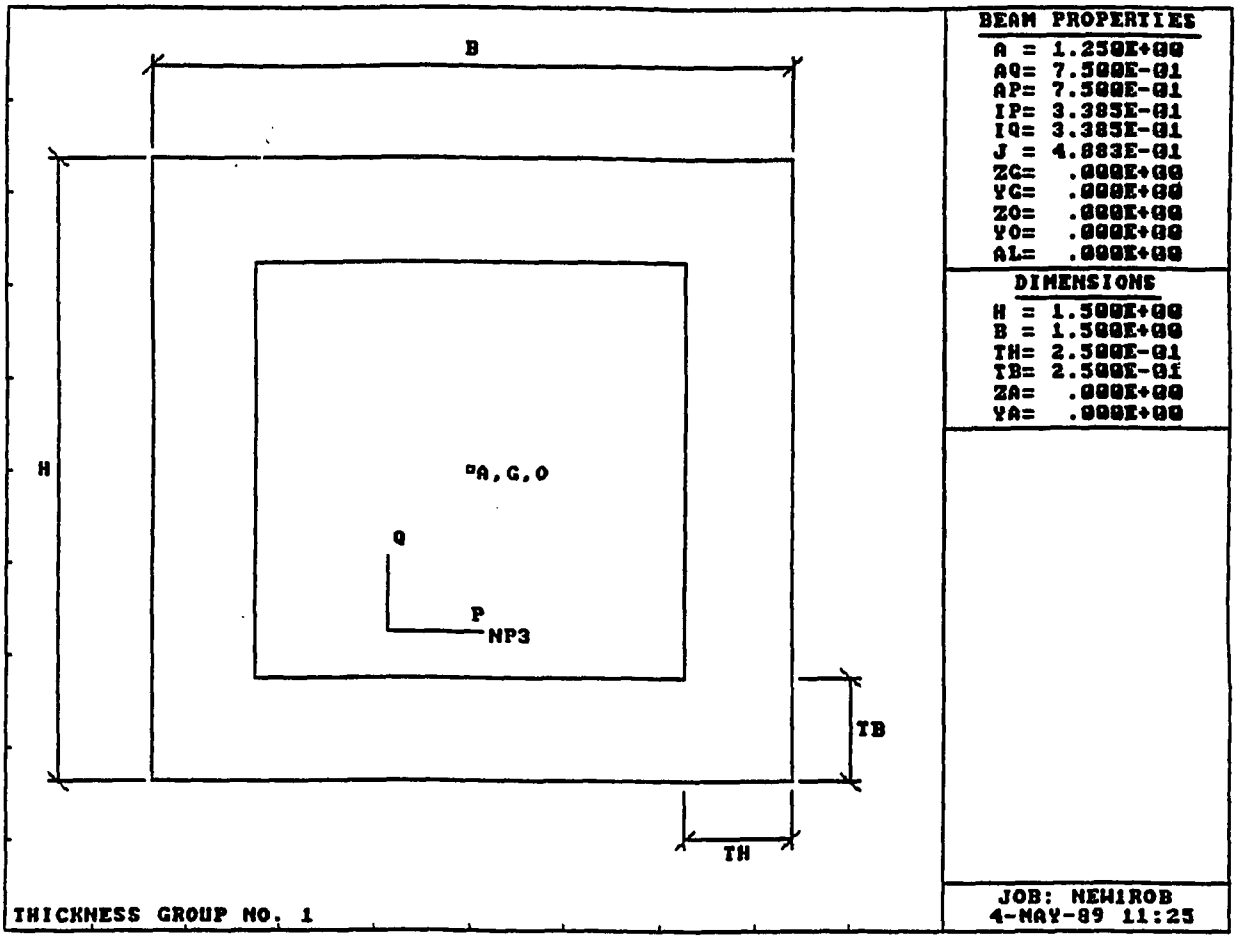

FIGURE 5.3 BEAM ELEMENTS BETWEEN NODES 6-12-13-2 & 5-14-15-3

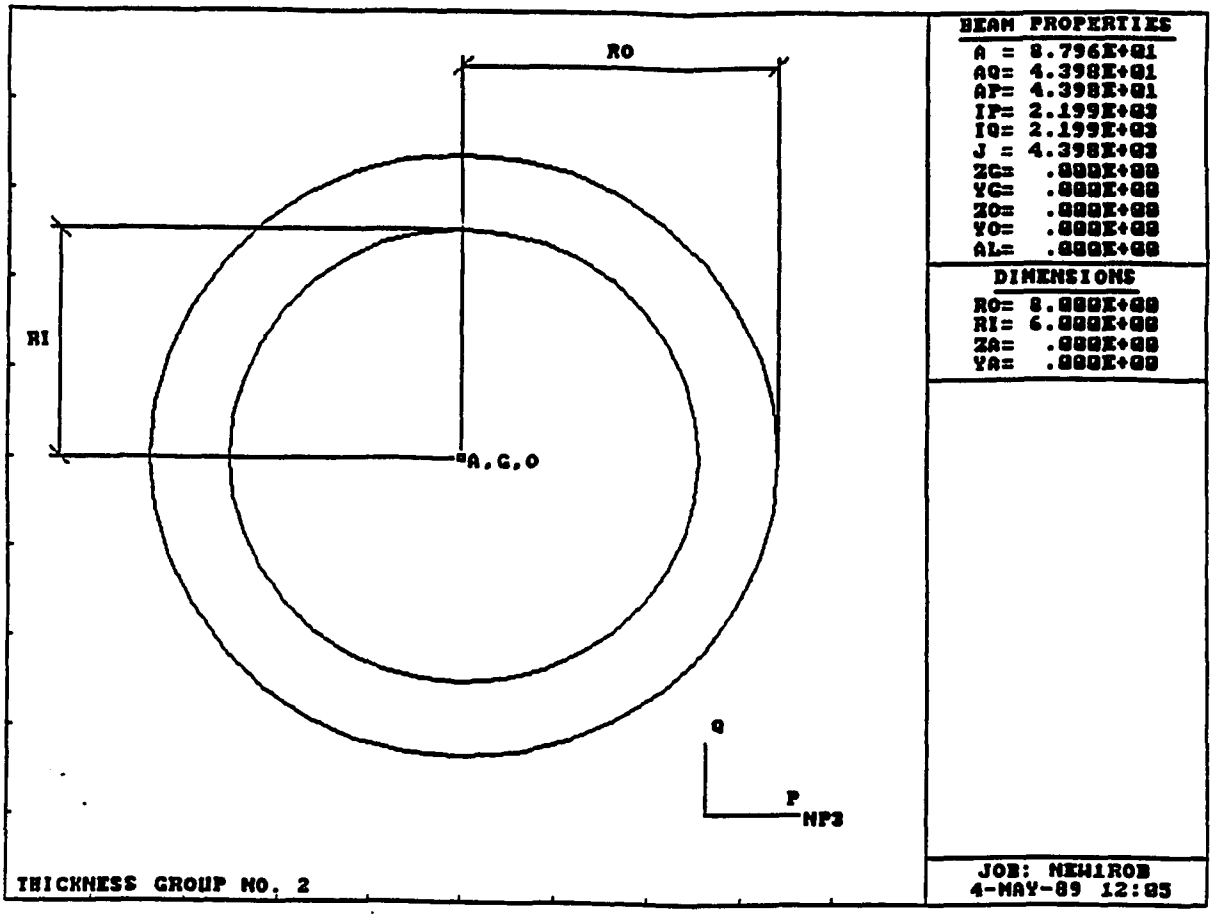

FIGURE 5.4 BEAM ELEMENTS BETWEEN NODES 10-9-21-1

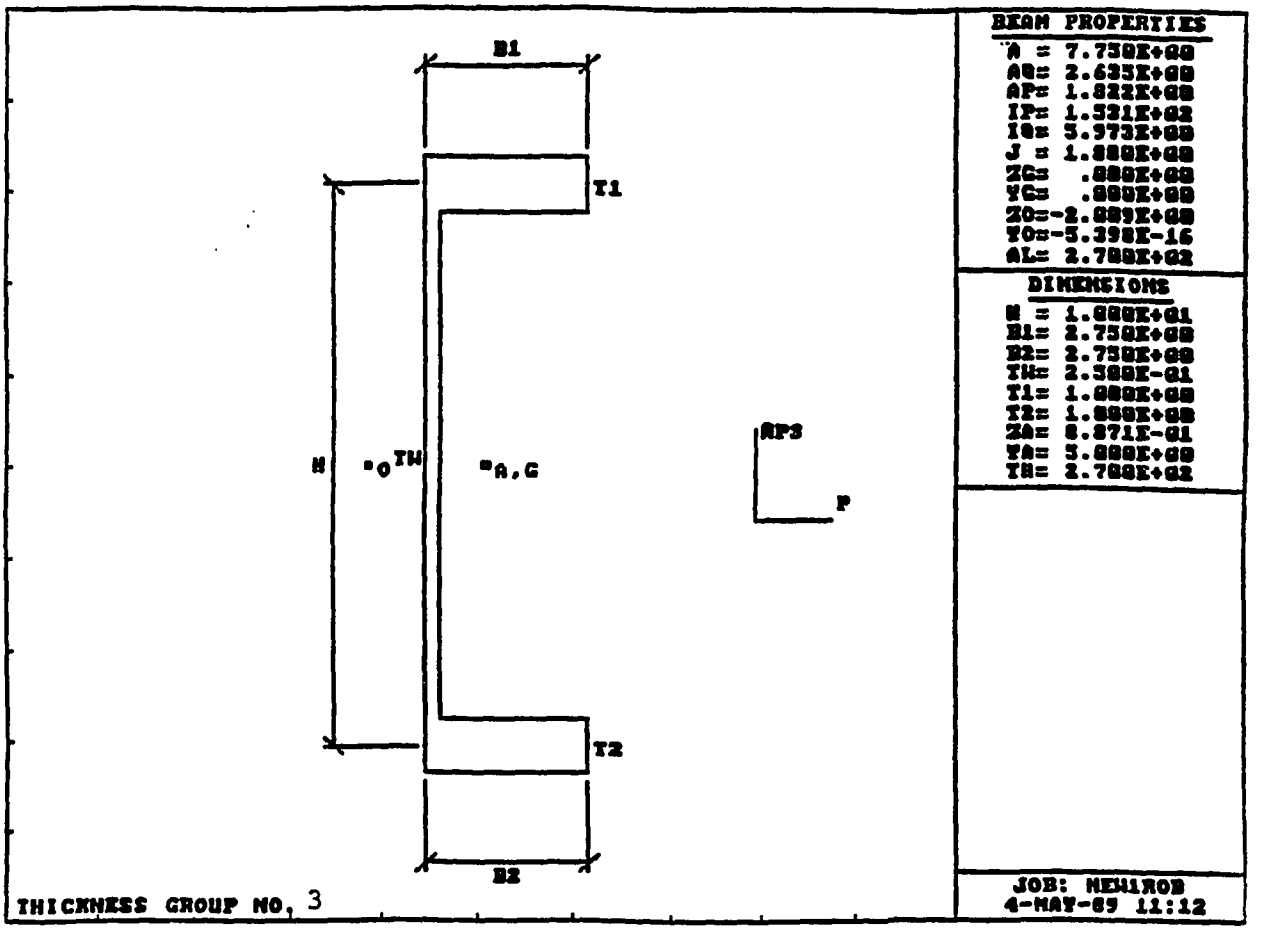

FIGURE 5.5 BEAM ELEMENTS BETWEEN NODES 1 -20-6

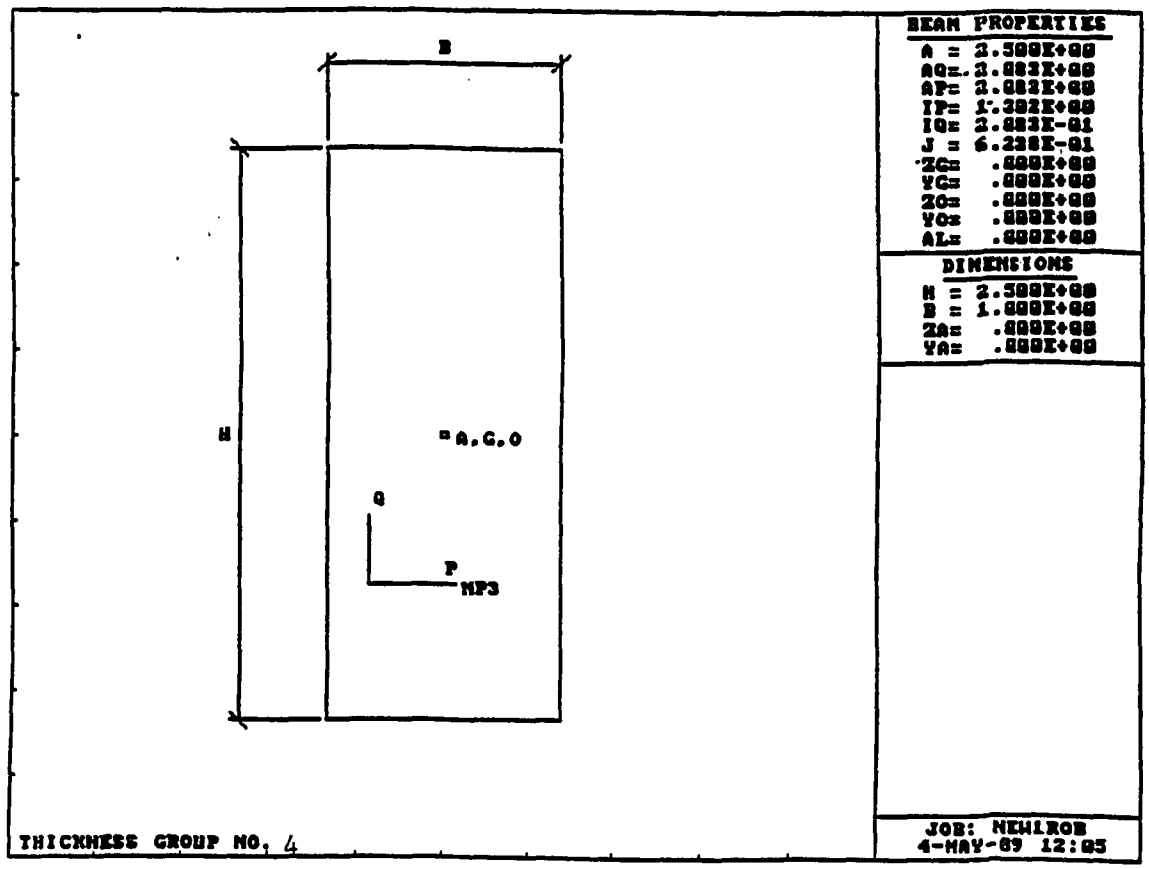

FIGURE 5.6 BEAM ELEMENTS BETWEEN NODES 7 -5

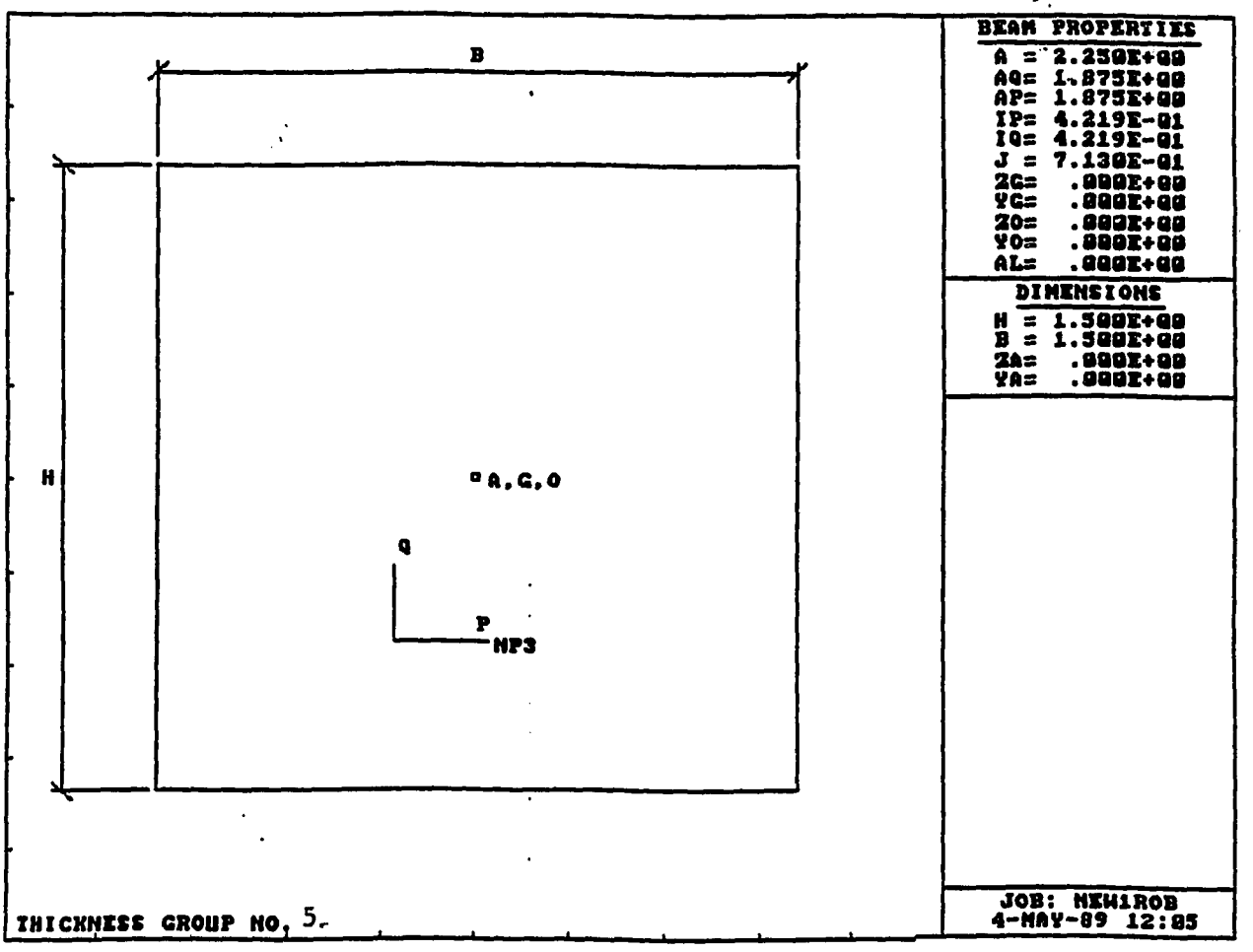

FIGURE 5.7 BEAM ELEMENTS BETWEEN NODES 3-4

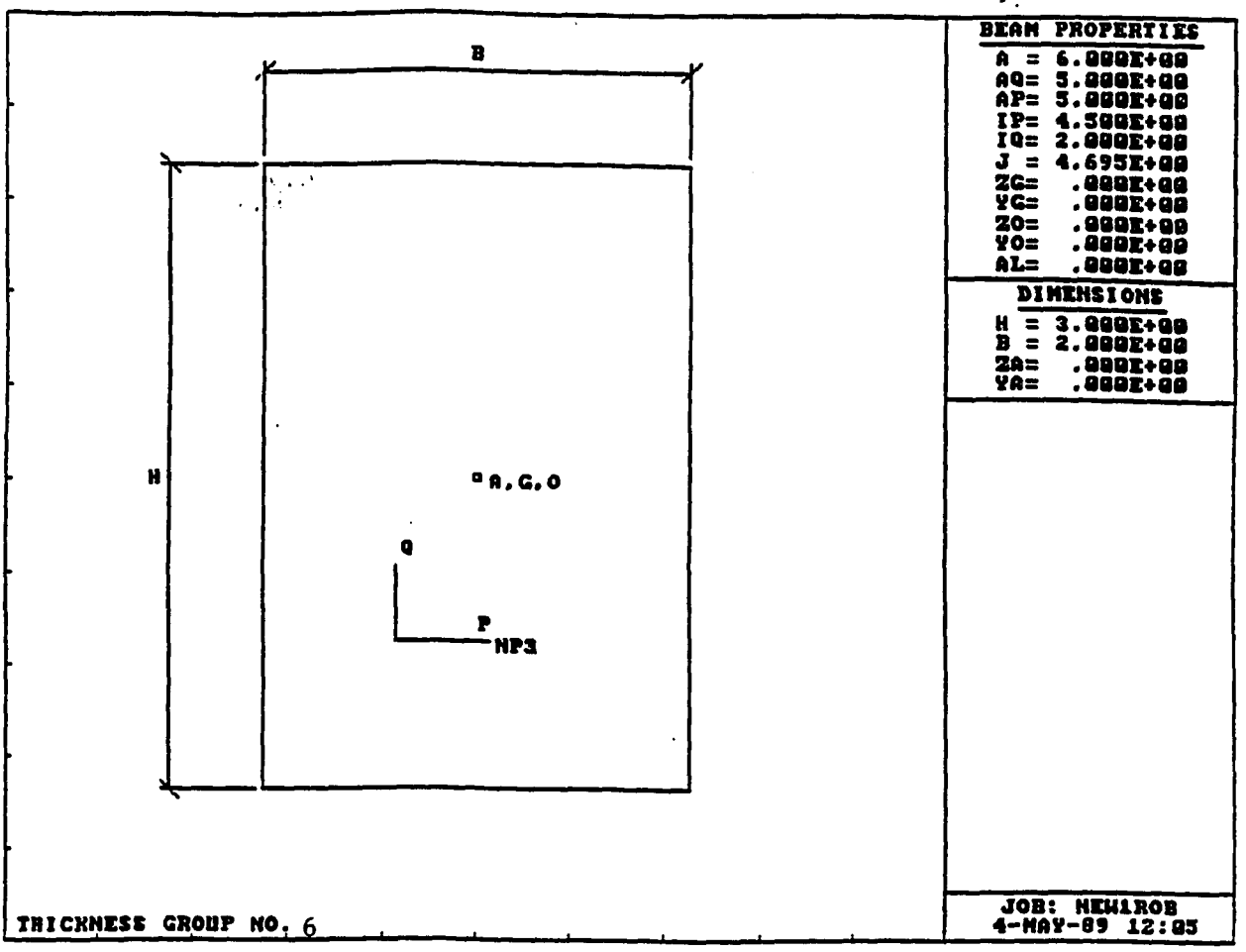

FIGURE 5.8 BEAM ELEMENTS BETWEEN NODES 11-20

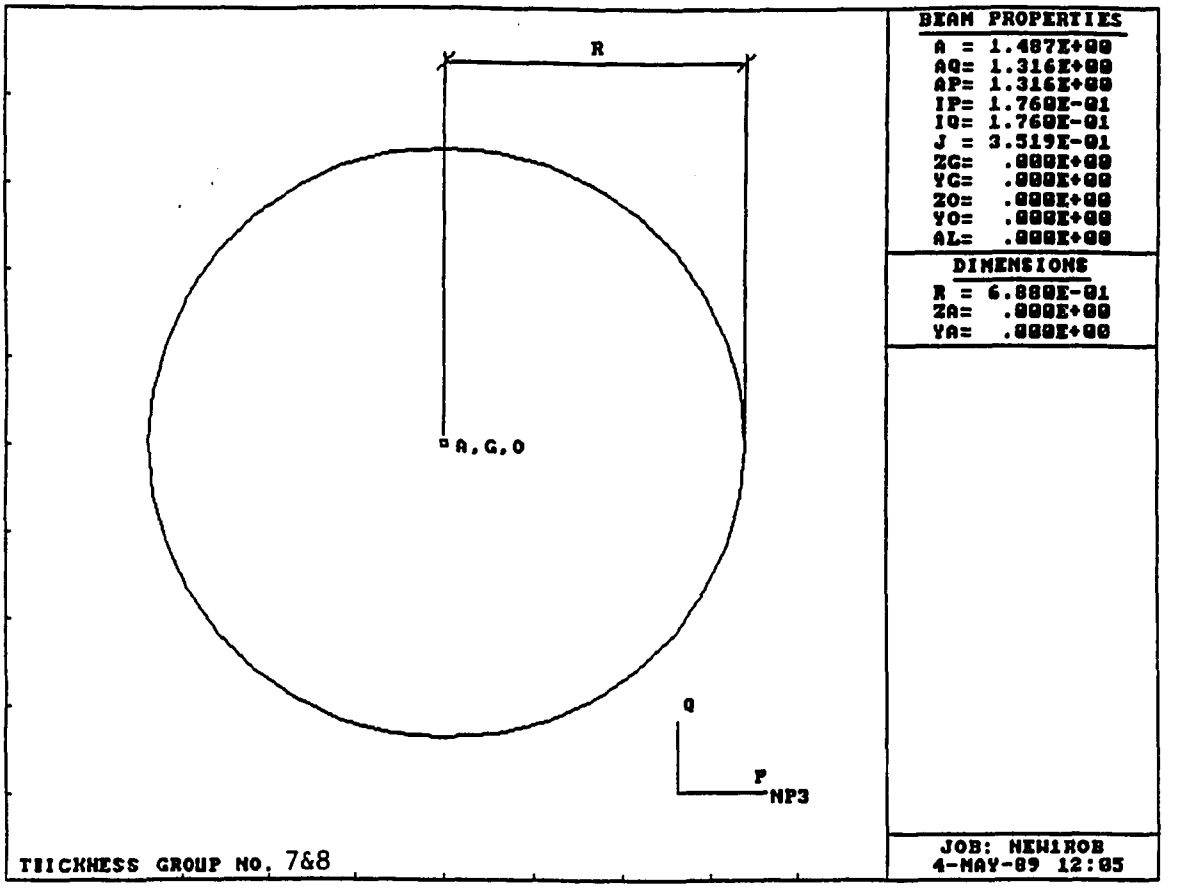

FIGURE 5.9 ROD ELEMENTS BETWEEN NODES 11-7 & 8-6

APPENDIX–B

Fortran77 Program Code "STRAIN.FOR"

NOMENCLATURE

For Fortran77 Program **STRAIN.FOR**

A1 Fixed dimension (figure 3.11, = 22.804 inches).

A2 Fixed dimension (figure 3.11, = 13.0 inches).

AN123 General numerator calculation equations 3.18,3.21,3.24,3.36,& 3.39.

AN4 AN123/DENOM.

ALFA Thesis angle α equation (3.106) figure 3.11.

B1 Fixed dimension (figure 3.11, = 9.50 inches).

B2 Fixed dimension (figure 3.11, = 65.5 inches).

CF(1) Cosine of FE(1) (Thesis ϕ_1).

CF(2) Cosine of FE(2) (Thesis ϕ_2).

CF(3) Cosine of FE(3) (Thesis ϕ_3).

DENOM General denominator calculation equations 3.18,3.21,3.24,3.36,& 3.39.

DALFA Incremental change in ALFA (α) Thesis equation (3.106).

DPHI Incremental change in PHI (φ) Thesis equation (3.96).

Ey(i,j) Strain gage reading from strain gage pair on positive and negative y–face on link i (i=2,3) at location j (j=1,2,3) where:

Ey(2,1) = y–face link 2 location 1 (Thesis ${}^{2}_{y}\epsilon_1$ figure 3.8).

Ey(2,2) = y–face link 2 location 2 (Thesis ${}^{2}_{y}\epsilon_2$ figure 3.8).

Ey(2,3) = y–face link 2 location 3 (Thesis ${}^{2}_{y}\epsilon_3$ figure 3.8).

Ey(3,1) = y–face link 3 location 1 (Thesis ${}^{3}_{y}\epsilon_1$ figure 3.9a).

Ey(3,2) = y–face link 3 location 2 (Thesis ${}^{3}_{y}\epsilon_2$ figure 3.9a).

Ey(3,3) = y–face link 3 location 3 (Thesis ${}^{3}_{y}\epsilon_3$ figure 3.9a).

Ez(i,j) Strain gage reading from strain gage pair on positive and negative

z–face on link i (i=2,3) at location j (j=1,2,3) where:

Ez(2,1) = z–face link 2 location 1 (Thesis ${}^{2}_{z}\epsilon_{1}$ figure 3.8).

Ez(2,2) = z–face link 2 location 2 (Thesis ${}^{2}_{z}\epsilon_{2}$ figure 3.8).

Ez(2,3) = z–face link 2 location 3 (Thesis ${}^{2}_{z}\epsilon_{3}$ figure 3.8).

Ez(3,1) = z–face link 3 location 1 (Thesis ${}^{3}_{z}\epsilon_{1}$ figure 3.9a).

Ez(3,2) = z–face link 3 location 2 (Thesis ${}^{3}_{z}\epsilon_{2}$ figure 3.9a).

Ez(3,3) = z–face link 3 location 3 (Thesis ${}^{3}_{z}\epsilon_{3}$ figure 3.9a).

ERR1 Fluctuation in fluid flow rate in actuator ab in units of strain.

ERR2 Fluctuation in fluid flow rate in actuator de in units of strain.

FE(1) Angle ϕ_1 in the XY global plane at joint 1 (figure 3.1).

FE(2) Angle ϕ_2 in the XY global plane at joint 2 (figure 3.1).

FE(3) Angle ϕ_3 in the XY global plane at joint 3 (figure 3.1).

FE21 Angle ϕ_2 minus ϕ_1.

FE31 Angle ϕ_3 minus ϕ_1.

FE32 Angle ϕ_3 minus ϕ_2.

GAMA(2) Shear strain from rosette gage set at X4 link 2 (figure 3.8).

GAMA(3) Shear strain from rosette gage set at X4 link 3 (figure 3.9a).

h Out to out dimension of the steel tube for link 2 and 3 along the y and z axes set at 1.50 inches.

PI Archemedes' number π.

PHI Thesis angle φ figure 3.11.

QXL(2,1) Angular rotational displacement ${}^{2}_{2}\theta_{x1}$ at joint 2 in local x–direction.

QXL(3,1) Angular rotational displacement ${}^{3}_{3}\theta_{x1}$ at joint 3 in local x–direction.

QYL(2,1) Angular rotational displacement ${}^{2}_{2}\theta_{y1}$ at joint 2 in local y–direction.

QYL(3,1) Angular rotational displacement ${}^{3}_{3}\theta_{y1}$ at joint 3 in local y–direction.

QZL(2,1) Angular rotational displacement ${}^{2}_{2}\theta_{z1}$ at joint 2 in local z–direction.

QZL(3,1)	Angular rotational displacement ${}^{3}_{3}\theta_{z1}$ at joint 3 in local z–direction.
R20	Rosette gage set orientated at 0^{o} to the local x–axis link 2.
R245	Rosette gage set orientated at 45^{o} to the local x–axis link 2.
R290	Rosette gage set orientated at 90^{o} to the local x–axis link 2.
R30	Rosette gage set orientated at 0^{o} to the local x–axis link 3.
R345	Rosette gage set orientated at 45^{o} to the local x–axis link 3.
R390	Rosette gage set orientated at 90^{o} to the local x–axis link 3.
SF(1)	Sine of FE(1) (Thesis ϕ_1).
SF(2)	Sine of FE(2) (Thesis ϕ_2).
SF(3)	Sine of FE(3) (Thesis ϕ_3).
UL(2,1)	Local axial displacement ${}^{2}_{2}u_1$ at joint 2.
UL(3,1)	Local axial displacement ${}^{3}_{3}u_1$ at joint 3.
ULT(2)	Sum of all local displacements in the x–direction at joint 2 in relation to link 2.
ULT(3)	Sum of all local displacements in the x–direction at joint 3 in relation to link 3.
ULT(4)	Sum of all local displacements in the x–direction at EECP 4 in relation to link 4.
VL(2,1)	Local flexural displacement ${}^{2}_{2}v_1$ at joint 2.
VL(3,1)	Local flexural displacement ${}^{3}_{3}v_1$ at joint 3.
VLT(2)	Sum of all local displacements in the y–direction at joint 2 in relation to link 2.
VLT(3)	Sum of all local displacements in the y–direction at joint 3 in relation to link 3.
VLT(4)	Sum of all local displacements in the y–direction at EECP 4 in relation to link 4.

WL(2,1) Local flexural displacement ${}^{2}_{2}w_{1}$ at joint 2.

WL(3,1) Local flexural displacement ${}^{3}_{3}w_{1}$ at joint 3.

WLT(2) Sum of all local displacements in the z–direction at joint 2 in relation o link 2.

WLT(3) Sum of all local displacements in the z–direction at joint 3 in relation to link 3.

WLT(4) Sum of all local displacements in the z–direction at EECP 4 in relation to link 4.

XLAM The angle *lamda* between link 3 and the actuator de connector arm (figure 3.1, $\lambda = 126.87^{o}$).

XL(2) Length in inches of link 2 (figure 3.1, XL(2)=56.0").

XL(3) Length in inches of link 3 (figure 3.1, XL(3)=36.5").

XL(4) Length in inches of the end effector link (figure 3.1, XL(3)=7.0").

X(i,j) Location j (j=1,2,3) of single element strain gage sets from the clamped end of link i (i=2,3) where:

X(2,1) = 7.0" (figure 3.8).

X(2,2) = 22.0" (figure 3.8).

X(2,3) = 43.0" (figure 3.8).

X(3,1) = 2.5" (figure 3.9a).

X(3,2) = 15.0" (figure 3.9a).

X(3,3) = 29.0" (figure 3.9a).

XG(1) Initial location of Joint 1 along the global x–axis.

XG(2) Initial location of Joint 2 along the global x–axis.

XG(3) Initial location of Joint 3 along the global x–axis.

XG(4) Initial location of the *end effector center point* 4 along the global x–axis.

XX(2)	Global X coordinate of joint 2.
XX(3)	Global X coordinate of joint 3.
XX(4)	Global X coordinate of EECP 4.
YG(1)	Initial location of Joint 1 along the global y–axis.
YG(2)	Initial location of Joint 2 along the global y–axis.
YG(3)	Initial location of Joint 3 along the global y–axis.
YG(4)	Initial location of the *end effector center point* 4 along the global y–axis.
YY(2)	Global Y coordinate of joint 2.
YY(3)	Global Y coordinate of joint 3.
YY(4)	Global Y coordinate of EECP 4.
Z1	h/2.0.
ZG(1)	Initial location of Joint 1 along the global z–axis.
ZG(2)	Initial location of Joint 2 along the global z–axis.
ZG(3)	Initial location of Joint 3 along the global z–axis.
ZG(4)	Initial location of the *end effector center point* 4 along the global z–axis.
ZZ(2)	Global Z coordinate of joint 2.
ZZ(3)	Global Z coordinate of joint 3.
ZZ(4)	Global Z coordinate of joint 4.

```
c  filename ----------"STRAIN.FOR"
c
c  ********************************************************
c  * THIS PROGRAM WAS WRITTEN BY ROBERT F. MARCEAU FOR THE *
c  * DEGREE OF MASTERS OF SCIENCE IN CIVIL ENGINEERING AT  *
c  * THE UNIVERSITY OF NEVADA, LAS VEGAS.                  *
c  ********************************************************
c  PROGRAM WRITTEN IN FORTRAN77 TO DETERMINE DISPLACEMENTS
c  AT EACH JOINT UTILZING STRAIN GAGES AND LAGRANGE
c  POLYNOMIALS FOR A THREE-LINK ROBOTIC MECHANISM.
c
c  ASSUMPTIONS:
c    1) Tension is assumed positive and Compression is
c       negative .
c    2) I have assumed that the strain gage readings are +
c       for tensile strain and - for compressive strain.
c    3) All rotations are + counter-clockwize (right hand
c       rule).
c    4) All displacements follow right hand rule +.
c    5) Any link deformations associated with the end
c       effector link are considered negligible.
c    6) All angles are measured counter-clockwize + from
c       horizontal global X-axis.
c
c                       *PROGRAM KEY*
c
c  Key for joint displacements resulting from static and
c  dynamic forces and rigid body motions.
c  Example: UL(j,s)
c    The first letter indicates axis displacement direction
c    (u,v,w = x,y,z)
c    The second letter (L or G)
c       L = implys LOCAL coordinates
c       G = implys GLOBAL coordinates
c    The third letter indicates the joint number.
c    The fourth letter indicates the displacement
c    designation corresponding to separate displacements as
c    noted in Thesis sections 3.2.1 through 3.2.6.
c
      DIMENSION X(3,3),DX(3,5),DENOM(3),AN4(3),XL(4),FE(3)
      DIMENSION Ey(3,3),Ez(3,3),CF(3),SF(3),XG(4),YG(4)
      DIMENSION ZG(4),UL(5,10),VL(5,10),WL(5,10),GAMA(3)
      DIMENSION QXL(5,10),QYL(5,10),QZL(5,10),XX(5),YY(5)
      DIMENSION ZZ(5),ULT(5),VLT(5),WLT(5),QXLT(5),QYLT(5)
      DIMENSION QZLT(5),UG(5),VG(5),WG(5),QXG(5),QYG(5)
      DIMENSION QZG(5)
      DOUBLE PRECISION E,Ey,Ez
      DOUBLE PRECISION R20,R245,R290,R30,R345,R390
      OPEN(UNIT=1,FILE='GEN1.DAT',STATUS='OLD')
      OPEN(UNIT=6,FILE='GEN1.OUT',STATUS='NEW')
c
c ******************* FORMAT STATEMENTS ******************
c
 1000 FORMAT(4F12.6)
```

```
 1002 FORMAT(3F20.17)
 1005 FORMAT(3F15.6)
 1006 FORMAT(6F10.4)
 1999 FORMAT(/'                          *** INPUT ***')
 2000 FORMAT(' ENCODER SENSOR READINGS FE1,FE2,& FE3,(radian
     1s)')
 2010 FORMAT(/' STRAIN GAGE READINGS @ X1,X2,X3 (Y-FACE) lin
     1k 2.')
 2020 FORMAT(/' STRAIN GAGE READINGS @ X1,X2,X3 (Z-FACE) lin
     1k 2.')
 2030 FORMAT(/' STRAIN GAGE READINGS @ X1,X2,X3 (Y-FACE) lin
     1k 3.')
 2040 FORMAT(/' STRAIN GAGE READINGS @ X1,X2,X3 (Z-FACE) lin
     1k 3.')
 2050 FORMAT(/' ROSETTE GAGE READINGS @ X4 (Y-FACE) link 2.'
     1)
 2060 FORMAT(/' ROSETTE GAGE READINGS @ X4 (Y-FACE) link 3.'
     1)
 2090 FORMAT(/' FLUCTUATION IN ACTUATOR ab & de (units of st
     1rain)')
 2061 FORMAT(///'                          *** OUTPUT ***')
 2200 FORMAT(//' *SUMMARY OF LOCAL JOINT DISPLACEMENTS*')
 2300 FORMAT(/' Local Displacements at Joint 2.')
 2400 FORMAT(/' Local Displacements at Joint 3.')
 2500 FORMAT(/' Local Displacements at EECP 4.')
 2700 FORMAT(//' *SUMMARY OF GLOBAL JOINT DISPLACEMENTS*')
 2800 FORMAT(/' Global Displacements at Joint 2.')
 2900 FORMAT(/' Global Displacements at Joint 3.')
 3000 FORMAT(/' Global Displacements at EECP 4.')
 3100 FORMAT(//' *LOCATION OF JOINTS 2,3 AND EECP 4 IN XYZ C
     1OORDINATES*')
 3200 FORMAT(/' Final Location of Joint 2. (X,Y,Z)')
 3300 FORMAT(/' Final Location of Joint 3. (X,Y,Z)')
 3400 FORMAT(/' Final Location of EECP 4. (X,Y,Z)')
C
C ********************************************************
C  All fixed robot dimensions are defined here as noted:
C  For reference see chapter 3 figures.
C
C  XL(2) = length in inches of link No. 2.
C  XL(3) = length in inches of link No. 3.
C  XL(4) = length in inches of the end effector link.
C  h     = out to out dimension of steel tube cross sections
C          of link No. 2 and No. 3.(Same for both)
C  XLAM  = greek symbol lamda see figure 3.1
C  A1    = see figure 3.11
C  A2    = see figure 3.11
C  B1    = see figure 3.11
C  B2    = see figure 3.11
C  X(2,1)= location from clamped end on link No. 2 of single
C          element strain gage set at x1 (figure 3.8).
C  X(2,2)= location from clamped end on link No. 2 of single
C          element strain gage set at x2 (figure 3.8).
C  X(2,3)= location from clamped end on link No. 2 of single
```

```
c          element strain gage set at x3 (figure 3.8).
c  X(3,1)= location from clamped end on link No. 3 of single
c          element strain gage set at x1 (figure 3.9a).
c  X(3,2)= location from clamped end on link No. 3 of single
c          element strain gage set at x2 (figure 3.9a).
c  X(3,3)= location from clamped end on link No. 3 of single
c          element strain gage set at x3 (figure 3.9a).
c ***********************************************************
c
      XL(2)=56.0
      XL(3)=36.50
      XL(4)=7.0
      A1=22.804
      A2=13.0
      B1=9.50
      B2=65.50
      h=1.5
      XLAM=2.21430
      X(2,1)=7.0
      X(2,2)=22.0
      X(2,3)=43.0
      X(3,1)=2.5
      X(3,2)=15.0
      X(3,3)=29.0
      PI=3.14159265
c
c ***********************************************************
c     The angles in global about the z-axis at joints 1,2,
c     and 3 are FE(1),FE(2),and FE(3). Encoder sensors on
c     the robot read these angles as a function of time and
c     this input must be input at this point in this
c     program.
c ***********************************************************
c
      READ(1,1000)FE(1),FE(2),FE(3)
      FE21=FE(2)-FE(1)
      FE31=FE(3)-FE(1)
      FE32=FE(3)-FE(2)
      WRITE(6,1999)
      WRITE(6,2000)
      WRITE(6,1005)FE(1),FE(2),FE(3)
c
c ***********************************************************
c          SINGLE ELEMENT STRAIN GAGE SETS:
c
c     Key for strain gage notation: Ey(i,j)
c     Where:
c           y  The second letter designates the strain gage
c              set plane (either y or z face plane).
c           i  The third letter relates to the link number
c              (2 for link 2 and 3 for link 3).
c           j  The fourth letter relates to the position of
c              the strain gage sets on link 2 & 3 from the
c              clamped end (j=1,2,3 for x1,x2,and x3
```

```
c              figure 3.8 & 3.9a).
c ***********************************************************
c
      DO 10 i=2,3
      READ(1,1002)(Ey(i,j),j=1,3)
      READ(1,1002)(Ez(i,j),j=1,3)
      IF (i-2) 11,11,12
   11 WRITE(6,2010)
      GO TO 13
   12 WRITE(6,2030)
   13 WRITE(6,1002)(Ey(i,j),j=1,3)
      IF (i-2) 14,14,15
   14 WRITE(6,2020)
      GO TO 16
   15 WRITE(6,2040)
   16 WRITE(6,1002)(Ez(i,j),j=1,3)
   10 CONTINUE
c
c ***********************************************************
c          THREE ELEMENT ROSETTE STRAIN GAGES:
c
c     Strain readings from the rosettes for each link at
c     each location 2 and 3 include three pairs of readings
c     at each location.
c     2 location is on link No. 2 from left to right at x4
c     (figure 3.6).
c     3 location is on link No. 3 from left to right at x4
c     (figure 3.7)
c     Each rosette gage pair is at 0,45,and 90 degrees in
c     orientation.
c ***********************************************************
c
      READ(1,1002)R20,R245,R290
      WRITE(6,2050)
      WRITE(6,1002)R20,R245,R290
      READ(1,1002)R30,R345,R390
      WRITE(6,2060)
      WRITE(6,1002)R30,R345,R390
      GAMA(2)=R245-(R20+R290)/2.0
      GAMA(3)=R345-(R30+R390)/2.0
      READ(1,1002)ERR1,ERR2
      WRITE(6,2090)
      WRITE(6,1002)ERR1,ERR2
      WRITE(6,2061)
c
c                        * PART A *
c ***********************************************************
c Part A locates joints 1,2,3, and the end effector center
c point 4 in global coordinates at a time t. (Joint 1 is set
c at 0,0,0.)
c
      DO 17 j=1,3
      CF(j)=COS(FE(j))
      SF(j)=SIN(FE(j))
```

```
   17 CONTINUE
      XG(2)=B2*CF(1)
      XG(3)=XG(2)+XL(3)*CF(2)
      XG(4)=XG(3)+XL(4)*CF(3)
      YG(2)=B2*SF(1)
      YG(3)=YG(2)+XL(3)*SF(2)
      YG(4)=YG(3)+XL(4)*SF(3)
c
c          * PART B *    THESIS SECTIONS 3.1.1 TO 3.1.6 (s=1)
c ***********************************************************
c  This part of the program calculates displacements u(i,1),
c  v(i,1),& w(i,1) in local coordinates at joints 2 and 3
c  from Thesis equations 3.18,3.21,3.24,3.36 & 3.39.
c ***********************************************************
c
c  Ey(k,j) used for bending strain to calculate v(i,1)
c  displacements and THETAz (QZL(i,1),QZL(i,1) angular
c  displacements (xy plane).
c  Ez(k,j) used for bending strain to calculate w(i,1)
c  displacements and THETAy (QYL(i,1),QYL(i,1) angular
C  displacements (xz plane).
c  NOTE: THESE VALUES ARE FROM STRAIN GAGE PAIRS AND MUST BE
c        DIVIDED BY 2 FOR USE IN PART B.
c
      DO 18 k=2,3
      DO 19 j=1,3
      Ey(k,j)=Ey(k,j)/2.0
      Ez(k,j)=Ez(k,j)/2.0
   19 CONTINUE
   18 CONTINUE
c
c  Z1= 1/2 the out to out dimension (h) of the steel tube
c  (inches).
c
      AN=3.0
      DO 202 M=2,3
      P=0.0
      Z=1.0
      T=1.0
      DO 201 L=1,5
      J=2
      K=J+1
      D=0.0
      DO 200 I=1,3
      IF(J-I)30,20,30
   20 J=J-1
   30 IF(K-I)60,50,60
   50 K=K-1
   60 DENOM(I)=(X(M,I)-X(M,J))*(X(M,I)-X(M,K))
      AN123=(XL(M))**(AN+P)/(AN*T)-1.0*(XL(M))**(AN+P-1.)*(X
     1(M,J)+X(M,K))/(Z*(AN-1.))+X(M,J)*X(M,K)*(XL(M))**(P+1.
     1)/(P+1.)
      IF(L-2)21,41,33
   33 IF(L-4)31,21,41
```

```
   31 E1=0.0
      GO TO 22
   21 E1=Ey(M,I)
      Z1=H/2.0
      GO TO 22
   41 E1=Ez(M,I)
      Z1=H/2.0
   22 AN4(I)=(AN123*E1/(Z1*DENOM(I)))+D
      D=AN4(I)
      DX(M,L)=D
  200 CONTINUE
      IF(L-2)201,201,34
   34 P=1.0
      Z=3.0
      T=4.0
  201 CONTINUE
  202 CONTINUE
      DO 65 i=2,3
      QXL(i,1)=XL(i)*GAMA(i)/Z1
      QZL(i,1)=DX(i,1)
      QYL(i,1)=-1.0*DX(i,2)
      UL(i,1)=DX(i,3)
      VL(i,1)=DX(i,4)
      WL(i,1)=DX(i,5)
   65 CONTINUE
C
C                 * PART C *       THESIS SECTION 3.2.3 (s=2)
C ************************************************************
C  RIGID BODY MOTION EFFECTS IN THE LOCAL XY PLANE
C
      UL(3,2)=VL(2,1)*SIN(FE21)
      VL(3,2)=VL(2,1)*COS(FE21)
      UL(4,2)=VL(2,1)*SIN(FE31)+VL(3,1)*SIN(FE32)-XL(4)*QZL(
     13,1)*SIN(QZL(3,1)/2.0)
      VL(4,2)=VL(2,1)*COS(FE31)+VL(3,1)*COS(FE32)+XL(4)*QZL(
     13,1)*COS(QZL(3,1)/2.0)
      QZL(4,2)=QZL(3,1)
C
C                 * PART D *       THESIS SECTION 3.2.4 (s=3)
C ************************************************************
C RIGID BODY MOTION EFFECTS IN THE LOCAL XZ PLANE
C
      UL(3,3)=-1.*XL(3)*QYL(2,1)*SIN(QYL(2,1)/2.0)+WL(3,1)*S
     1IN(QYL(2,1))
      WL(3,3)=WL(2,1)-1.*XL(3)*QYL(2,1)*COS(QYL(2,1)/2.0)+WL
     1(3,1)*COS(QYL(2,1))
      UL(4,3)=-1.*(XL(3)+XL(4))*QYL(2,1)*SIN(QYL(2,1)/2.0)+W
     1L(3,1)*SIN(QYL(2,1))-1.*XL(4)*QYL(3,1)*SIN(QYL(2,1)+QY
     1L(3,1)/2.0)
      WL(4,3)=WL(2,1)-1.*(XL(3)+XL(4))*QYL(2,1)*COS(QYL(2,1)
     1/2.0)+WL(3,1)*COS(QYL(2,1))-1.*XL(4)*QYL(3,1)*COS(QYL(
     12,1)+QYL(3,1)/2.0)
      QYL(3,3)=QYL(2,1)
      QYL(4,3)=QYL(2,1)+QYL(3,1)
```

```
C
C                  * PART E *       THESIS SECTION 3.2.5 (s=4)
C ************************************************************
C RIGID BODY MOTION EFFECTS FROM ROTATIONAL DISPLACEMENTS
C THETA X
C
      R1=XL(3)*SIN(FE21)
      R2=R1*(COS(QXL(2,1))-1.0)
      R3=R1+XL(4)*SIN(FE31)
      R4=R3*(COS(QXL(2,1))-1.0)
      R5=XL(4)*SIN(FE32)
      R6=R5*(COS(QXL(3,1))-1.0)
      UL(3,4)=R2*SIN(FE21)
      IF (FE2-FE1) 73,74,74
   74 VL(3,4)=R2*COS(FE21)
      GO TO 75
   73 VL(3,4)=-1.0*R2*COS(FE21)
   75 IF (FE3-FE1) 76,77,77
   77 VL(4,4)=R4*COS(FE32)
      GO TO 78
   76 VL(4,4)=-1.0*R4*COS(FE32)
   78 IF (FE3-FE2) 79,81,81
   81 VL(4,4)=VL(4,4)+R6*COS(FE32)
      GO TO 82
   79 VL(4,4)=VL(4,4)-R6*COS(FE32)
   82 WL(3,4)=R1*SIN(QXL(2,1))
      QXL(3,4)=QXL(2,1)*COS(FE21)
      UL(4,4)=R4*SIN(FE32)+R6*SIN(FE32)
      WL(4,4)=R3*SIN(QXL(2,1))+R5*SIN(QXL(3,1))
      QXL(4,4)=QXL(3,4)*COS(FE32)+QXL(3,1)*COS(FE32)
C
C                  * PART F *       THESIS SECTION 3.2.6 (s=5)
C ************************************************************
C  RIGID BODY MOTIONS EFFECTS FROM ACTUATOR FLUCTUATIONS
C
      PHI=PI/2.0+FE1-ATAN(6.0/22.0)
      C1=((A1)**2.+(B1)**2.-2.*A1*B1*COS(PHI))**.5
      DPHI=ERR1*C1/(A1*B1*SIN(PHI))
      ALFA=FE1+PI-XLAM-FE2
      C2=((A2)**2.+(B2)**2.-2.*A2*B2*COS(ALFA))**.5
      DALFA=ERR2*C2/(A2*B2*SIN(ALFA))
      UL(2,5)=B2*DPHI*SIN(DPHI/2.)
      VL(2,5)=B2*DPHI*COS(DPHI/2.)
      UL(3,5)=B2*DPHI*SIN(FE21+DPHI/2.)+XL(3)*DALFA*SIN(DALF
     1A/2.)
      VL(3,5)=B2*DPHI*COS(FE21+DPHI/2.)+XL(3)*DALFA*COS(DALF
     1A/2.)
      UL(4,5)=B2*DPHI*SIN(FE31+DPHI/2.)+XL(3)*DALFA*SIN(FE32
     11+DALFA/2.)
      VL(4,5)=B2*DPHI*COS(FE31+DPHI/2.)+XL(3)*DALFA*COS(FE32
     11+DALFA/2.)
C
C                       * PART G *
C ************************************************************
```

```
c DEAD LOAD DISPLACEMENTS AT JOINT 2,3 AND 4.
c
c NOTE: ALL RIGID BODY MOTION EFFECTS ARE ALSO INCLUDED HERE
c       SIMILAR TO THESIS SECTION 3.2.3.
c
c E*I = .3385*29000000 = 9816500 LBS-IN2. LINKS 2&3.
c                LIST OF CONCENTRATED LOADS:
c P1: END EFFECTOR GRIPPER         = 3.0 LBS @ 6" FROM JT. 3.
c P2: END EFFECTOR STEPPER MOTOR   = 5.0 LBS @ JT. 3.
c P3: END EFFECTOR ENCODER SENSOR = 2.0 LBS @ JT. 3.
c P4: END EFFECTOR SHAFT           = 2.55 LBS @ 2" FROM JT.3.
c P5: ACTUATOR CONNECTOR ARM de    = 12.0 LBS @ JT. 2.
c P6: SIDE PLATES AT JT. 2         = 10.0 LBS @ JT. 2.
c P7: PORTION OF ACTUATOR de       = 12.0 LBS @ JT. 2.
c                     UNIFORM WEIGHTS:
c Q1: UNIFORM WEIGHT OF LINK 2 & 3 = 0.355 LBS/INCH.
c
      EI=9816500.0
      P1=3.0
      P2=5.0
      P3=2.0
      P4=2.55
      P5=12.0
      P6=10.0
      P7=12.0
      Q1=0.355
      P=P1+P2+P3+P4
      PP=P+P5+P6+P7+XL(3)*Q1
      XM=CF(3)*(P1*6.+P4*2.)
      XM1=XM+XL(3)*CF(2)*P
      ZETA=ATAN((13.*SIN(ALFA)-4.)/(62.5-13.*COS(ALFA)))
      ZETA1=PI/2.-ZETA-ALFA
      P8=XM1*SIN(ZETA)/(13.*COS(ZETA1))
      VL(2,6)=-1.*CF(1)*XL(2)**3.*(PP/3.+Q1*XL(2)/8.)/EI-1.*
     1P8*XL(2)**3./(3.*EI)
      QZL(2,6)=-1.*CF(1)*XL(2)**2.*(PP/2.+Q1*XL(2)/6.)/EI
      UL(3,6)=VL(2,6)*SIN(FE21)
      VL(3,6)=-1.*CF(2)*XL(3)**3.*(P/3.+Q1*XL(3)/8.)/EI-XM*X
      L(3)**2./(2.*EI)
      QZL(3,6)=-1.*CF(2)*XL(3)**2.*(P/2.+Q1*XL(3)/6.)/EI-XM*
      XL(3)/EI
      UL(4,6)=VL(2,6)*SIN(FE31)+VL(3,6)*SIN(FE32)-XL(4)*QZL(
      3,6)*SIN(QZL(3,6)/2.)
      VL(4,6)=VL(2,6)*COS(FE31)+VL(3,6)*COS(FE32)+XL(4)*QZL(
      3,6)*COS(QZL(3,6)/2.)
      VL(3,6)=VL(3,6)+VL(2,6)*COS(FE21)
      QZL(4,6)=QZL(3,6)
c
c                        * PART H *       THESIS SECTION 3.2.7
c ***********************************************************
c SUMMARY OF ALL LOCAL JOINT DISPLACEMENTS
      DO 80 i=2,4
      U=0.0
      V=0.0
```

```
      W=0.0
      QX=0.0
      QY=0.0
      QZ=0.0
      DO 70 IS=1,6
      ULT(i)=UL(i,IS)+U
      U=ULT(i)
      VLT(i)=VL(i,IS)+V
      V=VLT(i)
      WLT(i)=WL(i,IS)+W
      W=WLT(i)
      QXLT(i)=QXL(i,IS)+QX
      QX=QXLT(i)
      QYLT(i)=QYL(i,IS)+QY
      QY=QYLT(i)
      QZLT(i)=QZL(i,IS)+QZ
      QZ=QZLT(i)
   70 CONTINUE
   80 CONTINUE
      WRITE(6,2200)
      WRITE(6,2300)
      WRITE(6,1006)ULT(2),VLT(2),WLT(2),QXLT(2),QYLT(2),QZLT
     1(2)
      WRITE(6,2400)
      WRITE(6,1006)ULT(3),VLT(3),WLT(3),QXLT(3),QYLT(3),QZLT
     1(3)
      WRITE(6,2500)
      WRITE(6,1006)ULT(4),VLT(4),WLT(4),QXLT(4),QYLT(4),QZLT
     1(4)
C
C                        * PART I *          THESIS SECTION 3.3
C ***************************************************************
C LOCAL TO GLOBAL COORDINATE TRANSFORMATIONS
C
      DO 71 j=2,4
      UG(j)=ULT(j)*COS(FE(j-1))-VLT(j)*SIN(FE(j-1))
      VG(j)=ULT(j)*SIN(FE(j-1))+VLT(j)*COS(FE(j-1))
      WG(j)=WLT(j)
      QXG(j)=QXLT(j)*COS(FE(j-1))-QYLT(j)*SIN(FE(j-1))
      QYG(j)=QXLT(j)*SIN(FE(j-1))+QYLT(j)*COS(FE(j-1))
      QZG(j)=QZLT(j)
   71 CONTINUE
      WRITE(6,2700)
      WRITE(6,2800)
      WRITE(6,1006)UG(2),VG(2),WG(2),QXG(2),QYG(2),QZG(2)
      WRITE(6,2900)
      WRITE(6,1006)UG(3),VG(3),WG(3),QXG(3),QYG(3),QZG(3)
      WRITE(6,3000)
      WRITE(6,1006)UG(4),VG(4),WG(4),QXG(4),QYG(4),QZG(4)
C
C                        * PART J *
C ***************************************************************
C LOCATION OF JOINTS 2,3 AND EECP 4 IN XYZ COORDINATES.
C
```

```
      DO 72 i=2,4
      XX(i)=XG(i)+UG(i)
      YY(i)=YG(i)+VG(i)
      ZZ(i)=ZG(i)+WG(i)
   72 CONTINUE
      WRITE(6,3100)
      WRITE(6,3200)
      WRITE(6,1005)XX(2),YY(2),ZZ(2)
      WRITE(6,3300)
      WRITE(6,1005)XX(3),YY(3),ZZ(3)
      WRITE(6,3400)
      WRITE(6,1005)XX(4),YY(4),ZZ(4)
      END
```

*** INPUT *** From a 5 lb load.

```
ENCODER SENSOR READINGS FE1,FE2,& FE3,(radians)
 5.846900  5.846900  4.712400

STRAIN GAGE READINGS @ X1,X2,X3 (Y-FACE) link 2.
 -.000060  -.000039  -.000011

STRAIN GAGE READINGS @ X1,X2,X3 (Z-FACE) link 2.
  .000000   .000000   .000000

STRAIN GAGE READINGS @ X1,X2,X3 (Y-FACE) link 3.
 -.000028  -.000016  -.000006

STRAIN GAGE READINGS @ X1,X2,X3 (Z-FACE) link 3.
  .000000   .000000   .000000

ROSETTE GAGE READINGS @ X4 (Y-FACE) link 2.
  .000000   .000000   .000000

ROSETTE GAGE READINGS @ X4 (Y-FACE) link 3.
  .000000   .000000   .000000

FLUCTUATION IN ACTUATOR ab & de (units of strain)
  .000000   .000000

                *** OUTPUT ***

*SUMMARY OF LOCAL JOINT DISPLACEMENTS*

Local Displacements at Joint 2. u,v,w,Qx,Qy,Qz.
    .0000    -.0459     .0000     .0000     .0000    -.0012

Local Displacements at Joint 3. u,v,w,Qx,Qy,Qz.
    .0000    -.0544     .0000     .0000     .0000    -.0004

Local Displacements at EECP 4.  u,v,w,Qx,Qy,Qz.
    .0493    -.0254     .0000     .0000     .0000    -.0004

*SUMMARY OF GLOBAL JOINT DISPLACEMENTS*

Global Displacements at Joint 2. U,V,W,QX,QY,QZ.
   -.0194    -.0416     .0000     .0000     .0000    -.0012

Global Displacements at Joint 3. U,V,W,QX,QY,QZ.
   -.0230    -.0493     .0000     .0000     .0000    -.0004

Global Displacements at EECP 4.  U,V,W,QX,QY,QZ.
   -.0254    -.0493     .0000     .0000     .0000    -.0004

*LOCATION OF JOINTS 2,3 AND EECP 4 IN XYZ COORDINATES*

Final Location of Joint 2. (X,Y,Z)
    59.3451   -27.7203      .0000

Final Location of Joint 3. (X,Y,Z)
    92.4224   -43.1520      .0000

Final Location of EECP 4. (X,Y,Z)
    92.4201   -50.1520      .0000
```

INPUT ### From a 10 lb. load.

ENCODER SENSOR READINGS FE1,FE2,& FE3,(radians)
5.846900 5.846900 4.712400

STRAIN GAGE READINGS @ X1,X2,X3 (Y-FACE) link 2.
-.000107 -.000072 -.000020

STRAIN GAGE READINGS @ X1,X2,X3 (Z-FACE) link 2.
.000000 .000000 .000000

STRAIN GAGE READINGS @ X1,X2,X3 (Y-FACE) link 3.
-.000054 -.000032 -.000010

STRAIN GAGE READINGS @ X1,X2,X3 (Z-FACE) link 3.
.000000 .000000 .000000

ROSETTE GAGE READINGS @ X4 (Y-FACE) link 2.
.000000 .000000 .000000

ROSETTE GAGE READINGS @ X4 (Y-FACE) link 3.
.000000 .000000 .000000

FLUCTUATION IN ACTUATOR ab & de (units of strain)
.000000 .000000

OUTPUT

#SUMMARY OF LOCAL JOINT DISPLACEMENTS#

Local Displacements at Joint 2. u,v,w,Qx,Qy,Qz.
.0000 -.0828 .0000 .0000 .0000 -.0021

Local Displacements at Joint 3. u,v,w,Qx,Qy,Qz.
.0000 -.0994 .0000 .0000 .0000 -.0007

Local Displacements at EECP 4. u,v,w,Qx,Qy,Qz.
.0901 -.0467 .0000 .0000 .0000 -.0007

#SUMMARY OF GLOBAL JOINT DISPLACEMENTS#

Global Displacements at Joint 2. U,V,W,QX,QY,QZ.
-.0330 -.0731 .0000 .0000 .0000 -.0021

Global Displacements at Joint 3. U,V,W,QX,QY,QZ.
-.0420 -.0901 .0000 .0000 .0000 -.0007

Global Displacements at EECP 4. U,V,W,QX,QY,QZ.
-.0467 -.0901 .0000 .0000 .0000 -.0007

#LOCATION OF JOINTS 2,3 AND EECP 4 IN XYZ COORDINATES#

Final Location of Joint 2. (X,Y,Z)
59.3295 -27.7538 .0000

Final Location of Joint 3. (X,Y,Z)
92.4034 -43.1928 .0000

Final Location of EECP 4. (X,Y,Z)
92.3988 -50.1928 .0000

INPUT ###From a 15 lb. load.

ENCODER SENSOR READINGS FE1,FE2,& FE3,(radians)
5.846900 5.846900 4.712400

STRAIN GAGE READINGS @ X1,X2,X3 (Y-FACE) link 2.
-.000159 -.000106 -.000031

STRAIN GAGE READINGS @ X1,X2,X3 (Z-FACE) link 2.
.000000 .000000 .000000

STRAIN GAGE READINGS @ X1,X2,X3 (Y-FACE) link 3.
-.000082 -.000048 -.000015

STRAIN GAGE READINGS @ X1,X2,X3 (Z-FACE) link 3.
.000000 .000000 .000000

ROSETTE GAGE READINGS @ X4 (Y-FACE) link 2.
.000000 .000000 .000000

ROSETTE GAGE READINGS @ X4 (Y-FACE) link 3.
.000000 .000000 .000000

FLUCTUATION IN ACTUATOR ab & de (units of strain)
.000000 .000000

OUTPUT

#SUMMARY OF LOCAL JOINT DISPLACEMENTS#

Local Displacements at Joint 2. u,v,w,Qx,Qy,Qz.
.0000 -.1230 .0000 .0000 .0000 -.0032

Local Displacements at Joint 3. u,v,w,Qx,Qy,Qz.
.0000 -.1480 .0000 .0000 .0000 -.0010

Local Displacements at EECP 4. u,v,w,Qx,Qy,Qz.
.1341 -.0696 .0000 .0000 .0000 -.0010

#SUMMARY OF GLOBAL JOINT DISPLACEMENTS#

Global Displacements at Joint 2. U,V,W,QX,QY,QZ.
-.0520 -.1114 .0000 .0000 .0000 -.0032

Global Displacements at Joint 3. U,V,W,QX,QY,QZ.
-.0625 -.1341 .0000 .0000 .0000 -.0010

Global Displacements at EECP 4. U,V,W,QX,QY,QZ.
-.0696 -.1341 .0000 .0000 .0000 -.0010

#LOCATION OF JOINTS 2,3 AND EECP 4 IN XYZ COORDINATES#

Final Location of Joint 2. (X,Y,Z)
59.3125 -27.7902 .0000

Final Location of Joint 3. (X,Y,Z)
92.3829 -43.2368 .0000

Final Location of EECP 4. (X,Y,Z)
92.3759 -50.2368 .0000

INPUT ### From a 20 lb. load.

```
ENCODER SENSOR READINGS FE1,FE2,& FE3,(radians)
 5.846900  5.846900  4.712400

STRAIN GAGE READINGS @ X1,X2,X3 (Y-FACE) link 2.
 -.000210  -.000141  -.000042

STRAIN GAGE READINGS @ X1,X2,X3 (Z-FACE) link 2.
  .000000   .000000   .000000

STRAIN GAGE READINGS @ X1,X2,X3 (Y-FACE) link 3.
 -.000108  -.000064  -.000019

STRAIN GAGE READINGS @ X1,X2,X3 (Z-FACE) link 3.
  .000000   .000000   .000000

ROSETTE GAGE READINGS @ X4 (Y-FACE) link 2.
  .000000   .000000   .000000

ROSETTE GAGE READINGS @ X4 (Y-FACE) link 3.
  .000000   .000000   .000000

FLUCTUATION IN ACTUATOR ab & de (units of strain)
  .000000   .000000
```

OUTPUT

```
#SUMMARY OF LOCAL JOINT DISPLACEMENTS#

Local Displacements at Joint 2. u,v,w,Qx,Qy,Qz.
    .0000    -.1630     .0000     .0000     .0000    -.0042

Local Displacements at Joint 3. u,v,w,Qx,Qy,Qz.
    .0000    -.1961     .0000     .0000     .0000    -.0013

Local Displacements at EECP 4.  u,v,w,Qx,Qy,Qz.
    .1777    -.0921     .0000     .0000     .0000    -.0013

#SUMMARY OF GLOBAL JOINT DISPLACEMENTS#

Global Displacements at Joint 2. U,V,W,QX,QY,QZ.
   -.0689    -.1477     .0000     .0000     .0000    -.0042

Global Displacements at Joint 3. U,V,W,QX,QY,QZ.
   -.0829    -.1777     .0000     .0000     .0000    -.0013

Global Displacements at EECP 4.  U,V,W,QX,QY,QZ.
   -.0921    -.1777     .0000     .0000     .0000    -.0013

#LOCATION OF JOINTS 2,3 AND EECP 4 IN XYZ COORDINATES#

Final Location of Joint 2. (X,Y,Z)
    59.2956   -27.8264      .0000

Final Location of Joint 3. (X,Y,Z)
    92.3626   -43.2804      .0000

Final Location of EECP 4. (X,Y,Z)
    92.3534   -50.2804      .0000
```

*** INPUT *** From a 25 lb. load.

ENCODER SENSOR READINGS FE1,FE2,& FE3,(radians)
5.846900 5.846900 4.712400

STRAIN GAGE READINGS @ X1,X2,X3 (Y-FACE) link 2.
-.000264 -.000178 -.000055

STRAIN GAGE READINGS @ X1,X2,X3 (Z-FACE) link 2.
.000000 .000000 .000000

STRAIN GAGE READINGS @ X1,X2,X3 (Y-FACE) link 3.
-.000134 -.000079 -.000023

STRAIN GAGE READINGS @ X1,X2,X3 (Z-FACE) link 3.
.000000 .000000 .000000

ROSETTE GAGE READINGS @ X4 (Y-FACE) link 2.
.000000 .000000 .000000

ROSETTE GAGE READINGS @ X4 (Y-FACE) link 3.
.000000 .000000 .000000

FLUCTUATION IN ACTUATOR ab & de (units of strain)
.000000 .000000

*** OUTPUT ***

SUMMARY OF LOCAL JOINT DISPLACEMENTS

Local Displacements at Joint 2. u,v,w,Qx,Qy,Qz.
.0000 -.2056 .0000 .0000 .0000 -.0053

Local Displacements at Joint 3. u,v,w,Qx,Qy,Qz.
.0000 -.2465 .0000 .0000 .0000 -.0016

Local Displacements at EECP 4. u,v,w,Qx,Qy,Qz.
.2234 -.1156 .0000 .0000 .0000 -.0016

SUMMARY OF GLOBAL JOINT DISPLACEMENTS

Global Displacements at Joint 2. U,V,W,QX,QY,QZ.
-.0869 -.1863 .0000 .0000 .0000 -.0053

Global Displacements at Joint 3. U,V,W,QX,QY,QZ.
-.1042 -.2234 .0000 .0000 .0000 -.0016

Global Displacements at EECP 4. U,V,W,QX,QY,QZ.
-.1156 -.2234 .0000 .0000 .0000 -.0016

LOCATION OF JOINTS 2,3 AND EECP 4 IN XYZ COORDINATES

Final Location of Joint 2. (X,Y,Z)
59.2776 -27.8650 .0000

Final Location of Joint 3. (X,Y,Z)
92.3413 -43.3261 .0000

Final Location of EECP 4. (X,Y,Z)
92.3299 -50.3261 .0000

INPUT ### From a 30 lb. load.

```
ENCODER SENSOR READINGS FE1,FE2,& FE3,(radians)
 5.846900  5.846900  4.712400

STRAIN GAGE READINGS @ X1,X2,X3 (Y-FACE) link 2.
 -.000318  -.000214  -.000067

STRAIN GAGE READINGS @ X1,X2,X3 (Z-FACE) link 2.
  .000000   .000000   .000000

STRAIN GAGE READINGS @ X1,X2,X3 (Y-FACE) link 3.
 -.000161  -.000095  -.000027

STRAIN GAGE READINGS @ X1,X2,X3 (Z-FACE) link 3.
  .000000   .000000   .000000

ROSETTE GAGE READINGS @ X4 (Y-FACE) link 2.
  .000000   .000000   .000000

ROSETTE GAGE READINGS @ X4 (Y-FACE) link 3.
  .000000   .000000   .000000

FLUCTUATION IN ACTUATOR ab & de (units of strain)
  .000000   .000000
```

OUTPUT

```
#SUMMARY OF LOCAL JOINT DISPLACEMENTS#

Local Displacements at Joint 2. u,v,w,Qx,Qy,Qz.
    .0000    -.2476     .0000     .0000     .0000    -.0064

Local Displacements at Joint 3. u,v,w,Qx,Qy,Qz.
    .0000    -.2958     .0000     .0000     .0000    -.0020

Local Displacements at EECP 4.  u,v,w,Qx,Qy,Qz.
    .2689    -.1391     .0000     .0000     .0000    -.0020

#SUMMARY OF GLOBAL JOINT DISPLACEMENTS#

Global Displacements at Joint 2. U,V,W,QX,QY,QZ.
   -.1046    -.2244     .0000     .0000     .0000    -.0064

Global Displacements at Joint 3. U,V,W,QX,QY,QZ.
   -.1254    -.2690     .0000     .0000     .0000    -.0020

Global Displacements at EECP 4.  U,V,W,QX,QY,QZ.
   -.1391    -.2689     .0000     .0000     .0000    -.0020

#LOCATION OF JOINTS 2,3 AND EECP 4 IN XYZ COORDINATES#

Final Location of Joint 2. (X,Y,Z)
    59.2598   -27.9031       .0000

Final Location of Joint 3. (X,Y,Z)
    92.3200   -43.3717       .0000

Final Location of EECP 4. (X,Y,Z)
    92.3064   -50.3717       .0000
```

INPUT ### From a 35 lb. load.

```
ENCODER SENSOR READINGS FE1,FE2,& FE3,(radians)
 5.846900  5.846900  4.712400

STRAIN GAGE READINGS @ X1,X2,X3 (Y-FACE) link 2.
 -.000368  -.000250  -.000079

STRAIN GAGE READINGS @ X1,X2,X3 (Z-FACE) link 2.
  .000000   .000000   .000000

STRAIN GAGE READINGS @ X1,X2,X3 (Y-FACE) link 3.
 -.000187  -.000111  -.000032

STRAIN GAGE READINGS @ X1,X2,X3 (Z-FACE) link 3.
  .000000   .000000   .000000

ROSETTE GAGE READINGS @ X4 (Y-FACE) link 2.
  .000000   .000000   .000000

ROSETTE GAGE READINGS @ X4 (Y-FACE) link 3.
  .000000   .000000   .000000

FLUCTUATION IN ACTUATOR ab & de (units of strain)
  .000000   .000000
```

OUTPUT

```
*SUMMARY OF LOCAL JOINT DISPLACEMENTS*

Local Displacements at Joint 2. u,v,w,Qx,Qy,Qz.
    .0000    -.2877     .0000     .0000     .0000    -.0075

Local Displacements at Joint 3. u,v,w,Qx,Qy,Qz.
    .0000    -.3449     .0000     .0000     .0000    -.0023

Local Displacements at EECP 4.  u,v,w,Qx,Qy,Qz.
    .3125    -.1618     .0000     .0000     .0000    -.0023

*SUMMARY OF GLOBAL JOINT DISPLACEMENTS*

Global Displacements at Joint 2. U,V,W,QX,QY,QZ.
   -.1216    -.2607     .0000     .0000     .0000    -.0075

Global Displacements at Joint 3. U,V,W,QX,QY,QZ.
   -.1458    -.3125     .0000     .0000     .0000    -.0023

Global Displacements at EECP 4.  U,V,W,QX,QY,QZ.
   -.1618    -.3125     .0000     .0000     .0000    -.0023

*LOCATION OF JOINTS 2,3 AND EECP 4 IN XYZ COORDINATES*

Final Location of Joint 2. (X,Y,Z)
    59.2429   -27.9394      .0000

Final Location of Joint 3. (X,Y,Z)
    92.2997   -43.4153      .0000

Final Location of EECP 4. (X,Y,Z)
    92.2837   -50.4153      .0000
```

*** INPUT *** From a 40 lb. load.

```
ENCODER SENSOR READINGS FE1,FE2,& FE3,(radians)
 5.845900  5.845900  4.712400

STRAIN GAGE READINGS @ X1,X2,X3 (Y-FACE) link 2.
 -.000422  -.000286  -.000093

STRAIN GAGE READINGS @ X1,X2,X3 (Z-FACE) link 2.
  .000000   .000000   .000000

STRAIN GAGE READINGS @ X1,X2,X3 (Y-FACE) link 3.
 -.000214  -.000127  -.000035

STRAIN GAGE READINGS @ X1,X2,X3 (Z-FACE) link 3.
  .000000   .000000   .000000

ROSETTE GAGE READINGS @ X4 (Y-FACE) link 2.
  .000000   .000000   .000000

ROSETTE GAGE READINGS @ X4 (Y-FACE) link 3.
  .000000   .000000   .000000

FLUCTUATION IN ACTUATOR ab & de (units of strain)
  .000000   .000000

                *** OUTPUT ***

*SUMMARY OF LOCAL JOINT DISPLACEMENTS*

Local Displacements at Joint 2. u,v,w,Qx,Qy,Qz.
    .0000    -.3301     .0000     .0000     .0000    -.0086

Local Displacements at Joint 3. u,v,w,Qx,Qy,Qz.
    .0000    -.3955     .0000     .0000     .0000    -.0026

Local Displacements at EECP 4.  u,v,w,Qx,Qy,Qz.
    .3385    -.1853     .0000     .0000     .0000    -.0026

*SUMMARY OF GLOBAL JOINT DISPLACEMENTS*

Global Displacements at Joint 2. U,V,W,QX,QY,QZ.
   -.1395    -.2992     .0000     .0000     .0000    -.0086

Global Displacements at Joint 3. U,V,W,QX,QY,QZ.
   -.1671    -.3385     .0000     .0000     .0000    -.0026

Global Displacements at EECP 4.  U,V,W,QX,QY,QZ.
   -.1853    -.3385     .0000     .0000     .0000    -.0026

*LOCATION OF JOINTS 2,3 AND EECP 4 IN XYZ COORDINATES*

Final Location of Joint 2. (X,Y,Z)
    59.2250   -27.9779      .0000

Final Location of Joint 3. (X,Y,Z)
    92.2783   -43.4612      .0000

Final Location of EECP 4. (X,Y,Z)
    92.2602   -50.4612      .0000
```

APPENDIX–C

Fortran77 Program Code "MODEL.FOR"

NOMENCLATURE

For Fortran77 Program **MODEL.FOR**

A	Cross–section area of each rod element (hydraulic Actuator rods = 1.485 in^2).
BEAM2	"CASA/GIFTS" nomenclature used to generate first–order beam elements.
D	Mass density of steel in slugs (.00073462).
E	Modulus of Elasticity of Steel (29,000,000 psi).
ELMAT	"CASA/GIFTS" nomenclature used to define isotropic materials.
END	Denotes the end of the file.
ETH	"CASA/GIFTS" nomenclature used to define element size.
FY	Yield Strength of A36 steel (36,000 psi).
FE1	Angle ϕ_1 in the XY global plane at joint 1 (figure 3.1).
FE2	Angle ϕ_2 in the XY global plane at joint 2 (figure 3.1).
FE3	Angle ϕ_3 in the XY global plane at joint 3 (figure 3.1).
I	Integer defining the node numbers (I = 1,2,3....22).
POINT	"CASA/GIFTS" nomenclature used to generate node points.
PTRM	"CASA/GIFTS" nomenclature used to set material pointer.
PTRTH	"CASA/GIFTS" nomenclature used to set thickness pointer.
RAD	One radian in degrees = $180/\pi$.
ROD2	"CASA/GIFTS" nomenclature used to generate first–order rod elements.
THETA	Set angle = 53.13 degrees.

U	Poisson's ratio μ (0.29).
XL109	Distance from node 10 to node 9 (17.39").
XL111	Distance from node 1 to node 11 (4.0").
XL120	Distance from node 1 to node 20 (3.0").
XL25	Distance from node 2 to node 5 (2.501").
XL206	Distance from node 20 to node 6 (6.5").
XL34	Distance from node 3 to node 4 (7.0").
XL53	Distance from node 5 to node 3 (36.501").
XL57	Distance from node 5 to node 7 (13.0").
XL514	Distance from node 5 to node 14 (12.167").
XL62	Distance from node 6 to node 2 (53.501").
XL612	Distance from node 6 to node 12 (17.833").
XL91	Distance from node 9 to node 1 (22.0").
XL98	Distance from node 9 to node 8 (6.0").
X(I)	Global X coordinate of nodal points I (I = 1,2,3...22).
Y(I)	Global Y coordinate of nodal points I (I = 1,2,3...22).
Z(I)	Global Z coordinate of nodal points I (I = 1,2,3...22).

```
c  ********************************************************
c  * This program is an INPUT GENERATOR called MODEL.FOR   *
c  * by Robert F. Marceau, for the "GIFTS" finite element  *
c  * program file called NEWxROB. This program receives    *
c  * screen input and places it in SRC files as "ROBx.SRC" *
c  * (x = 1,2,3,4,5....etc.).                             *
c  * Note: All units in lbs and inches.                    *
c  ********************************************************
c
      DIMENSION X(25),Y(25),Z(25)
      OPEN(UNIT=6,FILE='ROB.DAT',STATUS='NEW')
 1000 FORMAT(4E12.4)
 1001 FORMAT(3E12.4)
 1003 FORMAT(3F10.2)
 1004 FORMAT(5HELMATI7)
 1005 FORMAT(7HAUTOOFF)
 1006 FORMAT(2I6)
 1007 FORMAT(/5HPOINTI7)
 1111 FORMAT(4I6)
 1112 FORMAT(/3HEND)
 1113 FORMAT(I6)
 1114 FORMAT(4HROD2I8)
 1115 FORMAT(/4HPTRMI8)
 1116 FORMAT(5HPTRTHI7)
 1117 FORMAT(/3HETHI9)
 1010 FORMAT(/' NOTE: Separate multiple inputs on one line
     1by commas.')
 1020 FORMAT(' NOTE: All input must be in decimal form & in
     1degrees.')
 1030 FORMAT(/' INPUT:Angles fe1,fe2,& fe3 (counter
      1clockwise +)')
c Beam element lengths in inches as later defined in GIFTS.
c Yield strength for A36 steel
      FY=36000.0
c Young's Modulus
      E=29000000.0
c Poisson's ratio for steel
      U=.29
c Mass density of steel in slugs
      D=.00073462
      J=0
      XL109=17.39
      XL91=22.0
      XL98=6.0
      XL120=3.0
      XL206=6.5
      XL62=53.501
      XL25=2.501
      XL53=36.501
      XL34=7.0
      XL111=4.0
      XL57=13.0
      XL612=17.833
      XL514=12.167
```

```
      WRITE(*,1010)
      WRITE(*,1020)
      WRITE(*,1030)
      READ(*,1003)FE1,FE2,FE3
      RAD=180.0/3.14159265
      FE1=FE1/RAD
      FE2=FE2/RAD
      FE3=FE3/RAD
      THETA=53.13/RAD
c Point number 10 is reference point.
      X(10)=0.0
      Y(10)=0.0
      Z(10)=0.0
c Point number 9 is set.
      X(9)=0.0
      Y(9)=17.39
      Z(9)=0.0
c Point number 8 is set.
      X(8)=6.0
      Y(8)=17.39
      Z(8)=0.0
c Point number 1 is set.
      X(1)=0.0
      Y(1)=39.39
      Z(1)=0.0
c Point number 11 is set.
      X(11)=0.0
      Y(11)=43.39
      Z(11)=0.0
c Point number 21 is set.
      X(21)=0.0
      Y(21)=28.39
      Z(21)=0.0
c Find joint 20
      X(20)=XL1920*COS(FE1)
      Y(20)=XL109+XL91+XL1920*SIN(FE1)
      Z(20)=0.0
c Find joint 6
      X(6)=X(20)+XL206*COS(FE1)
      Y(6)=Y(20)+XL206*SIN(FE1)
      Z(6)=0.0
c Find joint 12
      X(12)=X(6)+XL612*COS(FE1)
      Y(12)=Y(6)+XL612*SIN(FE1)
      Z(12)=0.0
c Find joint 13
      X(13)=X(12)+XL612*COS(FE1)
      Y(13)=Y(12)+XL612*SIN(FE1)
      Z(13)=0.0
c Find joint 2
      X(2)=X(13)+XL612*COS(FE1)
      Y(2)=Y(13)+XL612*SIN(FE1)
      Z(2)=0.0
c Find joint 5
```

```
      X(5)=X(2)+XL25*COS(FE1)
      Y(5)=Y(2)+XL25*SIN(FE1)
      Z(5)=0.0
c Find joint 14
      X(14)=X(5)+XL514*COS(FE2)
      Y(14)=Y(5)+XL514*SIN(FE2)
      Z(14)=0.0
c Find joint 15
      X(15)=X(14)+XL514*COS(FE2)
      Y(15)=Y(14)+XL514*SIN(FE2)
      Z(15)=0.0
c Find joint 3
      X(3)=X(15)+XL514*COS(FE2)
      Y(3)=Y(15)+XL514*SIN(FE2)
      Z(3)=0.0
c Find joint 4
      X(4)=X(3)+XL34*COS(FE3)
      Y(4)=Y(3)+XL34*SIN(FE3)
      Z(4)=0.0
c Find joint 7
      X(7)=X(5)-XL57*COS(THETA-FE2)
      Y(7)=Y(5)+XL57*SIN(THETA-FE2)
      Z(7)=0.0
c Reference points for alignment of beam x-sections.
      X(19)=X(8)
      Y(19)=Y(8)
      Z(19)=50.0
      X(16)=X(5)
      Y(16)=Y(5)
      Z(16)=50.0
      X(17)=X(11)
      Y(17)=Y(11)
      Z(17)=50.0
      X(18)=X(4)
      Y(18)=Y(4)
      Z(18)=50.0
      X(22)=X(9)
      Y(22)=Y(9)
      Z(22)=50.0
c Generate SRC data file.
      WRITE(6,1005)
      WRITE(6,1004)4
      WRITE(6,1006)1,0
      WRITE(6,1000)FY,E,U,D
      WRITE(6,1007)0
      DO 10 I=1,22
      WRITE(6,1113)I
      WRITE(6,1001)X(I),Y(I),Z(I)
   10 CONTINUE
c Start BEAM2 input properties.******************************
      CALL SUB (J)
      WRITE(6,1111)6,12,16
      WRITE(6,1111)12,13,16
      WRITE(6,1111)13,2,16
```

```
      WRITE(6,1111)2,5,16
      WRITE(6,1111)5,14,16
      WRITE(6,1111)14,15,16
      WRITE(6,1111)15,3,16
      WRITE(6,1111)9,8,19
      CALL SUB (J)
      WRITE(6,1111)10,9,22
      WRITE(6,1111)9,21,22
      WRITE(6,1111)21,1,22
      CALL SUB (J)
      WRITE(6,1111)1,20,16
      WRITE(6,1111)20,6,16
      CALL SUB (J)
      WRITE(6,1111)5,7,16
      CALL SUB (J)
      WRITE(6,1111)3,4,18
      CALL SUB (J)
      WRITE(6,1111)20,11,17
      A=1.485
      WRITE(6,1117)1
      WRITE(6,1113)7
      WRITE(6,1001)A
      WRITE(6,1115)0
      WRITE(6,1113)1
      WRITE(6,1116)0
      WRITE(6,1113)7
      WRITE(6,1114)0
      WRITE(6,1111)11,7
      WRITE(6,1117)1
      WRITE(6,1113)8
      WRITE(6,1001)A
      WRITE(6,1115)0
      WRITE(6,1113)1
      WRITE(6,1116)0
      WRITE(6,1113)8
      WRITE(6,1114)0
      WRITE(6,1111)8,6
      WRITE(6,1112)
      STOP
      END
C ***************************************
C Subroutine SUB
C ***************************************
      SUBROUTINE SUB (J)
 1008 FORMAT(/4HPTRMI8)
 1009 FORMAT(5HPTRTHI7)
 1110 FORMAT(5HBEAM2I7)
 1002 FORMAT(I6)
      K=J+1
      WRITE(6,1008)0
      WRITE(6,1002)1
      WRITE(6,1009)0
      WRITE(6,1002)K
      WRITE(6,1110)
```

```
      J=K
      RETURN
      END
```

```
"NEW1.SRC"

AUTOOFF
ELMAT       4
     1      0
   .3600E+05    .2900E+08    .2900E+00    .7346E-03

POINT       0
     1
   .0000E+00    .3939E+02    .0000E+00
     2
   .5710E+02    .1277E+02    .0000E+00
     3
   .4394E+02   -.2137E+02    .0000E+00
     4
   .4098E+02   -.2772E+02    .0000E+00
     5
   .5936E+02    .1171E+02    .0000E+00
     6
   .8610E+01    .3538E+02    .0000E+00
     7
   .7209E+02    .1438E+02    .0000E+00
     8
   .6000E+01    .1739E+02    .0000E+00
     9
   .0000E+00    .1739E+02    .0000E+00
    10
   .0000E+00    .0000E+00    .0000E+00
    11
   .4409E+01    .4175E+02    .0000E+00
    12
   .2477E+02    .2784E+02    .0000E+00
    13
   .4093E+02    .2030E+02    .0000E+00
    14
   .5422E+02    .6815E+00    .0000E+00
    15
   .4908E+02   -.1035E+02    .0000E+00
    16
   .5936E+02    .1171E+02    .5000E+02
    17
   .4409E+01    .4175E+02    .5000E+02
    18
   .4098E+02   -.2772E+02    .5000E+02
    19
   .6000E+01    .1739E+02    .5000E+02
    20
   .2719E+01    .3812E+02    .0000E+00
    21
   .0000E+00    .2839E+02    .0000E+00
    22
   .0000E+00    .1739E+02    .5000E+02

PTRM        0
```

"NEW1.SRC continued"

```
      1
PTRTH        0
      1
BEAM2
      6     12     16
     12     13     16
     13      2     16
      2      5     16
      5     14     16
     14     15     16
     15      3     16
      9      8     19

PTRM         0
      1
PTRTH        0
      2
BEAM2
     10      9     22
      9     21     22
     21      1     22

PTRM         0
      1
PTRTH        0
      3
BEAM2
      1     20     16
     20      6     16

PTRM         0
      1
PTRTH        0
      4
BEAM2
      5      7     16

PTRM         0
      1
PTRTH        0
      5
BEAM2
      3      4     18

PTRM         0
      1
PTRTH        0
      6
BEAM2
     20     11     17

ETH          1
```

"NEW1.SRC continued"

```
      7
    .1485E+01

PTRM          0
      1
PTRTH         0
      7
ROD2          0
     11       7
ETH           1
      8
    .1485E+01

PTRM          0
      1
PTRTH         0
      8
ROD2          0
      8       6

END
```

```
"NEW3.SRC"

AUTOOFF
ELMAT       4
     1      0
   .3600E+05    .2900E+08    .2900E+00    .7346E-03

POINT       0
     1
   .0000E+00    .3939E+02    .0000E+00
     2
   .5710E+02    .1277E+02    .0000E+00
     3
   .9244E+02   -.3717E+01    .0000E+00
     4
   .9879E+02   -.6676E+01    .0000E+00
     5
   .5936E+02    .1171E+02    .0000E+00
     6
   .8610E+01    .3538E+02    .0000E+00
     7
   .5669E+02    .2443E+02    .0000E+00
     8
   .6000E+01    .1739E+02    .0000E+00
     9
   .0000E+00    .1739E+02    .0000E+00
    10
   .0000E+00    .0000E+00    .0000E+00
    11
   .4409E+01    .4175E+02    .0000E+00
    12
   .2477E+02    .2784E+02    .0000E+00
    13
   .4093E+02    .2030E+02    .0000E+00
    14
   .7039E+02    .6567E+01    .0000E+00
    15
   .8142E+02    .1425E+01    .0000E+00
    16
   .5936E+02    .1171E+02    .5000E+02
    17
   .4409E+01    .4175E+02    .5000E+02
    18
   .9879E+02   -.6676E+01    .5000E+02
    19
   .6000E+01    .1739E+02    .5000E+02
    20
   .2719E+01    .3812E+02    .0000E+00
    21
   .0000E+00    .2839E+02    .0000E+00
    22
   .0000E+00    .1739E+02    .5000E+02

PTRM        0
```

"NEW3.SRC continued"

```
      1
PTRTH        0
      1
BEAM2
      6     12     16
     12     13     16
     13      2     16
      2      5     16
      5     14     16
     14     15     16
     15      3     16
      9      8     19

PTRM         0
      1
PTRTH        0
      2
BEAM2
     10      9     22
      9     21     22
     21      1     22

PTRM         0
      1
PTRTH        0
      3
BEAM2
      1     20     16
     20      6     16

PTRM         0
      1
PTRTH        0
      4
BEAM2
      5      7     16

PTRM         0
      1
PTRTH        0
      5
BEAM2
      3      4     18

PTRM         0
      1
PTRTH        0
      6
BEAM2
     20     11     17

ETH          1
```

"NEW3.SRC continued"

```
      7
    .1485E+01

PTRM          0
      1
PTRTH         0
      7
ROD2          0
     11       7

ETH           1
      1
PTRTH         0
      7
ROD2          0
     11       7

ETH           1
      8
    .1485E+01

PTRM          0
      1
PTRTH         0
      8
ROD2          0
      8       6

END
```

```
"NEW5.SRC"

AUTOOFF
ELMAT       4
      1     0
    .3600E+05    .2900E+08    .2900E+00    .7346E-03

POINT       0
      1
    .0000E+00    .3939E+02    .0000E+00
      2
    .6300E+02    .3939E+02    .0000E+00
      3
    .1020E+03    .3939E+02    .0000E+00
      4
    .1090E+03    .3939E+02    .0000E+00
      5
    .6550E+02    .3939E+02    .0000E+00
      6
    .9500E+01    .3939E+02    .0000E+00
      7
    .5770E+02    .4979E+02    .0000E+00
      8
    .6000E+01    .1739E+02    .0000E+00
      9
    .0000E+00    .1739E+02    .0000E+00
     10
    .0000E+00    .0000E+00    .0000E+00
     11
    .3000E+01    .4339E+02    .0000E+00
     12
    .2733E+02    .3939E+02    .0000E+00
     13
    .4517E+02    .3939E+02    .0000E+00
     14
    .7767E+02    .3939E+02    .0000E+00
     15
    .8983E+02    .3939E+02    .0000E+00
     16
    .6550E+02    .3939E+02    .5000E+02
     17
    .3000E+01    .4339E+02    .5000E+02
     18
    .1090E+03    .3939E+02    .5000E+02
     19
    .6000E+01    .1739E+02    .5000E+02
     20
    .3000E+01    .3939E+02    .0000E+00
     21
    .0000E+00    .2839E+02    .0000E+00
     22
    .0000E+00    .1739E+02    .5000E+02

PTRM        0
```

"NEW5.SRC continued"

```
     1
PTRTH       0
     1
BEAM2
     6     12     16
    12     13     16
    13      2     16
     2      5     16
     5     14     16
    14     15     16
    15      3     16
     9      8     19

PTRM        0
     1
PTRTH       0
     2
BEAM2
    10      9     22
     9     21     22
    21      1     22

PTRM        0
     1
PTRTH       0
     3
BEAM2
     1     20     16
    20      6     16

PTRM        0
     1
PTRTH       0
     4
BEAM2
     5      7     16

PTRM        0
     1
PTRTH       0
     5
BEAM2
     3      4     18

PTRM        0
     1
PTRTH       0
     6
BEAM2
    20     11     17

ETH         1
```

"NEW5.SRC continued"

```
      7
    .1485E+01

PTRM          0
      1
PTRTH         0
      7
ROD2          0
     11       7

ETH           1
      8
    .1485E+01

PTRM          0
      1
PTRTH         0
      8
ROD2          0
      8       6

END
```

```
"NEW7.SRC"

AUTOOFF
ELMAT       4
     1      0
   .3600E+05    .2900E+08    .2900E+00    .7346E-03

POINT       0
     1
   .0000E+00    .3939E+02    .0000E+00
     2
   .5710E+02    .6601E+02    .0000E+00
     3
   .9244E+02    .8250E+02    .0000E+00
     4
   .9879E+02    .8546E+02    .0000E+00
     5
   .5936E+02    .6707E+02    .0000E+00
     6
   .8610E+01    .4340E+02    .0000E+00
     7
   .4790E+02    .7320E+02    .0000E+00
     8
   .6000E+01    .1739E+02    .0000E+00
     9
   .0000E+00    .1739E+02    .0000E+00
    10
   .0000E+00    .0000E+00    .0000E+00
    11
   .1028E+01    .4428E+02    .0000E+00
    12
   .2477E+02    .5094E+02    .0000E+00
    13
   .4093E+02    .5848E+02    .0000E+00
    14
   .7039E+02    .7221E+02    .0000E+00
    15
   .8142E+02    .7736E+02    .0000E+00
    16
   .5936E+02    .6707E+02    .5000E+02
    17
   .1028E+01    .4428E+02    .5000E+02
    18
   .9879E+02    .8546E+02    .5000E+02
    19
   .6000E+01    .1739E+02    .5000E+02
    20
   .2719E+01    .4066E+02    .0000E+00
    21
   .0000E+00    .2839E+02    .0000E+00
    22
   .0000E+00    .1739E+02    .5000E+02

PTRM        0
```

"NEW7.SRC continued"

```
      1
PTRTH       0
      1
BEAM2
      6     12     16
     12     13     16
     13      2     16
      2      5     16
      5     14     16
     14     15     16
     15      3     16
      9      8     19

PTRM        0
      1
PTRTH       0
      2
BEAM2
     10      9     22
      9     21     22
     21      1     22

PTRM        0
      1
PTRTH       0
      3
BEAM2
      1     20     16
     20      6     16

PTRM        0
      1
PTRTH       0
      4
BEAM2
      5      7     16

PTRM        0
      1
PTRTH       0
      5
BEAM2
      3      4     18

PTRM        0
      1
PTRTH       0
      6
BEAM2
     20     11     17

ETH         1
```

"NEW7.SRC continued"

```
      7
   .1485E+01

PTRM          0
      1
PTRTH         0
      7
ROD2          0
     11       7

ETH           1
      8
   .1485E+01

PTRM          0
      1
PTRTH         0
      8
ROD2          0
      8       6

END
```

```
"NEW8.SRC"

AUTOOFF
ELMAT       4
      1     0
    .3600E+05    .2900E+08    .2900E+00    .7346E-03

POINT       0
      1
    .0000E+00    .3939E+02    .0000E+00
      2
    .5710E+02    .6601E+02    .0000E+00
      3
    .7479E+02    .3399E+02    .0000E+00
      4
    .7775E+02    .2765E+02    .0000E+00
      5
    .5936E+02    .6707E+02    .0000E+00
      6
    .8610E+01    .4340E+02    .0000E+00
      7
    .6549E+02    .7854E+02    .0000E+00
      8
    .6000E+01    .1739E+02    .0000E+00
      9
    .0000E+00    .1739E+02    .0000E+00
     10
    .0000E+00    .0000E+00    .0000E+00
     11
    .1028E+01    .4428E+02    .0000E+00
     12
    .2477E+02    .5094E+02    .0000E+00
     13
    .4093E+02    .5848E+02    .0000E+00
     14
    .6451E+02    .5604E+02    .0000E+00
     15
    .6965E+02    .4502E+02    .0000E+00
     16
    .5936E+02    .6707E+02    .5000E+02
     17
    .1028E+01    .4428E+02    .5000E+02
     18
    .7775E+02    .2765E+02    .5000E+02
     19
    .6000E+01    .1739E+02    .5000E+02
     20
    .2719E+01    .4066E+02    .0000E+00
     21
    .0000E+00    .2839E+02    .0000E+00
     22
    .0000E+00    .1739E+02    .5000E+02

PTRM        0
```

"NEW8.SRC continued"

```
      1
PTRTH       0
      1
BEAM2
      6     12     16
     12     13     16
     13      2     16
      2      5     16
      5     14     16
     14     15     16
     15      3     16
      9      8     19

PTRM        0
      1
PTRTH       0
      2
BEAM2
     10      9     22
      9     21     22
     21      1     22

PTRM        0
      1
PTRTH       0
      3
BEAM2
      1     20     16
     20      6     16

PTRM        0
      1
PTRTH       0
      4
BEAM2
      5      7     16

PTRM        0
      1
PTRTH       0
      5
BEAM2
      3      4     18

PTRM        0
      1
PTRTH       0
      6
BEAM2
     20     11     17

ETH         1
```

"NEW8.SRC continued"

```
     7
   .1485E+01

PTRM        0
     1
PTRTH       0
     7
ROD2        0
    11      7

ETH         1
     8
   .1485E+01

PTRM        0
     1
PTRTH       0
     8
ROD2        0
     8      6

END
```

```
"NEW1BC.SRC"

AUTOOFF
CIRCH       0
     2
  8.0000E+00  6.0000E+00

RECTH       0
     1
  1.5000E+00  1.5000E+00
  2.5000E-01  2.5000E-01

RECTS       0
     4
  2.5000E+00  1.0000E+00
     5
  1.5000E+00  1.5000E+00
     6
  3.0000E+00  2.0000E+00

CHANNEL     1
     3
  1.0000E+01  2.7500E+00
  2.5000E-01  1.0000E+00
  9.0000E+01

END
```

```
"NEW1LD.SRC"

AUTOOFF
LOADP       2
      4
 -1.0000E+02

SUPP        0
     10

RELP        6
      2
      1

END
```

```
"NEW2LD.SRC"

AUTOOFF
SUPP         0
     10

MASS         0
MASSP        0
       3
   1.8116E-02
       4
   7.7700E-03
       2
   8.8000E-02

RELP         6
       2
       1

END
```

Static Procedure Results From GIFTS

For Robot Manipulator Configuration 1 (figure 4.1)

Called NEW1ROB:

Note: Geometrical input for the robot manipulator were obtained from the on–line–batch file NEW1.SRC .

JOB:NEW1ROB 24-JUN-89 19:11:33 PAGE 1
GIFTS PARAMETER STATUS

TOTAL NUMBER OF POINTS:	22
TOTAL NUMBER OF ELEMENTS:	18
NUMBER OF MATERIAL GROUPS:	1
NUMBER OF STRUCTURAL POINTS:	17
NUMBER OF ACTIVE ELEMENTS:	18
NUMBER OF THICKNESS GROUPS:	8
NUMBER OF LOAD CASES:	1
NUMBER OF ACTIVE LOAD CASES:	1
NUMBER OF UNKNOWNS:	96
COMPUTATIONAL HALF BANDWIDTH:	57.14018

JOB:NEW1ROB 24-JUN-89 19:16:20 PAGE 2
GIFTS STATUS LIST.

MODEL GENERATED.
POINT MASSES NOT GENERATED.
BANDWIDTH OPTIMIZED.
STIFFNESS DIRECTORY PRESENT.
STIFFNESS MATRIX NOT SAVED.
LOADS MODIFIED.
BOUNDARY CONDITIONS INTRODUCED.
STIFFNESS MATRIX DECOMPOSED.
DEFLECTIONS CALCULATED.
ELEMENT STRESSES COMPUTED.
ELEMENT STRAINS NOT PRESENT.
MODEL CAN BE SOLVED BY GIFTS.
TEMPERATURES NOT CALCULATED.
PRESCRIBED TEMPERATURES NOT APPLIED.
NO POINT CONVECTIONS APPLIED.
THERMAL GRADIENTS NOT CALCULATED.
PROBLEM CLASS:
3-D ELASTIC / PLASTIC

JOB:NEW1ROB 24-JUN-89 LOADING CASE 1 19:10:21 PAGE 1
DISPLACEMENT INFORMATION

POINT	U	V	W	RX	RY	RZ
1	4.796E-05	-7.429E-07	1.179E-22	-1.847E-23	-1.265E-22	-2.288E-06
2	-7.807E-02	-1.674E-01	-4.261E-06	3.631E-08	7.019E-08	-2.077E-03
3	-4.775E-02	-1.866E-01	-4.577E-06	3.631E-08	7.019E-08	2.476E-03
4	-3.166E-02	-1.941E-01	-4.600E-06	3.631E-08	7.019E-08	2.561E-03
5	-7.998E-02	-1.715E-01	-4.458E-06	3.631E-08	7.019E-08	-1.491E-03
6	-3.025E-04	-7.499E-04	-3.678E-08	3.631E-08	7.019E-08	-1.674E-04
7	-7.620E-02	-1.896E-01	-5.255E-06	3.631E-08	7.019E-08	-1.390E-03
8	7.485E-06	-7.549E-04	4.778E-22	9.023E-25	-5.645E-23	-1.715E-04
9	9.716E-06	-6.817E-07	1.391E-22	9.023E-25	-5.645E-23	-1.117E-06
10	.000E+00	.000E+00	.000E+00	.000E+00	.000E+00	.000E+00
11	2.390E-04	-1.903E-04	6.644E-08	-1.924E-08	-4.078E-08	-6.343E-05
12	-1.758E-02	-3.773E-02	-1.445E-06	3.631E-08	7.019E-08	-3.876E-03
13	-5.123E-02	-1.098E-01	-2.853E-06	3.631E-08	7.019E-08	-4.513E-03
14	-8.499E-02	-1.692E-01	-4.498E-06	3.631E-08	7.019E-08	4.687E-04
15	-7.189E-02	-1.753E-01	-4.538E-06	3.631E-08	7.019E-08	1.791E-03
20	9.512E-06	-8.354E-05	6.735E-08	-1.924E-08	-4.078E-08	-5.847E-05
21	2.562E-05	-7.123E-07	1.850E-22	-6.170E-24	-9.216E-23	-1.715E-06

JOB:NEW1ROB 24-JUN-89 19:14:29 PAGE 1

NODAL POINT INFORMATION

POINT NO.	SYS NO.	X	Y	Z	ACTIVE FREEDOMS
1	1	.00000E+00	3.93900E+01	.00000E+00	U, V, W,RX,RY,RZ
2	2	5.71000E+01	1.27700E+01	.00000E+00	U, V, W,RX,RY,RZ
3	3	4.39400E+01	-2.13700E+01	.00000E+00	U, V, W,RX,RY,RZ
4	4	4.09800E+01	-2.77200E+01	.00000E+00	U, V, W,RX,RY,RZ
5	5	5.93600E+01	1.17100E+01	.00000E+00	U, V, W,RX,RY,RZ
6	6	8.61000E+00	3.53800E+01	.00000E+00	U, V, W,RX,RY,RZ
7	7	7.20900E+01	1.43800E+01	.00000E+00	U, V, W,RX,RY,RZ
8	8	6.00000E+00	1.73900E+01	.00000E+00	U, V, W,RX,RY,RZ
9	9	.00000E+00	1.73900E+01	.00000E+00	U, V, W,RX,RY,RZ
10	10	.00000E+00	.00000E+00	.00000E+00	, , , , ,
11	11	4.40900E+00	4.17500E+01	.00000E+00	U, V, W,RX,RY,RZ
12	12	2.47700E+01	2.78400E+01	.00000E+00	U, V, W,RX,RY,RZ
13	13	4.09300E+01	2.03000E+01	.00000E+00	U, V, W,RX,RY,RZ
14	14	5.42200E+01	6.81500E-01	.00000E+00	U, V, W,RX,RY,RZ
15	15	4.90800E+01	-1.03500E+01	.00000E+00	U, V, W,RX,RY,RZ
-16	20	5.93600E+01	1.17100E+01	5.00000E+01	, , , , ,
-17	21	4.40900E+00	4.17500E+01	5.00000E+01	, , , , ,
-18	18	4.09800E+01	-2.77200E+01	5.00000E+01	, , , , ,
-19	19	6.00000E+00	1.73900E+01	5.00000E+01	, , , , ,
20	16	2.71900E+00	3.81200E+01	.00000E+00	U, V, W,RX,RY,RZ
21	17	.00000E+00	2.83900E+01	.00000E+00	U, V, W,RX,RY,RZ
-22	22	.00000E+00	1.73900E+01	5.00000E+01	, , , , ,

JOB:NEW1ROB 24-JUN-89 19:23:00 PAGE 1

MATERIAL INFORMATION

MAT NO.	MAT TYP	YOUNG'S MODULUS	POISSON'S RATIO	SHEAR MODULUS	YIELD STRESS	MASS DENSITY	THERMAL EXPANSION
1	1	2.9000E+07	2.9000E-01	1.1240E+07	3.6000E+04	7.3460E-04	6.5000E-06

JOB:NEW1ROB 24-JUN-89 19:17:41 PAGE 1

ELEMENT INFORMATION

ELEM NO.	SYS NO.	TYPE	MAT NO.	MAT ANG	THS NO.	CONNECTIVITY		
1	1	BEAM2	1		1	6	12	-16
2	2	BEAM2	1		1	12	13	-16
3	3	BEAM2	1		1	13	2	-16
4	4	BEAM2	1		1	2	5	-16
5	5	BEAM2	1		1	5	14	-16
6	6	BEAM2	1		1	14	15	-16
7	7	BEAM2	1		1	15	3	-16
8	8	BEAM2	1		1	9	8	-19
9	9	BEAM2	1		2	10	9	-22
10	10	BEAM2	1		2	9	21	-22
11	11	BEAM2	1		2	21	1	-22
12	12	BEAM2	1		3	1	20	-16
13	13	BEAM2	1		3	20	6	-16
14	14	BEAM2	1		4	5	7	-16
15	15	BEAM2	1		5	3	4	-18
16	16	BEAM2	1		6	20	11	-17
17	17	ROD2	1		7	11	7	
18	18	ROD2	1		8	8	6	

JOB:NEW1ROB 24-JUN-89 LOADING CASE 1 19:23:43 PAGE 1

LOADS

POINT	FORCE X	FORCE Y	FORCE Z	MOMENT X	MOMENT Y	MOMENT Z
4	0.	-1.000E+02	0.	0.	0.	0.

Static Procedure Results From GIFTS

For Robot Manipulator Configuration 3 (figure 4.1)

Called NEW3ROB:

Note: Geometrical input for the robot manipulator were obtained from the on–line–batch file NEW3.SRC .

JOB:NEW3ROB 24-JUN-89 20:00:22 PAGE 1

GIFTS PARAMETER STATUS

TOTAL NUMBER OF POINTS:	22
TOTAL NUMBER OF ELEMENTS:	18
NUMBER OF MATERIAL GROUPS:	1
NUMBER OF STRUCTURAL POINTS:	17
NUMBER OF ACTIVE ELEMENTS:	18
NUMBER OF THICKNESS GROUPS:	8
NUMBER OF LOAD CASES:	1
NUMBER OF ACTIVE LOAD CASES:	1
NUMBER OF UNKNOWNS:	96
COMPUTATIONAL HALF BANDWIDTH:	57.14018

JOB:NEW3ROB 24-JUN-89 20:03:34 PAGE 2

GIFTS STATUS LIST.

MODEL GENERATED.
POINT MASSES NOT GENERATED.
BANDWIDTH OPTIMIZED.
STIFFNESS DIRECTORY PRESENT.
STIFFNESS MATRIX NOT SAVED.
LOADS MODIFIED.
BOUNDARY CONDITIONS INTRODUCED.
STIFFNESS MATRIX DECOMPOSED.
DEFLECTIONS CALCULATED.
ELEMENT STRESSES COMPUTED.
ELEMENT STRAINS NOT PRESENT.
MODEL CAN BE SOLVED BY GIFTS.
TEMPERATURES NOT CALCULATED.
PRESCRIBED TEMPERATURES NOT APPLIED.
NO POINT CONVECTIONS APPLIED.
THERMAL GRADIENTS NOT CALCULATED.
PROBLEM CLASS:
3-D ELASTIC / PLASTIC

JOB:NEW3ROB 24-JUN-89 LOADING CASE 1 20:01:23 PAGE 1

DISPLACEMENT INFORMATION

POINT	U	V	W	RX	RY	RZ
1	1.160E-04	2.285E-07	3.857E-22	-4.201E-23	-3.295E-22	-5.563E-06
2	-1.737E-01	-3.705E-01	-6.664E-06	5.833E-08	1.131E-07	-6.487E-03
3	-3.474E-01	-7.428E-01	-1.162E-05	5.833E-08	1.131E-07	-1.406E-02
4	-3.894E-01	-8.329E-01	-1.251E-05	5.833E-08	1.131E-07	-1.424E-02
5	-1.802E-01	-3.842E-01	-6.982E-06	5.833E-08	1.131E-07	-5.551E-03
6	-6.785E-04	-1.658E-03	1.385E-07	5.833E-08	1.131E-07	-3.580E-04
7	-1.213E-01	-3.717E-01	-5.938E-06	5.833E-08	1.131E-07	-4.201E-03
8	1.849E-05	-1.670E-03	1.254E-21	4.292E-24	-1.479E-22	-3.795E-04
9	2.342E-05	-6.817E-07	3.673E-22	4.292E-24	-1.479E-22	-2.694E-06
10	.000E+00	.000E+00	.000E+00	.000E+00	.000E+00	.000E+00
11	7.078E-04	-5.064E-04	3.194E-07	-2.460E-08	-1.136E-07	-1.894E-04
12	-3.600E-02	-7.660E-02	-2.129E-06	5.833E-08	1.131E-07	-7.965E-03
13	-1.077E-01	-2.295E-01	-4.396E-06	5.833E-08	1.131E-07	-1.001E-02
14	-2.201E-01	-4.699E-01	-8.529E-06	5.833E-08	1.131E-07	-9.755E-03
15	-2.782E-01	-5.946E-01	-1.008E-05	5.833E-08	1.131E-07	-1.259E-02
20	2.633E-05	-1.912E-04	2.167E-07	-2.460E-08	-1.136E-07	-1.468E-04
21	6.182E-05	-2.266E-07	5.120E-22	-1.221E-23	-2.414E-22	-4.157E-06

JOB:NEW3ROB 24-JUN-89 20:05:57 PAGE 1

NODAL POINT INFORMATION

POINT NO.	SYS NO.	X	Y	Z	ACTIVE FREEDOMS
1	1	.00000E+00	3.93900E+01	.00000E+00	U, V, W,RX,RY,RZ
2	2	5.71000E+01	1.27700E+01	.00000E+00	U, V, W,RX,RY,RZ
3	3	9.24400E+01	-3.71700E+00	.00000E+00	U, V, W,RX,RY,RZ
4	4	9.87900E+01	-6.67600E+00	.00000E+00	U, V, W,RX,RY,RZ
5	5	5.93600E+01	1.17100E+01	.00000E+00	U, V, W,RX,RY,RZ
6	6	8.61000E+00	3.53800E+01	.00000E+00	U, V, W,RX,RY,RZ
7	7	5.66900E+01	2.44300E+01	.00000E+00	U, V, W,RX,RY,RZ
8	8	6.00000E+00	1.73900E+01	.00000E+00	U, V, W,RX,RY,RZ
9	9	.00000E+00	1.73900E+01	.00000E+00	U, V, W,RX,RY,RZ
10	10	.00000E+00	.00000E+00	.00000E+00	, , , , ,
11	11	4.40900E+00	4.17500E+01	.00000E+00	U, V, W,RX,RY,RZ
12	12	2.47700E+01	2.78400E+01	.00000E+00	U, V, W,RX,RY,RZ
13	13	4.09300E+01	2.03000E+01	.00000E+00	U, V, W,RX,RY,RZ
14	14	7.03900E+01	6.56700E+00	.00000E+00	U, V, W,RX,RY,RZ
15	15	8.14200E+01	1.42500E+00	.00000E+00	U, V, W,RX,RY,RZ
-16	20	5.93600E+01	1.17100E+01	5.00000E+01	, , , , ,
-17	21	4.40900E+00	4.17500E+01	5.00000E+01	, , , , ,
-18	18	9.87900E+01	-6.67600E+00	5.00000E+01	, , , , ,
-19	19	6.00000E+00	1.73900E+01	5.00000E+01	, , , , ,
20	16	2.71900E+00	3.81200E+01	.00000E+00	U, V, W,RX,RY,RZ
21	17	.00000E+00	2.83900E+01	.00000E+00	U, V, W,RX,RY,RZ
-22	22	.00000E+00	1.73900E+01	5.00000E+01	, , , , ,

JOB:NEW3ROB 24-JUN-89 20:07:17 PAGE 1

MATERIAL INFORMATION

MAT NO.	MAT TYP	YOUNG'S MODULUS	POISSON'S RATIO	SHEAR MODULUS	YIELD STRESS	MASS DENSITY	THERMAL EXPANSION
1	1	2.9000E+07	2.9000E-01	1.1240E+07	3.6000E+04	7.3460E-04	6.5000E-06

JOB:NEW3ROB 24-JUN-89 19:59:22 PAGE 1

ELEMENT INFORMATION

ELEM NO.	SYS NO.	TYPE	MAT NO.	MAT ANG	THS NO.	CONNECTIVITY		
1	1	BEAM2	1		1	6	12	-16
2	2	BEAM2	1		1	12	13	-16
3	3	BEAM2	1		1	13	2	-16
4	4	BEAM2	1		1	2	5	-16
5	5	BEAM2	1		1	5	14	-16
6	6	BEAM2	1		1	14	15	-16
7	7	BEAM2	1		1	15	3	-16
8	8	BEAM2	1		1	9	8	-19
9	9	BEAM2	1		2	10	9	-22
10	10	BEAM2	1		2	9	21	-22
11	11	BEAM2	1		2	21	1	-22
12	12	BEAM2	1		3	1	20	-16
13	13	BEAM2	1		3	20	6	-16
14	14	BEAM2	1		4	5	7	-16
15	15	BEAM2	1		5	3	4	-18
16	16	BEAM2	1		6	20	11	-17
17	17	ROD2	1		7	11	7	
18	18	ROD2	1		8	8	6	

JOB:NEW3ROB 24-JUN-89 LOADING CASE 1 20:08:36 PAGE 1

LOADS

POINT	FORCE X	FORCE Y	FORCE Z	MOMENT X	MOMENT Y	MOMENT Z
4	0.	-1.000E+02	0.	0.	0.	0.

Static Procedure Results From GIFTS

For Robot Manipulator Configuration 5 (figure 4.1)

Called NEW5ROB:

Note: Geometrical input for the robot manipulator were obtained from the on–line–batch file NEW5.SRC .

JOB:NEW5ROB 24-JUN-89 20:16:54 PAGE 1
GIFTS PARAMETER STATUS

TOTAL NUMBER OF POINTS:	22
TOTAL NUMBER OF ELEMENTS:	18
NUMBER OF MATERIAL GROUPS:	1
NUMBER OF STRUCTURAL POINTS:	17
NUMBER OF ACTIVE ELEMENTS:	18
NUMBER OF THICKNESS GROUPS:	8
NUMBER OF LOAD CASES:	1
NUMBER OF ACTIVE LOAD CASES:	1
NUMBER OF UNKNOWNS:	96
COMPUTATIONAL HALF BANDWIDTH:	57.14018

JOB:NEW5ROB 24-JUN-89 20:17:20 PAGE 2
GIFTS STATUS LIST.

MODEL GENERATED.
POINT MASSES NOT GENERATED.
BANDWIDTH OPTIMIZED.
STIFFNESS DIRECTORY PRESENT.
STIFFNESS MATRIX NOT SAVED.
LOADS MODIFIED.
BOUNDARY CONDITIONS INTRODUCED.
STIFFNESS MATRIX DECOMPOSED.
DEFLECTIONS CALCULATED.
ELEMENT STRESSES COMPUTED.
ELEMENT STRAINS NOT PRESENT.
MODEL CAN BE SOLVED BY GIFTS.
TEMPERATURES NOT CALCULATED.
PRESCRIBED TEMPERATURES NOT APPLIED.
NO POINT CONVECTIONS APPLIED.
THERMAL GRADIENTS NOT CALCULATED.
PROBLEM CLASS:
3-D ELASTIC / PLASTIC

JOB:NEW5ROB 24-JUN-89 LOADING CASE 1 20:14:01 PAGE 1
DISPLACEMENT INFORMATION

POINT	U	V	W	RX	RY	RZ
1	1.280E-04	4.410E-07	-3.431E-25	-1.048E-26	3.368E-26	-6.117E-06
2	-1.021E-03	-4.516E-01	9.560E-10	2.724E-12	-1.622E-11	-7.166E-03
3	-1.074E-03	-9.052E-01	1.589E-09	2.724E-12	-1.622E-11	-1.552E-02
4	-1.074E-03	-1.015E+00	1.702E-09	2.724E-12	-1.622E-11	-1.572E-02
5	-1.074E-03	-4.683E-01	9.966E-10	2.724E-12	-1.622E-11	-6.132E-03
6	1.074E-04	-2.006E-03	8.825E-11	2.724E-12	-1.622E-11	-3.923E-04
7	5.204E-02	-4.284E-01	8.984E-10	2.724E-12	-1.622E-11	-4.643E-03
8	1.978E-05	-1.870E-03	-1.874E-25	-7.201E-27	1.481E-26	-4.250E-04
9	2.584E-05	-6.817E-07	-9.859E-26	-7.201E-27	1.481E-26	-2.972E-06
10	.000E+00	.000E+00	.000E+00	.000E+00	.000E+00	.000E+00
11	9.495E-04	-2.265E-04	1.915E-11	1.623E-12	-6.481E-12	-2.073E-04
12	-2.686E-04	-9.335E-02	3.775E-10	2.724E-12	-1.622E-11	-8.786E-03
13	-6.448E-04	-2.798E-01	6.668E-10	2.724E-12	-1.622E-11	-1.104E-02
14	-1.074E-03	-5.729E-01	1.194E-09	2.724E-12	-1.622E-11	-1.077E-02
15	-1.074E-03	-7.245E-01	1.391E-09	2.724E-12	-1.622E-11	-1.390E-02
20	1.285E-04	-2.286E-04	1.266E-11	1.623E-12	-6.481E-12	-1.604E-04
21	6.826E-05	-1.203E-07	-2.119E-25	-9.661E-27	2.418E-26	-4.579E-06

JOB:NEW5ROB 24-JUN-89 20:21:32 PAGE 1

NODAL POINT INFORMATION

POINT NO.	SYS NO.	X	Y	Z	ACTIVE FREEDOMS
1	1	.00000E+00	3.93900E+01	.00000E+00	U, V, W,RX,RY,RZ
2	2	6.30000E+01	3.93900E+01	.00000E+00	U, V, W,RX,RY,RZ
3	3	1.02000E+02	3.93900E+01	.00000E+00	U, V, W,RX,RY,RZ
4	4	1.09000E+02	3.93900E+01	.00000E+00	U, V, W,RX,RY,RZ
5	5	6.55000E+01	3.93900E+01	.00000E+00	U, V, W,RX,RY,RZ
6	6	9.50000E+00	3.93900E+01	.00000E+00	U, V, W,RX,RY,RZ
7	7	5.77000E+01	4.97900E+01	.00000E+00	U, V, W,RX,RY,RZ
8	8	6.00000E+00	1.73900E+01	.00000E+00	U, V, W,RX,RY,RZ
9	9	.00000E+00	1.73900E+01	.00000E+00	U, V, W,RX,RY,RZ
10	10	.00000E+00	.00000E+00	.00000E+00	, , , , ,
11	11	3.00000E+00	4.33900E+01	.00000E+00	U, V, W,RX,RY,RZ
12	12	2.73300E+01	3.93900E+01	.00000E+00	U, V, W,RX,RY,RZ
13	13	4.51700E+01	3.93900E+01	.00000E+00	U, V, W,RX,RY,RZ
14	14	7.76700E+01	3.93900E+01	.00000E+00	U, V, W,RX,RY,RZ
15	15	8.98300E+01	3.93900E+01	.00000E+00	U, V, W,RX,RY,RZ
-16	20	6.55000E+01	3.93900E+01	5.00000E+01	, , , , ,
-17	21	3.00000E+00	4.33900E+01	5.00000E+01	, , , , ,
-18	18	1.09000E+02	3.93900E+01	5.00000E+01	, , , , ,
-19	19	6.00000E+00	1.73900E+01	5.00000E+01	, , , , ,
20	16	3.00000E+00	3.93900E+01	.00000E+00	U, V, W,RX,RY,RZ
21	17	.00000E+00	2.83900E+01	.00000E+00	U, V, W,RX,RY,RZ
-22	22	.00000E+00	1.73900E+01	5.00000E+01	, , , , ,

JOB:NEW5ROB 24-JUN-89 20:20:33 PAGE 1

MATERIAL INFORMATION

MAT NO.	MAT TYP	YOUNG'S MODULUS	POISSON'S RATIO	SHEAR MODULUS	YIELD STRESS	MASS DENSITY	THERMAL EXPANSION
1	1	2.9000E+07	2.9000E-01	1.1240E+07	3.6000E+04	7.3460E-04	6.5000E-06

JOB:NEW5ROB 24-JUN-89 20:19:13 PAGE 1

ELEMENT INFORMATION

ELEM NO.	SYS NO.	TYPE	MAT NO.	MAT ANG	THS NO.	CONNECTIVITY		
1	1	BEAM2	1		1	6	12	-16
2	2	BEAM2	1		1	12	13	-16
3	3	BEAM2	1		1	13	2	-16
4	4	BEAM2	1		1	2	5	-16
5	5	BEAM2	1		1	5	14	-16
6	6	BEAM2	1		1	14	15	-16
7	7	BEAM2	1		1	15	3	-16
8	8	BEAM2	1		1	9	8	-19
9	9	BEAM2	1		2	10	9	-22
10	10	BEAM2	1		2	9	21	-22
11	11	BEAM2	1		2	21	1	-22
12	12	BEAM2	1		3	1	20	-16
13	13	BEAM2	1		3	20	6	-16
14	14	BEAM2	1		4	5	7	-16
15	15	BEAM2	1		5	3	4	-18
16	16	BEAM2	1		6	20	11	-17
17	17	ROD2	1		7	11	7	
18	18	ROD2	1		8	8	6	

JOB:NEW5ROB 24-JUN-89 LOADING CASE 1 20:22:53 PAGE 1

LOADS

POINT	FORCE X	FORCE Y	FORCE Z	MOMENT X	MOMENT Y	MOMENT Z
4	0.	-1.000E+02	0.	0.	0.	0.

Modes Procedure Results From GIFTS

For Robot Manipulator Configurations 1, 3, 5, 7, 8, & 11 (figure 4.1)

Called:

NEW1ROB

NEW3ROB

NEW5ROB

NEW7ROB

NEW8ROB

NEW11ROB

Note: Geometrical input for the robot manipulator were obtained from the on–line–batch file NEW1.SRC, NEW3.SRC, NEW5.SRC, NEW7.SRC, NEW8.SRC, and NEW11.SRC.

JOB:NEW1ROB 5-MAY-89 3:10:06 PAGE 1

FREQUENCIES

MODE	FREQ	EIGV
1	3.80266E+00	5.70866D+02
2	6.04767E+00	1.44389D+03
3	6.21915E+00	1.52694D+03
4	1.58035E+01	9.85978D+03
5	4.26203E+01	7.17121D+04
6	9.47101E+01	3.54121D+05
7	1.06645E+02	4.48993D+05
8	1.32715E+02	6.95348D+05
9	1.38831E+02	7.60904D+05
10	2.22317E+02	1.95122D+06

JOB:NEW3ROB 5-MAY-89 3:22:39 PAGE 1

FREQUENCIES

MODE	FREQ	EIGV
1	3.33484E+00	4.39045D+02
2	5.30930E+00	1.11284D+03
3	1.51019E+01	9.00377D+03
4	2.07712E+01	1.70326D+04
5	2.69129E+01	2.85943D+04
6	9.04625E+01	3.23070D+05
7	1.09567E+02	4.73933D+05
8	1.39560E+02	7.73339D+05
9	1.47325E+02	8.56863D+05
10	2.18509E+02	1.88494D+06

JOB:NEW5ROB 5-MAY-89 3:58:00 PAGE 1

FREQUENCIES

MODE	FREQ	EIGV
1	3.33494E+00	4.39073D+02
2	5.30959E+00	1.11297D+03
3	1.51021E+01	9.00392D+03
4	2.07742E+01	1.70376D+04
5	2.69000E+01	2.85570D+04
6	9.04427E+01	3.22929D+05
7	1.09506E+02	4.73404D+05
8	1.39907E+02	7.72749D+05
9	1.47389E+02	8.57611D+05
10	2.12505E+02	1.78278D+06

JOB:NEW7ROB 5-MAY-89 3:59:34 PAGE 1

FREQUENCIES-

MODE	FREQ	EIGV
1	3.33453E+00	4.38964D+02
2	5.30451E+00	1.11084D+03
3	1.51034E+01	9.00558D+03
4	2.07694E+01	1.70297D+04
5	2.68883E+01	2.85421D+04
6	9.04049E+01	3.22653D+05
7	1.09248E+02	4.71179D+05
8	1.39798E+02	7.71550D+05
9	1.47328E+02	8.56901D+05
10	2.16561E+02	1.85148D+06

JOB:NEW8ROB 5-MAY-89 4:14:18 PAGE 1

FREQUENCIES

MODE	FREQ	EIGV
1	3.80245E+00	5.70802D+02
2	6.04853E+00	1.44437D+03
3	6.21201E+00	1.52344D+03
4	1.58054E+01	9.86217D+03
5	4.26135E+01	7.16959D+04
6	9.46292E+01	3.53517D+05
7	1.06285E+02	4.45966D+05
8	1.32703E+02	6.95222D+05
9	1.39012E+02	7.62497D+05
10	2.19458E+02	1.90135D+06

JOB:NEW11ROB 5-MAY-89 15:25:19 PAGE 1

FREQUENCIES

MODE	FREQ	EIGV
1	3.41103E+00	4.59337D+02
2	5.24230E+00	1.08494D+03
3	7.97913E+00	2.51345D+03
4	1.86059E+01	1.36667D+04
5	3.69631E+01	5.39383D+04
6	8.96024E+01	3.16956D+05
7	1.08954E+02	4.68647D+05
8	1.41384E+02	7.89153D+05
9	1.44307E+02	8.22114D+05
10	2.22921E+02	1.96182D+06

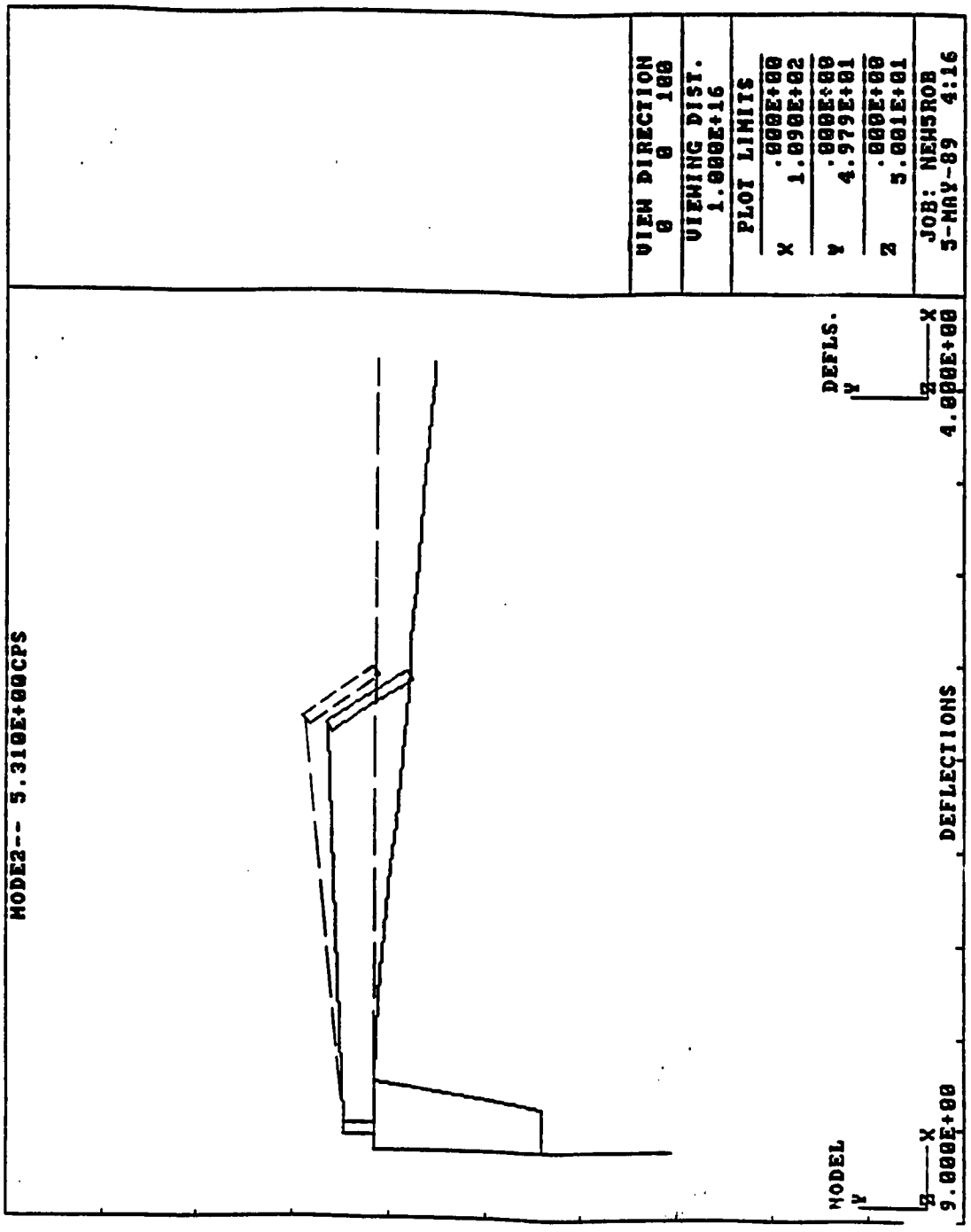
MODE2-- 5.310E+00CPS
VIEW DIRECTION
0 0 100
VIEWING DIST.
1.000E+16
PLOT LIMITS
X .000E+00
1.090E+02
Y .000E+00
4.979E+01
Z .000E+00
5.001E+01
JOB: NEWSROB
5-MAY-89 4:16
DEFLS.
4.000E+00
DEFLECTIONS
MODEL
9.000E+00

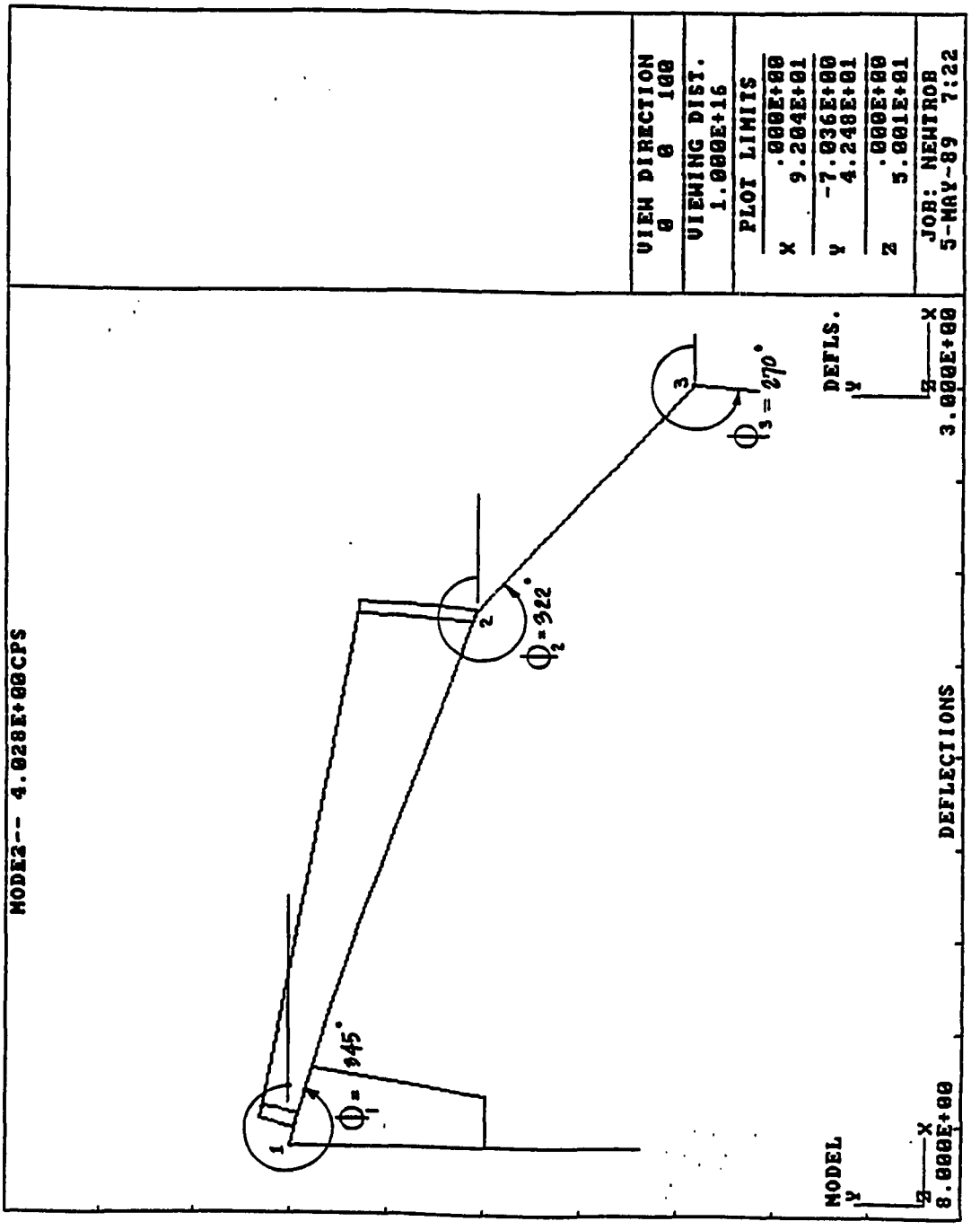
MODE2-- 4.028E+00CPS
VIEW DIRECTION
0 0 100
VIEWING DIST.
1.000E+16
PLOT LIMITS
X .000E+00
9.204E+01
Y -7.036E+00
4.248E+01
Z .000E+00
5.001E+01
JOB: NEWTROB
5-MAY-89 7:22
$\phi_1 = 145°$
$\phi_2 = 322°$
$\phi_3 = 270°$
1
2
3
DEFLS.
Y
Z
X
3.000E+00
MODEL
Y
Z
X
8.000E+00
DEFLECTIONS

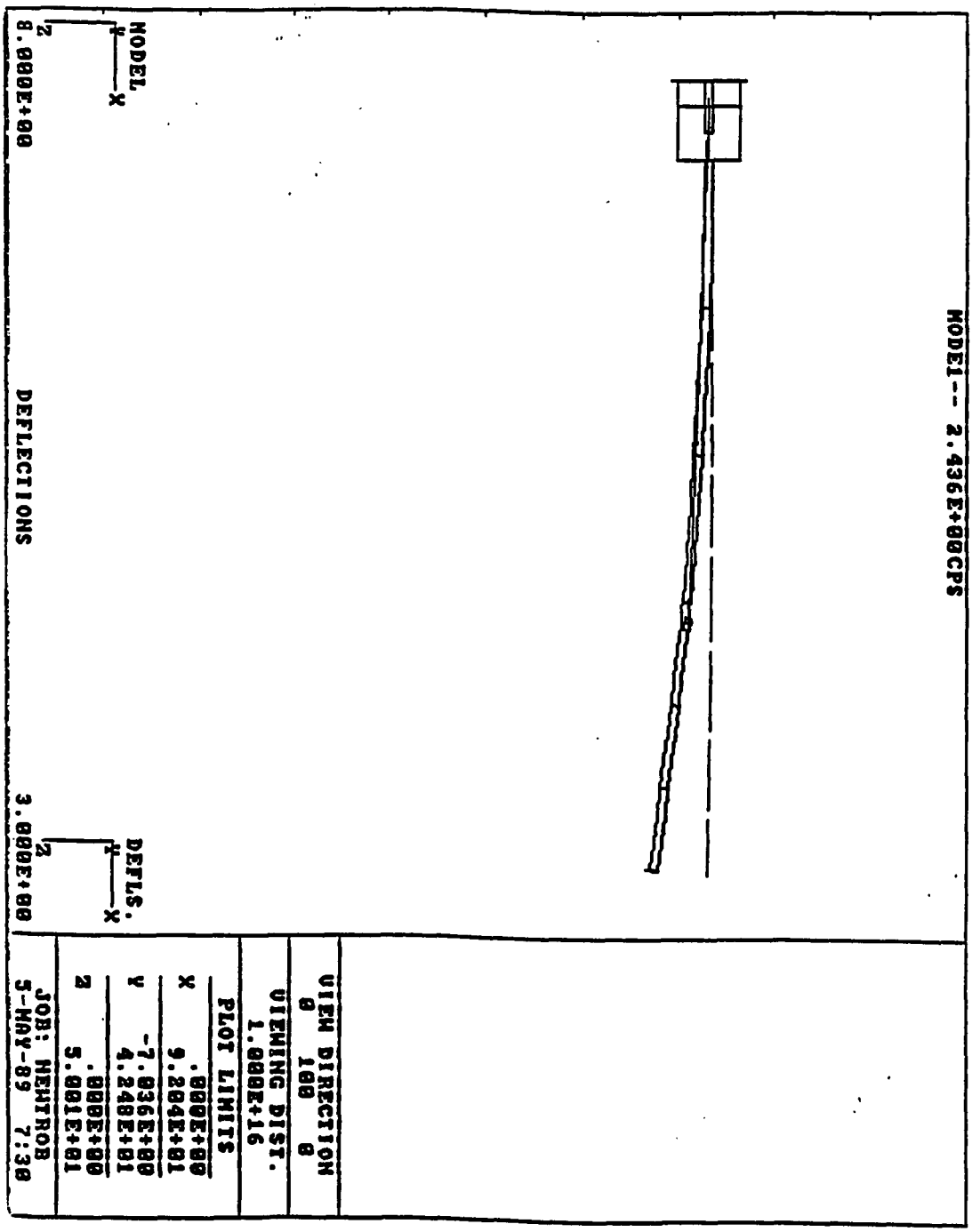
MODE1-- 2.436E+00CPS
DEFLECTIONS
MODEL
Z
X
8.000E+00
DEFLS.
Z
X
3.000E+00
VIEW DIRECTION
0 180 0
VIEWING DIST.
1.000E+16
PLOT LIMITS
X .000E+00
9.204E+01
Y -7.036E+00
4.248E+01
Z .000E+00
5.001E+01
JOB: NEWTROB
5-MAY-89 7:30